A CLAS Collaboration Proposal to PAC37

Meson Spectroscopy with low Q^2 electron scattering in CLAS12

M. Battaglieri*†, A. Bersani, A. Celentano, R. De Vita†, M. Osipenko, M. Ripani, M. Taiuti
Istituto Nazionale di Fisica Nucleare, Sezione di Genova
e Dipartimento di Fisica dell'Università, 16146 Genova, Italy

A. Afanasev, V. D. Burkert, L. Elouadrhiri, V. Kubarovsky,
P. Nadel-Turonski, E. Pasyuk, S. Stepanyan†, D. Weygand†
Jefferson Lab, Newport News, VA 23606, USA

D. I. Glazier†, D. P. Watts
Edinburgh University, Edinburgh EH9 3JZ, United Kingdom

C. Salgado†, M. Khandaker
Norfolk State University, Norfolk VA 23504, USA

A. Szczepaniak
Physics Department and Nuclear Theory Center, Indiana University, Bloomington, Indiana 47405

J. Ball, M. Garçon, B. Moreno, H. Moutarde, S. Procureur, F.Sabatié
CEA-Saclay, Service de Physique Nucleaire, F91191 Gif-sur-Yvette, France

A. Fradi, B. Guegan, M. Guidal, S. Niccolai, S.Pisano, D. Sokhan
Institut de Physique Nucleaire d'Orsay, IN2P3, BP 1, 91406 Orsay, France

K. Hicks
Ohio University, Department of Physics, Athens, OH 45701, USA

K. Joo, M. Ungaro
University of Connecticut, Storrs, Connecticut 06269

D. Ireland, R. Kaiser, K. Livingston, D. MacGregor, B. McKinnon,
D. Protopopescu, G. Rosner, B. Seitz
University of Glasgow, Glasgow G12 8QQ, United Kingdom

W. J. Briscoe, H. Haberzettl, A. Micherdzinska, M. Paris, I. I. Strakovsky
The George Washington University, Washington, D.C., 20052

A. Kubarovsky, P. Stoler
Rensselaer Polytechnic Institute, Department of Physics, Troy, NY 12181, USA

*Contact Person, email: Marco.Battaglieri@ge.infn.it
†Spokesperson

L. Guo
Florida International University, Miami, Florida 33199

B.Nefkens, A. Starostin
University of California at Los Angeles, Department of Physics and Astronomy, Los Angeles, CA 90095-1547, USA

A. D'Angelo, C. Shaerf, V. Vegna
Istituto Nazionale di Fisica Nucleare, Sezione di Roma 2 e Dipartimento di Fisica dell'Università di Roma Tor Vergata, Roma, Italy

M. Aghasyan, S. Anefalos Pereira, E. De Sanctis, D. Hasch, V. Lucherini, M. Mirazita, P. Rossi
Istituto Nazionale di Fisica Nucleare, Laboratori Nazionali di Frascati, P.O. 13, 00044 Frascati, Italy

M. Capogni, D.M. Castelluccio, E. Cisbani, S. Frullani, F. Garibaldi, F. Meddi, G. M. Urciuoli
Istituto Nazionale di Fisica Nucleare, Sezione di Roma e Gruppo Collegato Sanità, e Università La Sapienza, Italy

R. De Leo
Istituto Nazionale di Fisica Nucleare, Sezione di Bari e Dipartimento di Fisica dell'Università, Bari, Italy

R. Perrino
Istituto Nazionale di Fisica Nucleare, Sezione di Lecce 73100 Lecce, Italy

V. Bellini, A. Giusa, F. Mammoliti, G. Russo, M. L. Sperduto, C. M. Sutera
Istituto Nazionale di Fisica Nucleare, Sezione di Catania e Dipartimento di Fisica dell'Università, Catania, Italy

L. Barion, G. Ciullo, M. Contalbrigo, P. Lenisa, L. Pappalardo
Istituto Nazionale di Fisica Nucleare, Sezione di Ferrara e Dipartimento di Fisica dell'Università, Ferrara, Italy

J. Dumas, C. Maieron, Y. Perrin, E.Voutier
Laboratoire de Physique et de Cosmologie, CNRS/IN2P3, 38026 Grenoble, France

and the CLAS Collaboration

Abstract

Understanding quark and gluon confinement in Quantum Chromodynamics is one of the outstanding issues in physics. To this end, meson spectroscopy is a powerful tool to investigate how the QCD partons manifest themselves under the strong interaction at the energy scale of the nucleon mass (GeV).

We propose a comprehensive study of the meson spectrum with precise determination of resonance masses and properties with a high statistics and high resolution experiment. The meson spectrum in the mass range 1.5-2.5 GeV will be studied looking for rare $q\bar{q}$ states and unconventional mesons with exotic quantum numbers.

We will extend the Hall-B CLAS12 capability, to run experiments with quasi-real photons. The technique, electroscattering at very low Q^2 ($10^{-2} - 10^{-1}$ GeV^2) provides a high photon flux and a high degree of linear polarization and represents a competitive and complementary way to study the meson spectrum and production mechanisms with respect to real photoproduction experiments.

A Forward Tagger consisting of a calorimeter, scintillation hodoscope and tracking device will be added to the standard equipment to detect the scattered electrons in the angular range $\theta_{e'} = 2.5^\circ - 4.5^\circ$ and energy range $E_{e'} = 0.5 - 4.5$ GeV and fully determine the energy ($\nu = 6.5 - 10.5$ GeV) and the polarization ($P_\gamma = 70 - 10\%$) of the associated quasi-real photon. At the nominal luminosity of CLAS12 ($\sim 10^{35}$cm^{-2}s^{-1}) with an 11 GeV electron beam, the resulting hadronic rate will be equivalent to that achievable with a real photon flux of $10^8 - 10^9$ γ/s on the 5 cm LH_2 target, foreseen for electroproduction runs in Hall-B.

The CLAS12 detector will be used to identify and measure the decay products of produced mesons. Good efficiency for multi-particle final states, including neutrals, excellent particle identification with kaon/pion discrimination up to $p \sim 3$ GeV, and precise determination of momenta and angles are the key features available to CLAS12 to identify exclusive channels, measure the resonance masses with good accuracy over a broad range and extend the search to the strangeness-rich meson spectrum.

Quantum numbers of meson resonances will be defined via partial wave analysis (PWA) of their decay products. The experience with the CLAS 6 GeV data analysis and the detailed studies of PWA for benchmark channels of this proposal give us confidence that, with the addition of the Forward Tagger, CLAS12 will become a powerful tool for meson spectroscopy studies, in particular in the strangeness sector. The technique of electroproduction at very small angles will provide a precise knowledge of the photon polarization on event-by-event basis, giving a vital tool to disentangle contributions of different production mechanisms and reduce background from other isobars decaying in the same final state.

A beam time of 80 days at full luminosity of $\sim 10^{35}$cm^{-2}s^{-1} will be sufficient to accumulate enough statistics to perform complete amplitude analysis for rare meson production, with cross sections at the level of 10 nb. In addition to the production run, 35 days of commissioning will be required to test and optimize the new experimental equipment and collect adequate statistics at low luminosity with a minimum bias trigger for systematic checks. The operation of the new device will be compatible with standard electron scattering experiments planned for Hall-B, allowing the proposed measurements to be run in parallel with the approved program.

The unique combination of CLAS12 with an additional Forward Tagger facility will give access to an extensive physics program of hadron spectroscopy using quasi-real photoproduction. This will be highly complementary to the approved program of the GLUEX Collaboration in Hall-D. We believe the constructive interference of these different experiments will strengthen the role of Jefferson Lab in this field.

Contents

1 Introduction

It has been more than thirty years since QCD was postulated as the theory of strong interactions. While much progress has been made in understanding the high energy phenomena through this theory, the strong-interaction in the non-perturbative regime has remained obscure. A clear understanding of this regime is necessary since it is where we have the dominant manifestation of the strong force, *i.e.* hadrons that constitute the bulk of the visible mass of the universe.

The phenomenology of hadrons and in particular the study of their spectrum led more than forty years ago to the development of the quark model, where baryons and mesons are described as bound systems of three quarks and of a quark-antiquark pair, respectively. While this picture still holds and has been proven to reproduce many features of the hadron spectrum, now we know that the hadron mass cannot be explained only in terms of the quark masses, but it is mainly due to the dynamics of the gluons that bind them. Measuring the spectrum of hadrons, studying their properties and inner structure is therefore crucial to achieve a deep knowledge of the strong force.

Mesons, being made by a quark and an anti-quark, are the simplest quark bound system and therefore the ideal benchmark to study the interaction between quarks, understand what the role of gluons is and investigate the origin of confinement. The quark model predicts the existence of multiplets of mesons with similar properties, that are classified according to their total angular momentum J, the parity P, and charge conjugation C. While most of the lowest mass states have been clearly identified and studied [1], several open issues related to the mass hierarchy and decays of excited states remain and still await for a thorough experimental investigation. In addition phenomenological models [2, 3, 4, 5, 6, 7] and lattice QCD calculations [8, 9] suggest that states beyond the simple $q\bar{q}$ configuration, as hybrids (qqg), tetraquarks ($qq\bar{q}\bar{q}$) and glueballs, should also exist. If so, we should expect to find a much richer spectrum than that predicted by the quark model and, in particular, we should be able to observe new meson multiplets corresponding to these unconventional configurations. Hybrid mesons are of particular interest as they are the cleanest experimental signature for the presence of gluons in the dynamical mass generation process. A precise determination of their spectrum and properties can provide a unique opportunity to study the role of the glue and to understand the phenomenon of confinement. An unambiguous identification of these states can in general be rather difficult, since they can mix with ordinary mesons having the same quantum numbers (J^{PC}). However, the additional degrees of freedom present in these states can also lead to *exotic* quantum numbers that are not allowed in $q\bar{q}$ systems and therefore provide a unique signature of their unusual structure.

In this proposal we present an experiment to study meson spectroscopy via quasi-real photoproduction in Hall B, using the CLAS12 detector and a new Forward Tagger facility (FT). The 12 GeV electron beam available after the upgrade of Jefferson Lab, the excellent characteristics of the CLAS12 detector and of the new FT facility will give the possibility of exploring a broad mass range accumulating data of unprecedented accuracy and statistics.

The proposal is organized as follows. In Section 2 we summarize the present knowledge of meson spectroscopy, discussing the open issues, the topics that will be addressed by this experiment and future perspectives. In Section 3 we describe the analysis techniques that will be used to identify meson signals. In Section 4 we outline the goals of the proposed experiment and the technique that will be adopted. In Section 5 we discuss the experimental setup and running conditions. In Section 6 we describe Monte Carlo simulations that were performed to determine the acceptances for the reactions of interest and the detailed systematic studies on partial wave analysis of CLAS12 pseudo-data. Finally in Section 7 and 8 we present the beam time request and the experiment summary. Since this proposal follows from a Letter of Intent [10] endorsed by PAC35, in Appendix we address the issues raised by the Committee in their report.

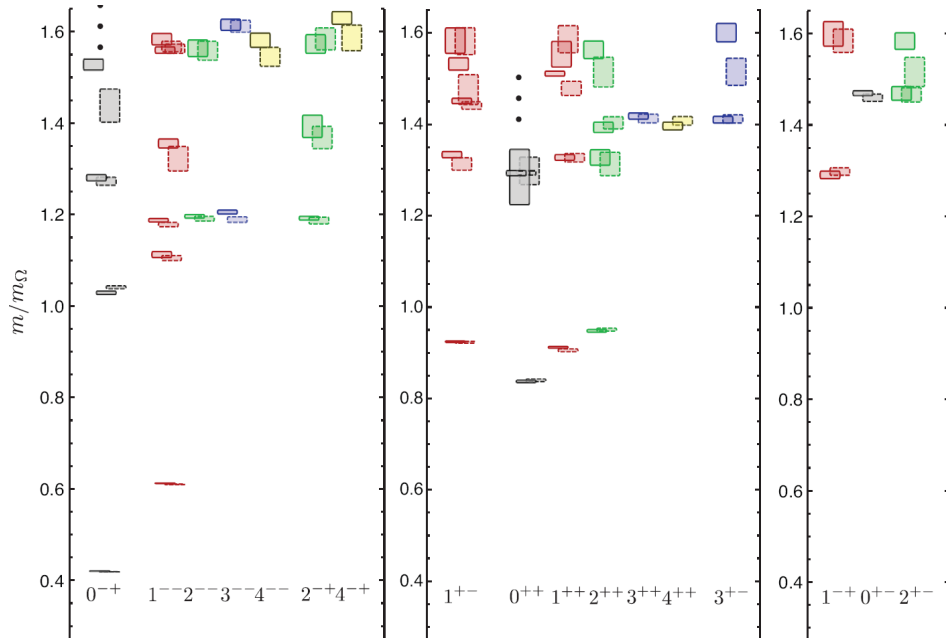

Figure 1: Lattice results from JLab lattice collaboration [9] for the low-lying isovector mesons. Masses are given in units of the Ω^- baryon mass (1.672 GeV).

2 Meson Spectroscopy

Over the last several decades significant efforts have been dedicated to the investigation of the meson spectrum, both from the experimental and theoretical perspective. Research has focused on two main topics: the search for unconventional states, such as hybrids, glueballs or tetraquarks, and the study of highly excited $q\bar{q}$ states, that are either poorly established or not experimentally observed. With the recent advances in lattice QCD calculations, first predictions of the masses, widths and decays of several states are becoming available with increasing reliability. These results give fundamental guidance for experimental investigations aiming to provide definitive proof of the existence of the unobserved states and precise determination of their properties. In the following, we discuss in more detail the physics topics that we consider more relevant in this field and that will be the main focus of the proposed experiment.

2.1 Hybrid Mesons and Exotics

For many years, there has been speculation on the existence of hybrid mesons ($q\bar{q}g$) and other resonances beyond those predicted by the quark model. The existence of these states and predictions for masses and decay widths have been based on various models, *e.g.* the bag model [2, 3, 4], the flux tube model [5, 6] or the constituent glue model [7]. Recently, first principle computations using lattice gauge techniques have shown signals for such states. Discrimination among the various dynamical assumptions of the models has become possible with these emerging lattice results giving confidence that hybrid mesons exist and should be experimentally accessible. The calculations also indicate that the decay characteristics of theses states are similar to those of regular resonances and that masses of the lowest states are around 2 GeV.

Recently an unquenched calculation with two light quark flavors and an heavier third quark tuned to the strange quark mass was performed, predicting the full light-quark isovector meson

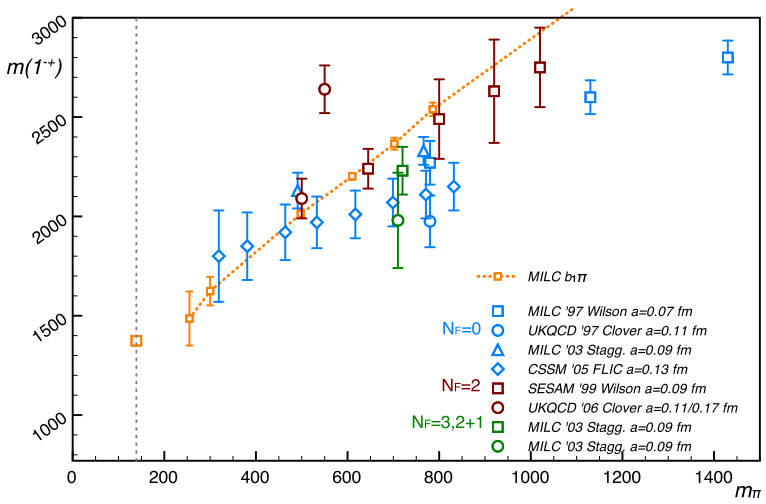

Figure 2: Summary of lattice results for the mass of the $J^{PC} = 1^{-+}$ exotic meson. Data are from Refs. [11, 12, 13, 14, 15, 16].

spectrum [8, 9]. The significant innovations adopted in this calculation, the fine lattice spacing and large operator basis allowed the authors to predict a large number of states, determining their spin assignments and providing, for the first time, indications of their nature. Figure 1 shows the predicted spectrum for both ordinary and exotic states. The good agreement between lattice computations and experimental data for conventional states, both in terms of number of states and mass hierarchy, proves the advanced stage of these calculations. In the exotic sector, states with J^{PC} quantum number 1^{-+}, 0^{+-} and 2^{+-} are predicted. The lightest is a 1^{-+} state, while the 0^{+-} and 2^{+-} ground states are almost degenerate and slightly heavier. Excited states with J^{PC} equal to 1^{-+} and 2^{+-} are also predicted. In the same calculation, states with exotic 0^{--} and 3^{-+} are found but with considerably higher masses. In Fig. 2, we show a compilation of several lattice results on the mass of the lightest $J^{PC} = 1^{-+}$ exotics as a function of the pion mass. It is evident that there is a good agreement between various lattice groups and convergence towards the physical pion mass limit is expected in the near future.

2.1.1 Experimental Evidence for Exotics

While theoretical efforts seem to be converging toward a coherent and comprehensive picture of exotics, the experimental situation is still rather confused. Most of the data on exotic mesons in the light quark sector have been collected in the last thirty years with hadronic probes, either in diffractive production from pion beams or anti-proton annihilation on protons or neutrons. More recently first photoproduction experiments have been performed at CLAS [17, 18, 19, 20, 21]. For a detailed review of the experimental situation, we refer the reader to recent reviews on the subject [22, 23, 24], while in the following we will summarize the main findings and open issues.

In the light-quark sector, experiments have given evidence for three possible exotics, the $\pi_1(1400)$, the $\pi_1(1600)$ and the $\pi_1(2105)$. The first has been observed in the decay to $\pi\eta$ in pion and anti-proton beam experiments [25, 26, 27, 28, 29]. However, the observation of the resonance in a single decay mode and some inconsistencies in the observed signals have raised doubts on its interpretation as an exotic meson and have lead to the belief that, while the structure may be real, it could be due to non-resonant effects as the opening a new channel or final state interaction [24, 30]. The

most solid but controversial state is the $\pi_1(1600)$. This has been observed in several decay modes, namely $\eta'\pi$, $b_1\pi$, $f_1\pi$, $\rho\pi$, and by several experiments. The signal reported by the E852 Collaboration in the $\pi^- p \to \pi^-\pi^-\pi^+ p$ channel [31] has been considered as the most robust evidence for this state. However, a later analysis, that used more statistics and a larger set of waves in the PWA [32], as well as negative observations from VES [33] and CLAS [17] raised strong doubts on the existence of this state. Adding to the controversy, a new positive result in the same decay was recently reported by the COMPASS Collaboration from the analysis of peripheral pion production on nuclear targets [34]. The observed signal appears again to be robust, but the limited published information and the absence of phase motion between the measured $\pi_1(1600)$ and $\pi_2(1670)$ signals bring some concerns. To solve this puzzling situation, high statistics and high accuracy data in the 3π final state are definitely needed to allow for a detailed analysis and systematic investigation of this decay mode. The evidence for the third exotic, the $\pi_1(2015)$ was reported by the E852 Collaboration [35] in the $b_1\pi$ and $f_1\pi$ decays. The limited data available and the absence of a confirmation again do not allow to draw conclusions about this possible exotic.

From a critical analysis of the experimental situation we can highlight two main points. First, an exotic signal to be convincing needs to be found in more than one decay mode. Phenomenological models can provide indications of the expected decays and widths and already suggest that these states should have multiple decay patterns with significant branching ratios. On the other hand, backgrounds that can affect the signal extraction will be different, giving different sensitivity to the signal. The measurement of multiple decay modes requires the capability of detecting complex final states, with neutral and charge particles and good particle-identification capabilities to include strange decays. Second, search for exotics in experiments with different probes is necessary, since we still don't know what production mechanisms are more favorable. So far most experiments used hadronic probes and only recently electromagnetic probes have been used. In the future data will be collected using very different techniques by BES-III [36] in Beijing using e^+e^- annihilation, by GLUEX [37] at JLab using a bremsstrahlung photon beam on a proton target and by PANDA [38] at GSI using proton-antiproton annihilation. The present experiment proposes the use of quasi-real photoproduction as a complementary and powerful method to search for exotics, contributing to the world-wide effort in the field.

2.1.2 Hybrids with Hidden Strangeness

One very attractive method to identify exotic mesons is through strangeness-rich final states, as the $\phi\pi$ decay mode. Any $s\bar{s}$-meson decay to $\phi\pi$ is forbidden due to the conservation of isotopic spin. This decay mode is forbidden by the Okubo-Zweig-Iizuka (OZI) rule for any $n\bar{n}$-meson (where n is u or d quarks) as well. On the other hand, multiquark or hybrid mesons are expected to have a strong coupling to the $\phi\pi$ system. The discovery of a $\phi\pi$ resonance would indicate a new kind of hadron and suggest a $q\bar{q}g$ or $q\bar{q}q\bar{q}$ state. This is true for $f'\pi$ and $J/\psi\pi$ decay modes as well [39].

Some experimental evidence for the existence of a resonance with strong $\phi\pi$ coupling is available. In experiments at the LEPTON-F spectrometer [40, 41], a new meson C(1480), with mass 1480 ± 40 MeV, width 130 ± 60 MeV and an anomalous large branching ratio to $\phi\pi$, was observed. At the present time, the only consistent explanation of these properties can be obtained with the assumption that the $C(1480)$ meson is a four quark or hybrid state. At the Ω–spectrometer [42] the cross section for the reaction $\gamma p \to \phi\pi^0 p$ was measured. Although the number of events was not large (~ 25), an excess of events in the mass spectrum of the $\phi\pi^0$ system at $\sim$1.4 GeV was observed. The $\phi\pi^0$ photoproduction cross section was estimated to be $\sigma(\gamma p \to \phi\pi^0 p) = 6 \pm 3$nb (at 95% C.L.). The existence of a structure in the same mass range was confirmed with the study of inclusive $\phi\pi^+$ production with a pion beam [43] and by recent $e^+e^- \to \phi\pi^0$ data from Ref. [44].

A clean identification of this final state can be obtained by detecting the K^+K^- pair from the charged decay of the ϕ meson. This can be achieved in CLAS12, exploting the good particle-identification capabilities of the detector, opening therefore a unique window on the search of exotics with hidden strangeness.

2.2 Spectroscopy of Conventional Mesons

Beside exotic mesons, the spectroscopy of conventional states still shows many interesting aspects. While the lowest mass multiplets are well established, at higher mass a number of states predicted by the quark model has not been observed yet. In addition in specific sectors, the quark model assignment of some observed state is still uncertain. As an example, in the following we briefly review the situation for scalar mesons and strangeonia.

2.2.1 Scalar Mesons

Spectroscopy of low-lying scalar mesons is one topic of high interest. The first nonet is assumed to include the σ, κ, $f_0(980)$, and $a_0(980)$ mesons but the mass ordering, disfavoring the naive $q\bar{q}$ picture, suggests an interpretation in terms of diquark-antidiquark bound states [45, 46]. Assignments to the excited nonets are even more doubius because of the surplus of scalar states with masses between 1.3 and 1.7 GeV. This excess has been interpreted as due to the possible presence of glueballs in the same mass range [47]. So far, scalar mesons have been observed in hadron-hadron collisions, $\gamma\gamma$ collisions in decays of various mesons such as $\phi, J/\Psi, D$ and B while very few studies with electromagnetic probes were attempted. Decays to several multi-particle final states such as $\pi^+\pi^-$, K^+K^-, $2\pi^+2\pi^-$, $\pi^0\eta$, ... have been observed. Production cross sections are relatively small compared to the dominant vector meson states; however S-wave parameters can be extracted by performing a partial wave analysis and exploiting the interference with the dominant P-waves. First study of low mass scalar mesons in the photoproduction of pion pairs was performed by the CLAS Collaboration [18]. This experiment led to the first evidence in photoproduction of the $f_0(980)$ but could not study higher mass states because of the limited beam energy. The extension of this measurement to the higher energies available with the 12 GeV upgrade would allow a detailed study of states such as the $f_0(1370)$, $f_0(1500)$, the $f_0(1710)$ and other scalars with masses up to 2.0-2.5 GeV. Estimates of the photoproduction cross sections for these states in the range of 10-50 nb have been made in Ref. [48] for the kinematic covered by Jefferson Lab at 12 GeV.

2.2.2 Strangeonia

Strangeonia are mesons containing $s\bar{s}$ pairs: these can be conventional states in the quark model or hybrids with or without exotic quantum numbers. While the strange meson spectrum is quite well understood, the details of the strangeonium spectrum are much less certain and only a handful of states have been confirmed. This, in itself, is a motivation for studying strangeonium spectroscopy. In addition, a number of the final states in which an exotic signal has been claimed are also final states in which strangeonia would be expected. Thus, a precise determination of the strangeonium spectrum is important to constrain the search of exotic candidates.

The masses are expected to be in the 1-3 GeV range, i.e. a transition region between light (relativistic) and heavy (non-relativistic) $q\bar{q}$ states[‡]. The conventional *strangeonia* mesons are associated with the radial and orbital excited states of the $\phi(1020)$ meson, the ground state of the

[‡]The relevance of this aspect was pointed out by Barnes, Page and Black [49]: "the similarity between the $s\bar{s}$ spectrum, the light meson $n\bar{n}$ and the heavy $Q\bar{Q}$ systems needs to be understood to bridge the gap between Heavy Quark Effective Theory (HQET) and the light quark world in which we live".

production	*mass* (MeV)	*width* (MeV)	*experiment*	*decay*	ref
e^+e^-	1650		DM1	K_LK_S	[50]
	1650			K^+K^-	[51]
	1650		VEPP-2M	K^+K^-	[52]
	1680		DM2	K^+K^-	[53]
	1677	102		$K_SK^+\pi^-$.	[54]
	1680	185	DM1	KK, $KK\pi$	[55]
	1657	146	DM2	K^+K^-	[56]
photo-	1748	80	CERN Omega	KK	[57]
	1760	80	CERN WA57	KK	[58]
	1726	121	Fermi E401	KK	[59]
	1753	122	Fermi FOCUS	KK	[60]

Table 1: Experimental data on the $\phi(1680)$.

$s\bar{s}$ system. Even these 'normal' strangeonia are poorly understood: among the 22 low mass (M < 2.5 GeV) strangeonium states expected, only 5 are well identified. A summary of the current data on the $\phi(1680)$, *i.e.* first radial excitation, is shown in Table 1. The interpretation of the current data is not conclusive. Photoproduction and e^+e^- annihilation experiments observed in fact different properties of the $\phi(1680)$ decay modes than hadroproduction experiments. In addition the resonance mass is consistently higher in photoproduction than in e^+e^- annihilation and there is no evidence of KK^* decay in photoproduction, which on the contrary is found to be dominant in e^+e^- experiments.

The different behavior of the $\phi(1680)$ observed in the two types of experiment may be explained by the presence of two resonances interfering with $n\bar{n}$ states. To understand this problem one could measure the relative branching ratios of the $\phi(1680)$ into the neutral and charged KK and KK^* pairs. Another possibility is to study the $\phi\eta$ decay mode since, according to the Zweig rule, the contribution of $s\bar{s}$ states is expected and interference with $n\bar{n}$ states should be highly suppressed. Just the mere identification of a resonance in the $\phi\eta$ system will prove the presence of a $s\bar{s}$ state. This argument can be extended to the $\phi(1850)$ and other higher mass excitations. This decay mode has not been yet observed and is one of the main reactions of interest for the proposed experiment. Preliminary analysis of data taken with CLAS [20] are promising, indicating that extraction of strangeonium resonances is feasible. However, due to the limited statistics and energy range, the current data will provide only a partial insight of the strangeonium sector. The higher energy and higher statistics of the proposed experiment would allow a much deeper investigation of these states.

3 Amplitude Analysis

The main goal of a meson spectroscopy program is to extract resonances from the measurement of their decay products and identify their quantum numbers. Resonances correspond to poles in partial waves, *i.e.* amplitudes for production of two or more resonance decay products, projected onto total angular momentum and isospin. In practice, as meson resonances are numerous, often broad and overlapping, the identification of a precise state requires the extraction of the corresponding waves from the measured distributions. This task is performed by parameterizing the cross sections in terms of partial waves which are then fitted to the experimental data using unbinned maximum

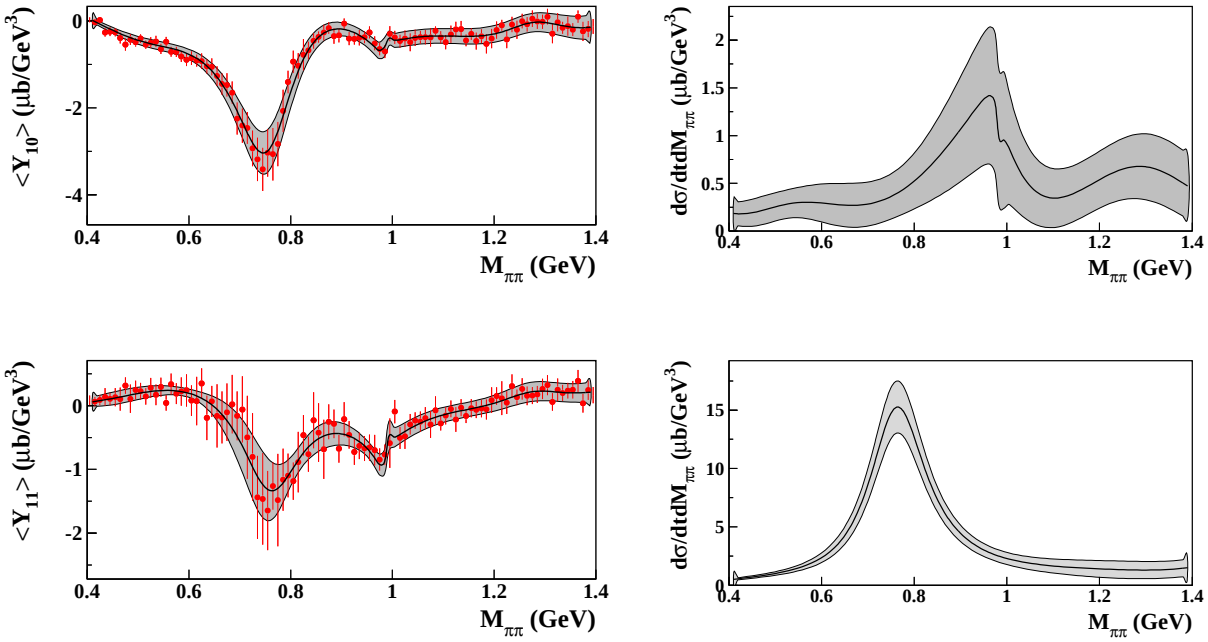

Figure 3: Left: Y_{10}, Y_{11} moments of the di-pion decay angular distribution in the photon energy range $E_\gamma = 3.2 - 3.4$GeV and momentum transfer range $-t = 0.5 - 0.6$ GeV^2 as a function of the di-pion mass. Right: differential cross section associated to the S (top) and P (bottom) waves.

likelihood fit, where the parameters are the wave intensities. Fits can be performed as a function of the invariant mass of the measured decay products and other relevant kinematic variables to derive information on the dependence of the fitted waves on those variables. This procedure is referred to as partial wave analysis or PWA.

The PWA is a crucial component for a meson spectroscopy experiment since the final results are strictly dependent on the reliability of the PWA tools and of the theoretical assumptions used in constructing the amplitudes. From the technical side, the goodness of the fit is related to the statistics and to the rank of the fit, as defined by the number of (complex) amplitudes. In the past, limitations to the number of amplitudes that could be included in a fit was coming from the computation time, since the fitting procedure can be very demanding both for the number of floating-point operations, necessary for the calculation of amplitudes, and for the memory usage. Nowadays, the advancements in computer technology and the recent introduction of Graphical Processing Units (GPUs) in scientific computing have lead to a dramatic reduction of the fitting time that will allow analysis of the large statistics data sets provided by this experiment and others in the near future with adequate number of waves. From the theoretical side, PWAs can be improved by reducing the rank of the fit via the implementation of known constraints on the amplitudes. In lepto- and photo- production, the knowledge of photon polarization simplifies the extraction of partial waves by giving information on the production mechanisms. In addition, amplitudes can be built including model-independent constraints originating from the general analytical properties of scattering amplitudes, as analyticity and unitarity. This is a challenging theoretical task which is currently being approached from several fronts and that will continue to progress as data from current and planned experiments are being collected. There is the EBAC effort at JLab, SAID at GW, the NABIS collaboration centered at Julich (and expanding onto the US) that focuses on

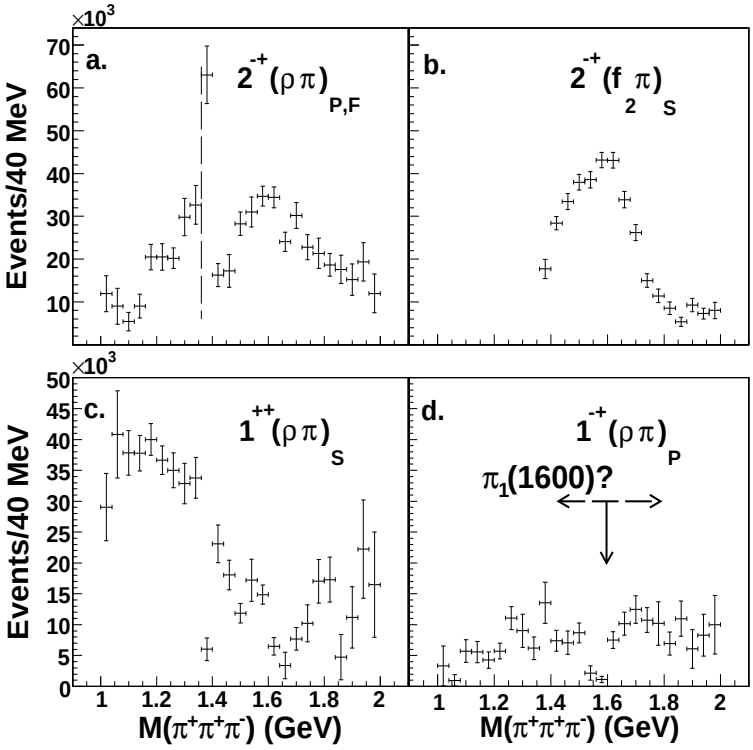

Figure 4: CLAS PWA results on 3π photoproduction [17].

Dalitz analysis of D and B meson decays, and ongoing amplitude analysis centers at BES III and GSI . These groups are actively sharing their experiences and resources through regular workshops and ongoing collaborations that include the authors of this proposal.

At Jefferson Lab, partial wave analysis aimed at the extraction of meson resonance signals have already been performed on photoproduction data collected with the CLAS detector. Recently data for two pion photoproduction were analyzed to look for a scalar meson signal [18]. Figure 3 shows the results of a partial wave analysis of the $\gamma p \to p\pi^+\pi^-$ channel. Moments of the pion relative angular distribution, shown in the left column, were extracted from the measured data distribution using an un-binned likelihood fit and then analyzed using dispersion relations to extract partial waves, shown in the right column. The final state is dominated by the contribution of the ρ-meson, whose prominent peak dominates the measured moments and final P-wave, shown in the bottom-right plot. However a narrow structure is observed at a mass close to 1 GeV in both the Y_{10} and Y_{11} moments. This structure, interpreted as evidence for the $f_0(980)$ meson, appears as a clear variation in the S-wave, shown in the top-right panel. It has to be noted that this is the first time that the $f_0(980)$ meson has been measured in a photoproduction experiment. The evidence of the $f_0(980)$ signal is a sign that photoproduction may indeed be a good tool for accessing meson resonances other than vector meson states.

Another example is given by the analysis of the 3π final states that was performed on data from the CLAS G6 run [19], looking for signal of the exotic $\pi_1(1600)$ [17]. A full partial wave analysis of about 83000 events for $\gamma p \to n\pi^+\pi^+\pi^-$ was completed. The results show clear signals for the $a_1(1270)$, $a_2(1320)$ and $\pi_2(1670)$, but show no signal for the $\pi_1(1600)$ decaying to three pions. The low statistics of this experiment, the significant background from baryon resonance production and the limited kinematics accessible with the 6 GeV beam energy prevent definitive conclusions.

Reactions
$\gamma p \to N\pi\pi\pi$
$\gamma p \to N\eta\pi$
$\gamma p \to NK\bar{K}\pi$
$\gamma p \to p\phi\pi^0$
$\gamma p \to p\phi\eta$

Table 2: List of the main reaction channels that will be studied by the proposed experiment.

These results, even if limited in physics reach because of the low beam energy and statistics, demonstrate that the PWAs with detectors like CLAS are feasible. A further confirmation comes from the recent analysis of ω photoproduction with CLAS [61] where a sophisticated PWA analysis was performed to single out signals of baryon resonances. The experience gained from the current analysis and the dedicated effort in developing and testing PWA tools for this proposal (see Section 6.2) give us confidence that reliable and accurate amplitude analyses of CLAS12 data can be performed and that the proposed meson spectroscopy program can be successfully completed.

4 Proposed Measurement

The proposed measurement aims at the study of meson spectroscopy using quasi-real photoproduction with CLAS12. As outlined in Sec. 2, an experimental program focused on search for exotics and the study of rare mesons requires measurements of a broad scope of final states in order to consolidate the possible evidence of a resonance by looking at different decay modes and explore poorly-studied reaction channels. The characteristics of the detector and the trigger conditions foreseen for the experiment - three prongs in the final state - will allow measurements of many final states simultaneously. A list of the reactions that will be discussed in detail in the rest of the proposal is given in Table 2.

These final states will be produced by the 11 GeV electron beam, scattering on a 5 cm long LH_2 target. While the hadrons will be detected in CLAS12, the electron scattered at very small angles (low Q^2) will be detected in the new Forward Tagger (FT) facility that will be built for this experiment. The combination of CLAS12 and of the new FT system presents unique properties as:

- high intensity photon beams with energies up to 10.5 GeV,
- large degree of linear polarization determined on an event-by-event basis with small systematic uncertainty,
- full determination of the initial state and final state four-momenta,
- large acceptance and good resolution for the measurement of the decay products,
- kaon identification to study strangeness production.

In the remaining part of this section we will briefly outline the advantages of low Q^2 electron scattering in meson spectroscopy.

4.1 Electroproduction at very small Q^2

Phenomenological models, like the flux-tube model, indicate that the photon may be more effective in producing exotics hybrids than, for example, the pion. The rational for this lies in the fact that the photon spin is 1 and it can fluctuate into a $q\bar{q}$ pair with spins aligned. When a $q\bar{q}$ pair with $\vec{S} = 1$ is excited into an hybrid, the production of exotic quantum numbers is expected to be favored. On the contrary, when in the initial state there is a $q\bar{q}$ pair with $\vec{S} = 0$, like for pion beams, the resulting hybrid mesons are more likely to be non-exotic. Phenomenological studies also indicate that exotic mesons can be produced with photon probes with cross sections that are comparable to ordinary mesons [62, 63]. Finally, the linear polarization of the quasi-real photons is expected to be a very powerful tool for high precision amplitude analysis, since it can provide information on the production mechanism and act as a filter on background from other processes.

The current photoproduction setup of the CLAS experiment, producing real bremsstrahlung photons tagged by a magnetic spectrometer, can not be operated at 11 GeV energies because of the limitation of the existing magnet.

Instead, we are planning to use quasi-real photons produced when electrons are scattered at very small angles (small Q^2).

Electron detection at very small angles, (Q^2 values of about 10^{-1} GeV^2 or lower) with the coincidence detection of the hadronic final states in CLAS12, is a very attractive alternative to pure photoproduction experiments [64]. This technique was used in the past to produce high energy ($\sim$ 100 GeV) photon beams at CERN (Ω [58] and COMPASS [65] Collaborations) and DESY (ZEUS [66] and H1 [67] experiments). First tests were performed with CLAS, by looking for hadronic events where the electron was undetected. Final states where the hadron four-momenta were compatible with an electron scattered at $\sim 0^\circ$ were selected. The reconstructed mass spectra of $\pi^0\pi^0$ and $\pi^0\eta$ show clear evidence of low cross section mesons expected in these channels ($f_0(980)$, $f_2(1270)$, $a_0(980)$) demonstrating the potential of this technique (see Fig. 5). Recently, the EG6 experiment used this technique to study coherent meson production on ^4He [21].

In the unpolarized electron scattering process (one-photon exchange approximation), the virtual photon polarization is:

$$\epsilon = [1 + 2\frac{(Q^2 + \nu^2)}{Q^2}\tan^2(\theta_{e'}/2)]^{-1}. \quad (1)$$

where ν is the photon energy and $\theta_{e'}$ the electron scattering angle. The longitudinal polarization is given by $\epsilon_L = \frac{Q^2}{\nu^2}\epsilon$, and the polarization density matrix can be written as [64]:

$$\begin{pmatrix} \frac{1}{2}(1+\epsilon) & 0 & -[\frac{1}{2}\epsilon_L(1+\epsilon)]^{1/2} \\ 0 & \frac{1}{2}(1-\epsilon) & 0 \\ -[\frac{1}{2}\epsilon_L(1+\epsilon)]^{1/2} & 0 & \epsilon_L \end{pmatrix}$$

At very low values of Q^2 the virtual photon beam becomes, for all practical purposes, almost a real photon beam, since

$$\epsilon_L = \frac{Q^2}{\nu^2}\epsilon = 10^{-3}\epsilon \approx 0,$$

and the matrix represents the spin density matrix of real (transverse) photons.

Via these relations, the photon polarization can be defined on an event-by-event basis, simply measuring the electron three-momentum. The polarization plane coincides with the electron scattering plane and the degree of polarization mainly depends on the energy. The associated systematic uncertainty is only affected by the electron detection resolution. These are significant advantages with respect to coherent bremsstrahlung beams, where only the average polarization can

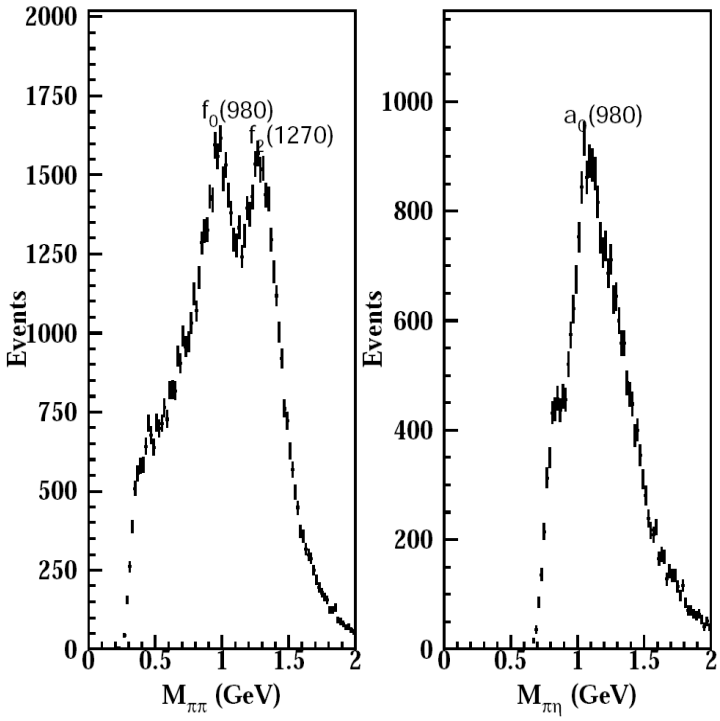

Figure 5: Invariant mass distribution for $\pi^0\pi^0$ (left) and $\pi^0\eta$ (right) for the reactions $ep \to p\pi^0\pi^0(e)$ and $ep \to p\pi^0\eta(e)$, respectively. In both cases, the protons and 4 photons from the meson decays were detected while the final state electron was unmeasured, being emitted at 0°.

be determined and its value is based on model calculations (or parallel measurement of reactions with known linear polarization asymmetries). Among other advantages of low Q^2 electroproduction is the possibility of running on thin targets and the better control on the absolute photon flux normalization. Since electrons are tagged after their target interactions, this technique allows the use of high electron currents, permitting to achieve high luminosity on thin (gas) targets not operable with photon bremsstrahlung beams. With no need for dedicated normalization equipment and procedures [69], the number of photons can be directly calculated from the measured electron beam current.

5 Experimental setup

In this section we outline the experimental setup that will be used in the proposed experiment, describing the CLAS12 configuration, the new Forward Tagger facility that will be build to detected small-angle electrons and the trigger system that is foreseen. The kinematics covered by the FT and the expected rates are discussed and results of detailed simulations are presented.

5.1 Hadron detection: the CLAS12 configuration

The goal of this experiment is to study meson spectroscopy looking for mesons with masses up to 2.5-3.0 GeV in different decay modes. To identify and measure the decay products of produced

mesons, the detector has to have:

- good efficiency for multi-particle final states since high mass meson resonances typically decay to more than three final state mesons,
- good efficiency for both neutral and charged particles,
- good particle identification, in particular good kaon/pion discrimination (up to $p \sim$3 GeV/c) to study strangeness-rich mesons,
- large kinematic coverage to study the production mechanisms exploiting information on energy and angular dependence,
- sufficient particle momentum and angle resolution to use the missing mass technique to reduce the number of particles that need to be detected to isolate exclusive final states suppressing background from other channels.

The baseline equipment of the CLAS12 detector [70] fulfills all of these requirements.

Charged particle detection and identification will be accomplished by tracking the particles in the magnetic field of the torus and solenoid magnets with the forward drift chambers and the central silicon tracker. Time-of-flight measurements in forward and central scintillation counters, together with momentum and path length measurements from the tracking and the Cherenkov counters information will allow us to separate pions, kaons and protons. Neutrals will be detected in the electromagnetic calorimeter and the FT.

The standard Hall-B cryogenic target will be used, with a 5 cm long cell located at the nominal CLAS12 center. This is the optimal target configuration foreseen for electroproduction experiments on proton.

The effect of the torus field setting has been studied for some benchmark reactions (see Sec. 6.1) showing that to increase the acceptance of multi particle final states, a half-strength-field is desirable. With this set-up, the CLAS12 resolution is good enough to apply the missing mass technique to reduce the necessary number of particles detected. Full-field running is also possible with improvement of the momentum resolution and moderate reduction of the acceptance. The latter is found to have negligible impact on the extraction of the mesonic resonance as shown by detailed studies reported in Sec. 6.2.2.

5.2 Electron detection: the Forward Tagger

The angular range of interest for electron detection, $2.5^\circ < \theta_{e'} < 4.5^\circ$, is outside of the CLAS12 acceptance region. Therefore a new detector component has to be added. The forward tagger will be made of: a *calorimeter*, to identify the electron, measure the electromagnetic shower energy and provide a fast trigger signal, a *tracker*, to measure the scattering angles ($\theta_{e'}$ and $\phi_{e'}$) with the required accuracy and a *scintillation counter* to provide e/γ separation. A dedicated trigger system will be develop to provide a fast signal to trigger the data acquisition in coincidence with signals from CLAS12. The list of the FT components and institutions responsible for the design is given in Table 3.

The calorimeter, the scintillation counter and one layer of the tracker will be placed between the High Threshold Cerenkov Counter (HTCC) and the torus support, at about 190 cm downstream of the target (nominal) position. The close proximity to the beam line (2.5° corresponds to $\sim$ 8 cm) and the limited space available (at most $\sim$ 40 cm along the beam axis), requires a compact

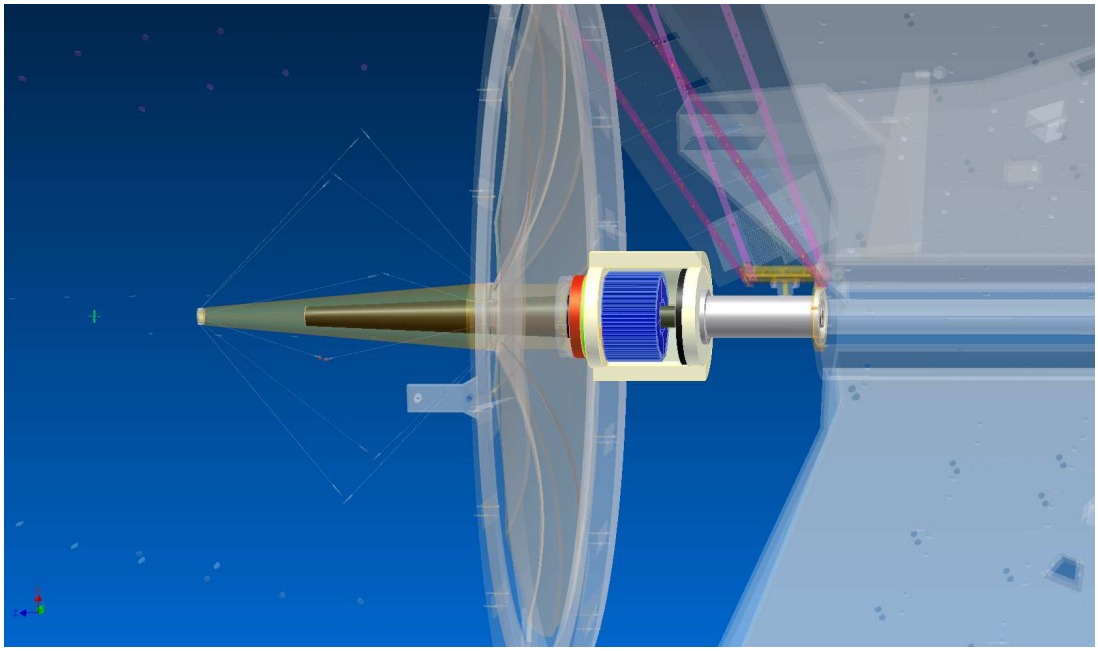

Figure 6: CAD drawing showing the integration of the FT in CLAS12. The FT is located in the free space between the HTCC and the first DC layer. The FT calorimeter shown in blue is located at about 190 cm from the interaction point, shown by the green cross, and is enclosed in a Rohacell case to provide thermal insulation. The scintillation counter (green) and first tracker layer (red) are located in front of the calorimeter. A tungsten cone in black shield the FT from Møller electrons and electromagnetic background created by the beam.

calorimeter with small radiation length and with very good radiation hardness. Figure 6 shows a CAD drawing of the FT integrated in CLAS12. The scintillation counter, placed in front of the calorimeter, will be made of plastic scintillator tiles read-out by silicon photomultipliers via wavelength shifting fibers. The first tracking plane will be located in front of the scintillation counter. The second tracking layer will be placed close to the target, extending the CLAS12 forward tracker down to 2.5 degrees. All these components will be designed to fit within a 5° cone around the beam axis to have no impact on the operation and acceptance of the CLAS12 equipment.

In the following specific requirements on the different FT components and the identified solutions are discussed in more detail.

5.2.1 The electromagnetic calorimeter

The electromagnetic calorimeter has to fulfill demanding requirements in terms of:

- high radiation hardness,
- high light yield,
- small radiation length and Moliere radius,
- fast recovery time,
- good energy and timing resolution.

As will be discussed in Sec. 6.1, the electron energy resolution is a crucial factor to determine precisely the photon energy and ensure the exclusivity of the measured reaction via missing mass technique. However, since we are interested in low energy electrons and high energy photons, the energy resolution on the latter will be significantly better than the resolution on the electron. For example, an electron energy resolution of 2% (at 1 GeV) would result in an energy resolution of $\sim 0.2\%$ for the corresponding 10 GeV photon and would allow the use the missing mass technique for the most part of the studied reactions.

The FT should also have a fast recovery time ($\tau \sim 10$ ns) to sustain high rates with small pile-up effects and provide the scattered electron interaction time with good accuracy (<1 ns) to reject background and identify the signals via coincidence with CLAS12.

Due to the expected high rate from electromagnetic background, the calorimeter should be highly segmented in the transverse direction in order to maintain each channel at a sustainable readout-rate. The size of each pixel should be comparable with the characteristic transverse size of the electromagnetic shower or Moliere radius to contain the signal induced by incident electrons to few pixels, thus minimizing pixel rates and pile-up.

Finally, the photodetectors for the light read-out will be placed in a sizable magnetic field and will have to be small in size to fit within the available space. The standard photomultiplier readout seems to be excluded while photodetectors based on semiconductors, e.g. Avalanche Photo Diode (APD) have been shown to meet the required criteria. Silicon Photo Multipliers (SiPM) can also be a valuable option but radiation hardness has to be tested.

To obtain the best performance we focused on a calorimeter based on homogeneous crystals. In fact, if the shower is longitudinally and transversely contained, the photoelectron fluctuations are the only sizable contribution to the energy and time resolution. In the recent years materials such as $PbWO_4$ have been extensively studied and shown to be very resistant to radiation damage. They are now used in large scale detectors involving up to hundreds of thousands of crystals, such as CMS-ECal [71], ALICE-PHOS [72]),PANDA-EMC [73] and CLAS-IC [74]. Against a very fast scintillation decay time (6.5 ns), a very small radiation length (0.9 cm) and one of the smaller Moliere radii (2.1 cm), the main disadvantage of the $PbWO_4$ is the poor light yield (only 0.3% of NaI(Tl)). A 5% energy resolution, at 1 GeV, has already been achieved by the existing CLAS-IC with an APD-based readout. According to the PANDA-EMC study, new crystal manufacturing procedures (PbWO-II from BTCP) and the operation at low temperature (-25° C) should ensure a better performance, with a gain of a factor of 8 in light [73]. With this design an energy resolution of $(2\%/\sqrt{E(GeV)} \oplus 1\%)$ is expected.

$PbWO_4$ is the leading option for the forward tagger calorimeter.

Other crystals as LSO/LYSO (or the very recent LaBr) share almost all the good specifications of the $PbWO_4$ with a light yield more than 100 times bigger. However, the lack of extensive studies on radiation hardness and limited experience in the manufacturing procedures prevent them to be considered as the main option. Nevertheless, tests of these new crystals and of different light sensors are planned in order to establish the ultimate performance in terms of radiation hardness, time, energy resolution and make the optimal choice.

5.2.2 The scintillation hodoscope

The primary aim of the hodoscope for the forward tagger is to discriminate between photons and electrons that produce electromagnetic shower in the calorimeter. In the design, the scintillation hodoscope will comprise of an array of plastic scintillators tiles covering individual or groupings of calorimeter elements. It should be possible to use larger tiles covering multiple calorimeter elements at the largest distance from the beam axis to reduce the level of instrumentation and

Component	*Institution*
Calorimeter	INFN-Genova, JLab, NSU
Scintillation Hodoscope	U. Edinburgh, JLab
Tracker	CEA - Saclay, NSU, JLab
Trigger	JLab, INFN-Genova

Table 3: Detector components of the FT facility and Institutions responsible for the design and construction.

readout required.

The high segmentation and restrictive geometry of the forward tagger precludes the use of light readout from the scintillator elements using standard light guides. Light readout with wavelength shifting (WLS) scintillating fibers embedded into the scintillator tile appears the most viable option and offers flexibility in routing away from the device. For effective operation the timing resolution of the hodoscope should be sufficient to select hodoscope-calorimeter coincident hits with a sufficiently low rate of accidentals. The timing resolution of the forward tagger calorimeter elements is expected to be 1 ns so the hodoscope timing should be comparable with this as not to compromise the achievable coincidence time resolution. Similar systems [75, 76, 77] have employed successful scintillator tile arrays achieving timing resolutions at the level of ns, using combination of WLS fiber coupled to optical fiber.

Measuring the energy deposits in the hodoscope elements with good energy resolution is not critical for our purpose. The vast majority of incident charged particles on the forward tagger will be highly relativistic resulting in a fixed minimum ionizing energy deposit regardless of particle type. The main requirements on the light collection are that sufficient photoelectrons are incident on the photon detection device considering the achievable light coupling in the scintillator and propagation in the fibres. Previous systems using WLS and optical fiber readout have sufficient photoelectrons per minimum ionizing interaction to achieve efficiencies for charged particle detection above 99.7% [76]. Readout sensors compatible with the high magnetic field present in the FT region are silicon photomultipliers (SiPM) that have already been used in this kind of detector. The scintillator hodoscope developed for the CLAS-IC produced 15 photoelectrons per minimum ionizing event from 1cm thick scintillator tiles with WLS fibers and 1x1-mm^2 SiPM readout [77].

5.2.3 The tracker

The role of the tracker is to provide the reconstruction of charged particles, essentially electrons, with polar angles between 2.5° and 4.5°. Charged particles with non-zero transverse momentum component are rotated by the 5 T solenoid field. The three-momentum can be reconstructed measuring the rotation in ϕ between the first tracker layer located within 50 cm downstream to the target, and the second layer placed about in front of the calorimeter. With a tracker spatial resolution of $\pm 200\mu$m a $\sim 1.7\%$ and 2.8° resolution on θ and ϕ electron angles respectively, are expected.

A Forward Vertex Tracker (FVT) is already planned as part of the standard CLAS12 equipment to improve the vertex resolution of charged particles at larger angles (5°-35°). In the current design, the FVT will be located 30 cm downstream the target, and will consist of 3 double disks of gaseous, Micromegas detectors.

Studies on a possible extension of the FVT to smaller angles are in progress. The background rate rapidly increases below 4°, up to several hundreds of kHz/mm^2. Assuming a 100 ns gate

	Range	*Resolution*
$E_{e'}$	0.5 - 4.5 GeV	$2\%/\sqrt{E_{e'}(GeV)} \oplus 1\%$
$\theta_{e'}$	2.5^o - 4.5^o	1.7 %
$\phi_{e'}$	0° - 360°	2.8°
E_γ	6.5 - 10.5 GeV	0.9 - 0.14 %
P_γ	70 - 10 %	
Q^2	0.01 - 0.3 GeV^2 ($< Q^2 >$ 0.1 GeV^2)	
W	3.6 - 4.5 GeV	

Table 4: Kinematic range and resolution of the FT.

for the Micromegas, 1 mm^2 pixels would lead to a few percent occupancy. In order to cover the proposed angular range, a doubling of the number of electronic channels is needed (6,000 to 13,000). Additional studies have to be performed on the tracking efficiency with this level of background, but the required 200 μm spatial resolution can be easily achieved with rectangular pixels.

In order to reconstruct the electron trajectory, a second layer of Micromegas will be installed in front of the calorimeter, at few centimeters from the front face of the crystals. The tracks reconstructed in both layers will be matched, allowing to determine the trajectory parameters in the presence of the solenoid field. The reconstructed trajectory will be correlated with the reconstructed hits in the scintillator hodoscope and calorimeter to reduce backgrounds and improve resolutions.

In addition to Micromegas, other options as silicon trackers or GEM foils are being considered. The optimal choice will be made based on the expected resolutions, rate limitations and space constraints.

5.3 Kinematics, rates and backgrounds

The kinematic range covered by the FT facility is shown in Tab. 4 for an incoming electron beam of 11 GeV. The energy range for electron detection was chosen to tag large energy photons and the angular range is the maximum allowed compatibly with the electromagnetic background.

The total electron scattering cross section contains contributions from one-photon exchange (Born process), from QED vacuum polarization loops, and from the emission of additional real photons (radiative corrections). The importance of the internal radiative corrections in relation to the Born process depends on the kinematics. Radiative corrections increase with decreasing Q^2 and increasing E_γ. We used the program RADGEN 1.0 [68] to calculate the contributions of internal radiative corrections to the total inclusive cross section. Including such effects, the total inclusive electron rate within the geometrical and momentum acceptance of the forward tagger will be of about 130 kHz (ΔE$_{e'}$=0.3-10.8 GeV and $\Delta\theta_{e'}$=2.5^o-4.5^o). Inelastic processes represent about 45% of the total cross section in our kinematic range. The remaining 55% is due to elastic events where at most one proton will go in the active area of CLAS12. It is, therefore, beneficial for our measurements to require a tight time coincidence between the forward tagger and the detection of multi-particle final states in the CLAS detector as discussed in Sec. 5.5.

The total rate of inelastic events in the forward tagger acceptance with E_γ=6.5-10.5 GeV, is expected to be about 6.5 kHz (while the radiative rate in the same energy range is about 40 kHz). The energy and the angular distributions of inelastic events are reported in Fig. 7. Figure 8 shows the Q^2 and the linear polarization for the same events.

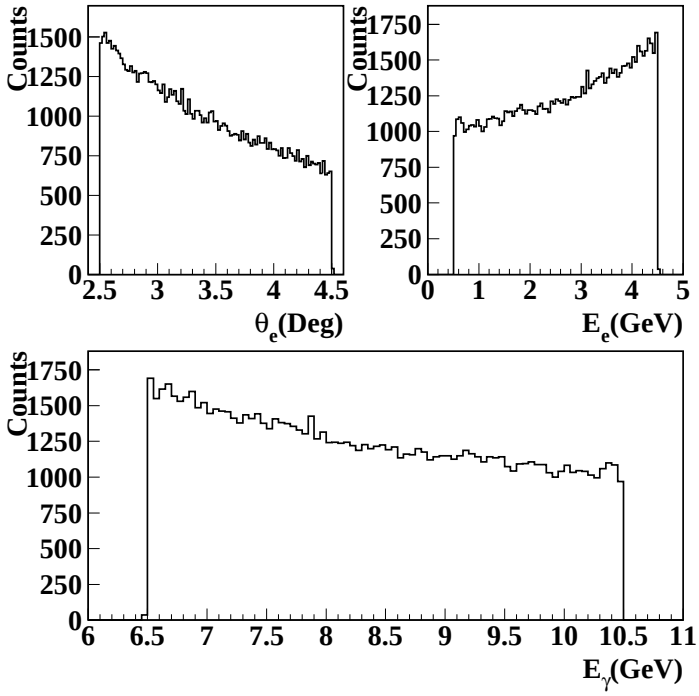

Figure 7: Angular and energy distribution of scattered electrons (top) and virtual photon energy distribution (bottom) within the geometrical and momentum acceptance of the FT.

Electromagnetic backgrounds in the FT include bremsstrahlung and Møller processes. Bremsstrahlung photon production peaks at very forward angles (about $\delta\theta \approx m_e/E_{Beam}$), therefore their contribution at angles $\theta > 0.5^o$ is very small. Møller electrons and their secondaries are the dominant contribution to the expected FT rate. The Møller cross section is almost flat within the FT acceptance with a sizable value of about $d\sigma/d\theta \sim$ 10-20 mb/rad. However, the Møller kinematics is highly constrained and, for angles above 2.5^o, the Møller electron energy is less than 0.5 GeV, i.e. outside the kinematic range of interest. These low energy electrons are bent in the 5T solenoidal field of CLAS12 and focused towards the beam line. Here they enter into a tungsten cone that shields CLAS12 and the FT from this background and from other secondaries produced along the beam line (low energy photons, X-rays, beam halo ...). These backgrounds have been studied using GEANT4 simulations. All details are reported in Sec. 5.4. The total expected electromagnetic rate is about 50 MHz, dominated by low energy ($<$ 100 MeV) secondaries that will be further suppressed by optimization of the shield. Suppression at the level of the on-line trigger is discussed in Sec. 5.5. This contribution can be almost totally rejected in the off-line analysis when a time coincidence of a few nanoseconds with the rest of CLAS12 will be required, since there are no hadrons associated with such events to reach the CLAS12 detector.

5.4 Detector Performance Studies

First simulations of the FT to understand kinematics, backgrounds and the detector response have been done with the GEANT4-based Monte Carlo code for CLAS12, GEMC [78]. The forward

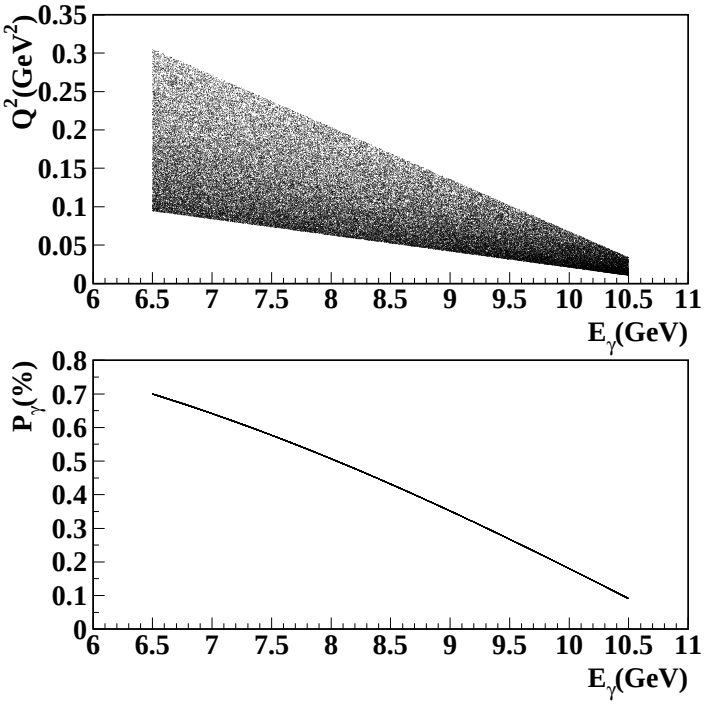

Figure 8: Q^2 and linear polarization of inelastic events within the geometrical and momentum acceptance of the FT.

tagger geometry was implemented in GEMC, assuming a FT calorimeter made of $PbWO_4$ crystals. The calorimeter, consisting of 408 crystals, was placed at a distance of 186 cm from the CLAS12 nominal center. The crystals have a rectangular shape with a section of 15×15 mm^2 and a length of 200 mm, corresponding to about 23 radiation lengths. The crystals are arranged around the beamline to cover angles from 2° to 5° to contain the electromagnetic shower produced by electrons in the angular range from 2.5 to 4.5 degrees. The crystals are placed inside a tungsten case to shield the forward part of CLAS12 from shower leakages. The scintillation hodoscope and first tracking plane are located directly in front of the calorimeter. The FT is shielded from Møller electrons produced by the interaction of the beam in the target by a tungsten cone covering polar angles up to 2.45°. The location and shape of the shield were chosen in order to minimize the radiation on the FT and on CLAS12, compatible with the most recent design of the CLAS12 beamline. The design of the shield will be finalized with further simulation studies.

The purpose of the simulations was to evaluate:

- the acceptance and resolution for the electron detection,
- the background rates on the calorimeter and the related impact on the electron reconstruction,
- the radiation dose on the calorimeter,
- the CLAS12 drift chamber occupancy to verify the compatibility of the FT with the CLAS12 operation at full luminosity.

The results of these studies are described in the next subsections.

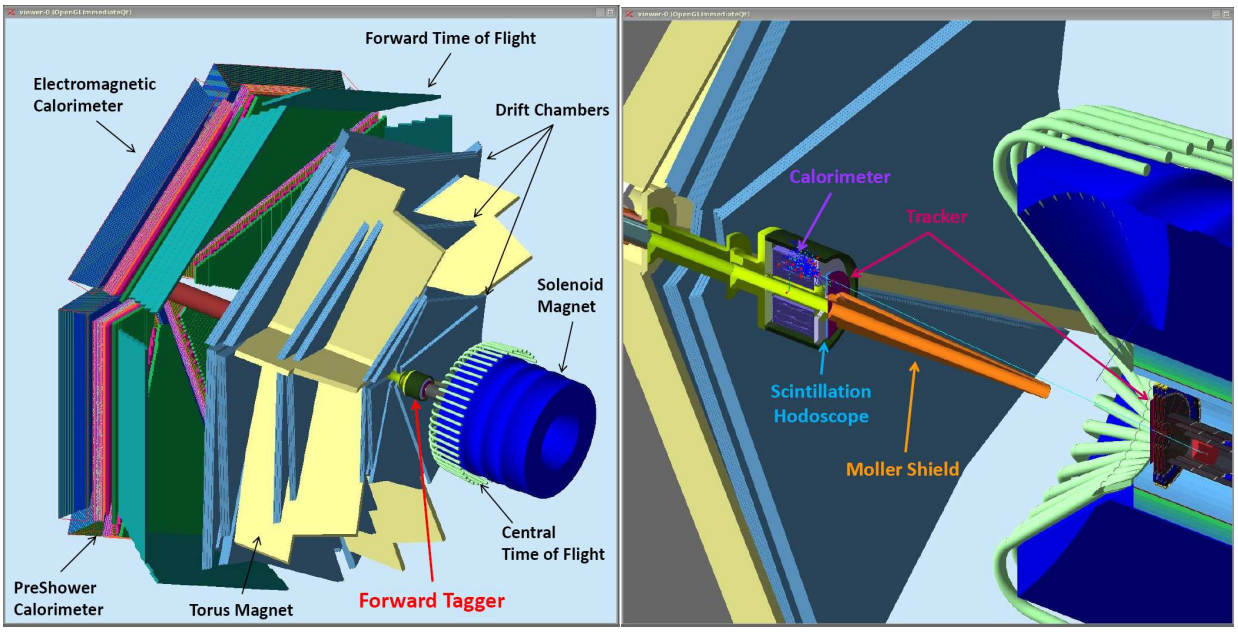

Figure 9: Left: schematic of the FT facility as implemented in the CLAS12 GEANT4 simulation, GEMC. The HTCC is not shown. Right: section of the FT with a 2 GeV, 3.5° electron interacting in the device.

5.4.1 FT acceptance and resolution

The GEMC simulations were first used to understand the electron kinematics and the forward tagger acceptance. For this purpose electrons with momentum from 0.05 to 5 GeV and polar angle from 1° to 35° were generated at the target location.

The trajectory of the electrons is affected by the 5-Tesla solenoid field, which induces a rotation of the particle around the beamline because of its non-zero transverse momentum component. This results in a significant shift of the azimuthal angle ϕ of the track, while the polar angle θ remains almost unchanged, except for very low momenta. This feature does not affect significantly the overall acceptance of the FT in the kinematics of interest The top panels of Fig. 10 show the difference between the azimuthal angle (top-left) and polar angle (top-right) of the electron tracks at the two tracking planes as a function of the momentum. The size of the ϕ rotation directly depends on the momentum and only marginally on the polar angle. By measuring this rotation it is therefore possible to infer the electron momentum as well as reconstruct the vertex angles. Assuming a spatial resolution of the tracker of 200 μm and the presence of air between the two tracking planes, the angular resolution estimated from these simulation is of ~ 2.8 degrees in ϕ and about 1.6% in θ.

Electrons entering in the FT calorimeter induce an electromagnetic shower that involves a certain number of crystals that represent a "cluster". The distribution of number of crystals with deposited energy greater than 10 MeV is shown in the top-left panel of Fig. 11. The energy deposited in single crystals is distributed between zero and several hundreds MeV, as shown by the top-right panel of the same figure. By summing up the energy "seen" by the crystals involved in a cluster, it is possible to reconstruct the electron energy: the difference between the reconstructed and generated energy as a function of the electron momentum is shown in the bottom-left panel. The overall acceptance is shown in the bottom-right panel of Fig. 11: the ratio of electrons absorbed in the FT calorimeter over the generated ones is shown as a function of the electron momentum

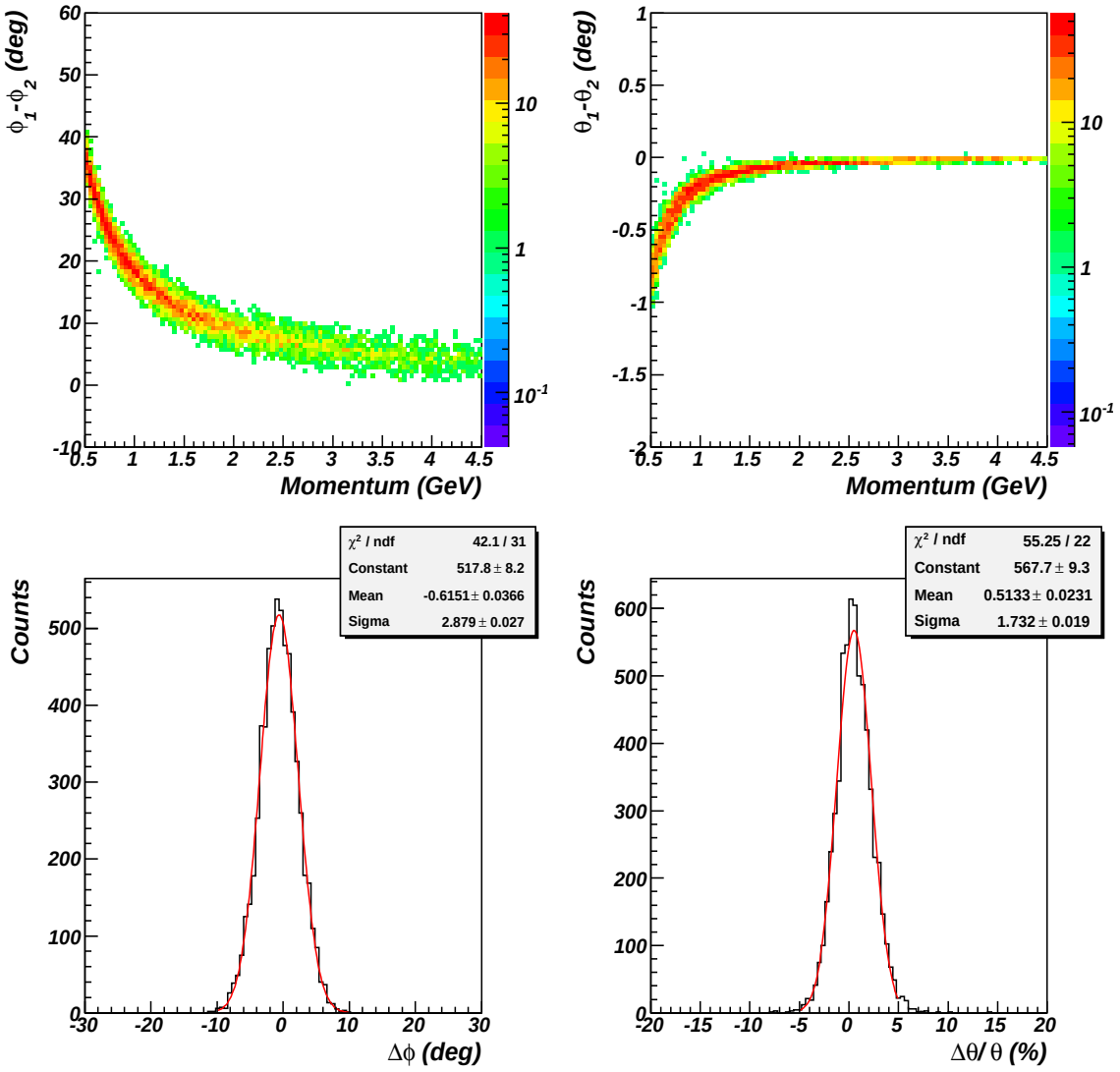

Figure 10: GEMC simulation results. Top: difference between the azimuthal and polar angles measured at two tracking planes as a function of the particle momentum . Bottom: resolution on the reconstruction of the particle vertex angles estimated from the simulation assuming 200 μm spatial resolution of the tracker and the presence of air in between the tracking planes.

and polar angle. Here an electron is considered as detected by the calorimeter if the reconstructed energy is within 10% of the generated one. The acceptance is very high and uniform throughout the region of interest for this proposal.

5.4.2 Electromagnetic background rates

The electromagnetic background produced by the interaction of the electron beam in the target at the nominal CLAS12 luminosity was also simulated[§]. Fig. 12 shows the energy deposited in the calorimeter in MeV/ns, the energy distribution of particle entering the calorimeter and the corresponding particle rates. The energy deposition per crystals is estimated to be less than 0.04 MeV/ns. Most of this dose is due to very low energy particles as shown by the right plot. The overall particle rate is of about 50 MHz with only 10% due to particles with energy above 100 MeV. In the energy range to be tagged (0.5-4.5 GeV) the overall particle rate is further reduced to about 200 KHz, equally shared between photons and hadrons. This is relevant for the trigger rates evaluation described in Sec. 5.5.

The background impact on the reconstruction of "good" electrons has been studied analyzing in detail the time structure of these events. The relevant background is the one that overlaps in time with the electron signal. The time window that has to be considered is set by the scintillating crystal properties and, in particular, by the $PbWO_4$ decay time, which is of about $\tau \sim 6.5$ ns. The rates and energy deposition were therefore evaluated in a time window of 3τ, i.e. $\sim$20 ns. The results are shown in Fig. 13. The left plot show the number of hits in the calorimeter in the chosen time window while the right plot shows the energy deposition in MeV. Considering the characteristic of the expected signal for "good" electrons (minimum number of crystals of the order of 4 and a minimum energy deposition per crystal of 100 MeV), this background is negligible.

5.4.3 Radiation dose

The results of the electromagnetic background study were used to estimate the radiation dose deposited in the FT crystals. Radiation dose can be a critical issue for the operation of scintillating crystals in high background environment since radiation induces a deterioration of the light transmission properties of the material due to the creation of color center in the lattice. This defects are not permanent and can be removed with an annealing procedure, that however may be unpractical during data taking.

The energy deposition in each crystal was evaluated from the background simulation and used to calculate the dose per unit of time. The overall radiation dose at 10^{35} $cm^{-2}s-1$ was estimated to be less than 1 rad/h when averaged over the entire calorimeter with a distribution on the calorimeter crystals as shown by Fig. 14. The maximum dose per crystal is of about 5 rad/h, which would result in an maximum integrated dose per crystal of about 3600 rad in 30 days of beam time. This is similar to what has been estimated for the existing CLAS-IC [74], where no significant worsening of the detector performance was observed.

[§]For this purpose, in each event, about 115000, 11 GeV, electrons were generated originating 10 cm upstream the target. The electrons were distributed randomly with the 2 ns radio-frequency structure of the CEBAF beam in a 250 ns window, which corresponds to the data acquisition window that will be used for the CLAS12 Drift Chambers. This number of electrons corresponds to the number of beam electrons that would pass through the target in the chosen time window at the nominal CLAS12 luminosity of 10^{35} cm $^{-2}s^{-1}$.

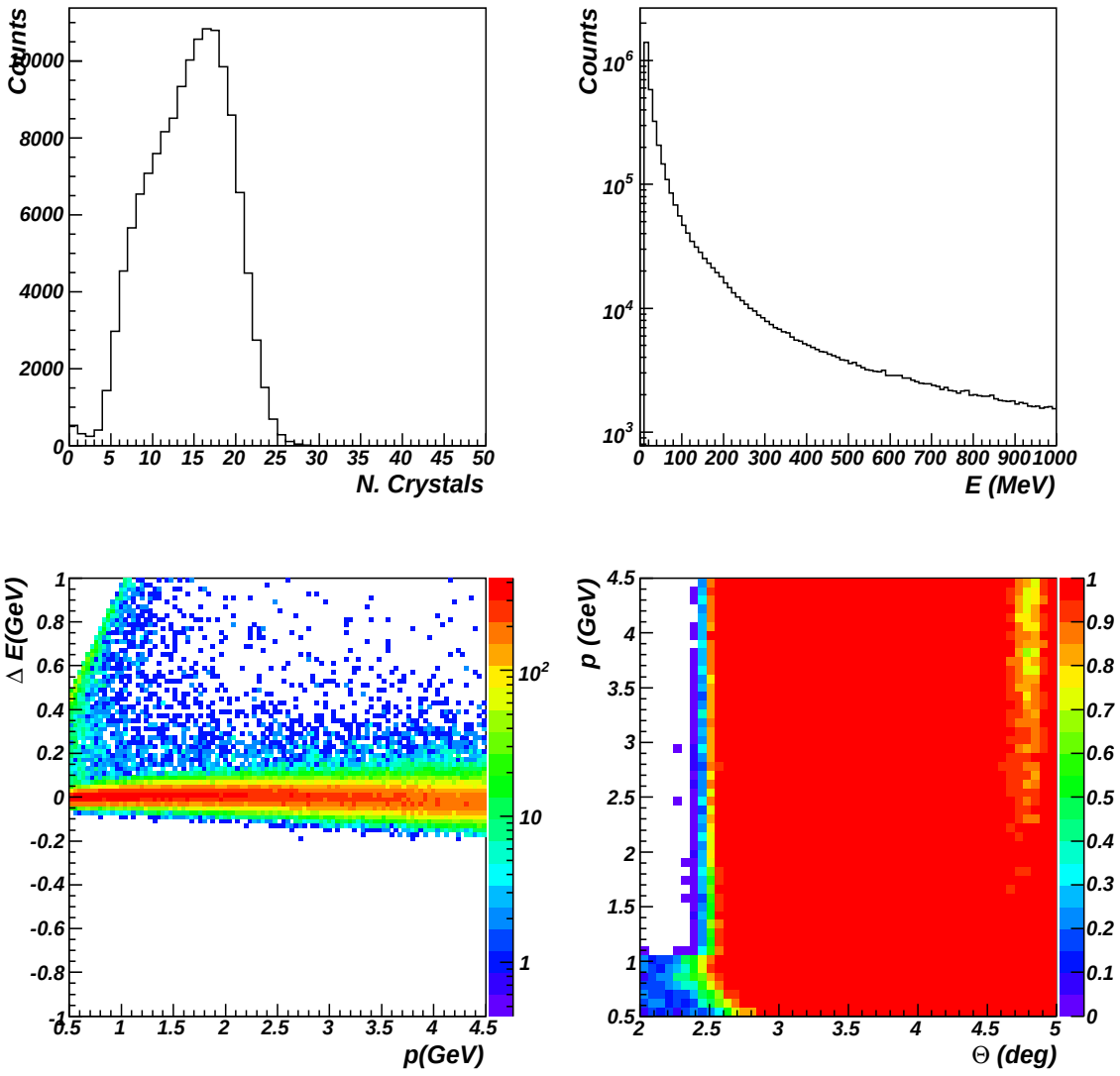

Figure 11: GEMC simulation results. Top-left: Number of crystals with deposited energy greater than 10 MeV involved in the cluster generated by an incoming electron with energy of 0.5-4.5 GeV. Top-right: energy deposited in a single crystal. Bottom-left: difference between the reconstructed and generated electron energy as a function of the electron momentum. Bottom-right: ratio between detected over generated electrons in the kinematic of interest. All plots are based on simulations of electrons generated uniformly in the momentum range 0.05-5 GeV and polar angle range 1°-35°.

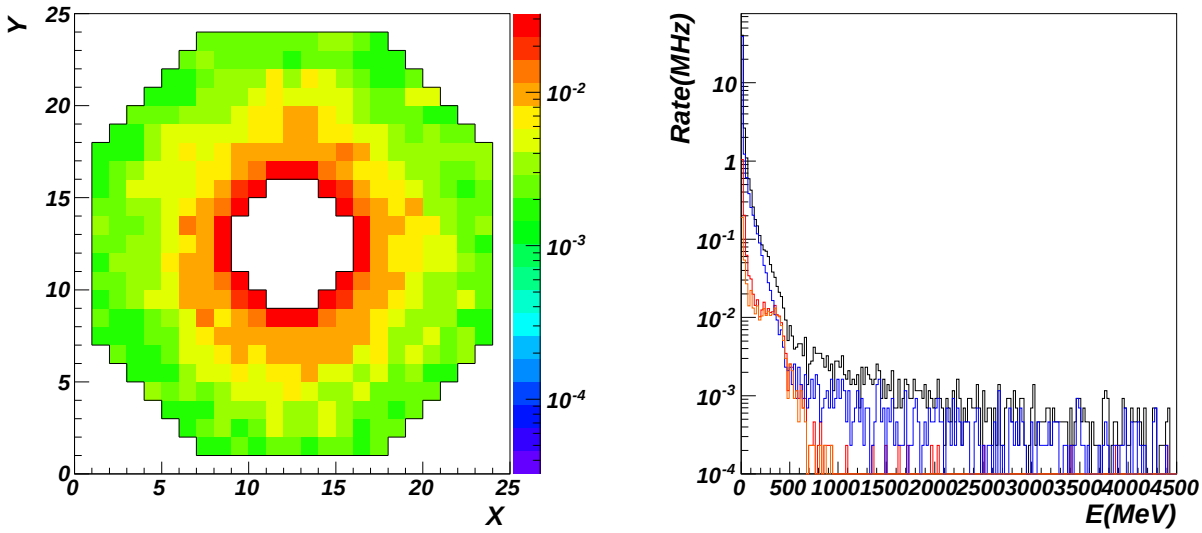

Figure 12: Simulation of the electromagnetic background with GEMC. Left: energy deposited in the calorimeter in MeV/ns. Right energy distribution of particles hitting the calorimeter front face (black-total, red-electrons, blue-photons).

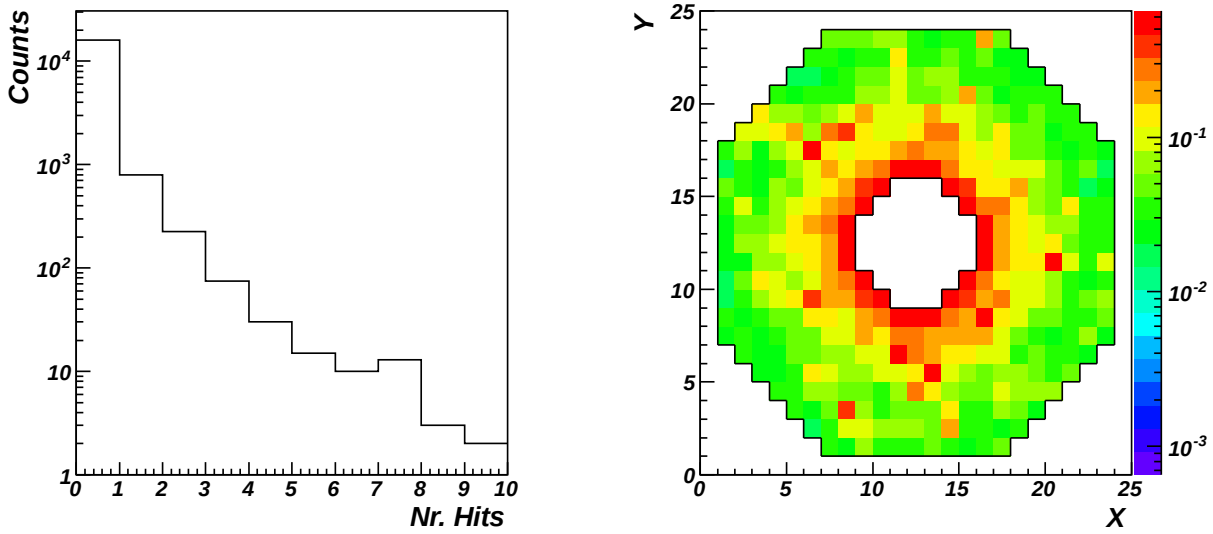

Figure 13: Left: number of crystals in the FT calorimeter with signal above threshold in a 20 ns time window due to the electromagnetic background at a luminosity of 10^{35} cm $^{-2}$s^{-1}. Right: distribution of the energy deposited in the calorimeter in a 20 ns window; the z-scale is in MeV.

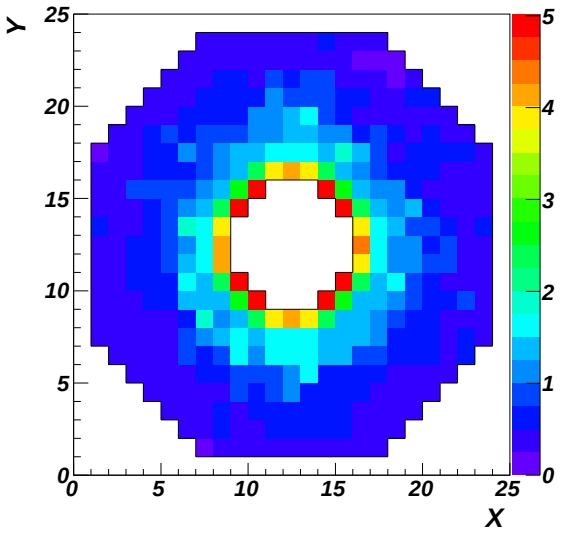

Figure 14: Radiation dose on the FT calorimeter crystals in rad/hour at 10^{35} cm^{-2}s-1 luminosity. The maximum values of about 5 rad/h are observed for the innermost crystals, i.e. at the smaller angles.

5.4.4 CLAS12 Drift Chamber occupancies

One of the limiting factors for the operation of CLAS12 at high luminosity is the Drift Chambers (DC) occupancy. In the CLAS12 configuration without the Forward Tagger, the DC occupancy is expected to be of the order of 1-2%, as estimated from GEANT3 simulations [79]. This value was obtained by inserting a Møller shield made of aluminum and tungsten and covering angles up to about 4 degrees. This shield is not compatible with the operation of the Forward Tagger. Therefore, we performed a dedicated study to evaluate the DC occupancy with the FT, optimizing the geometries of the FT mechanical structure and of the Møller shield. The interaction of the beam with the target was simulated generating electrons upstream to the interaction region, within a 250 ns window corresponding to the integration time of the DC readout. The secondaries that are produced were tracked throughout the CLAS12 volume and the rates of the different detector components were computed. The resulting DC occupancy for the nominal luminosity of 10^{35} cm^{-2}s^{-1} is shown in Fig. 15. The measured rates are higher in the first two superlayers of Region 1, since the background is dominated by low energy particles coming from the target region and the Møller shield. These secondaries are easily stopped by a small amounts of material, and therefore rates drop in Region 2 and 3. DC occupancy is always below 2.5% and therefore within acceptable values. It is worth to mention that, implementing the geometry of the standard CLAS12 shield in GEMC, we are able to reproduce the same results obtained with GEANT3 simulations.

5.5 Trigger

The hardware trigger for the proposed experiment should be designed to allow quasi-real photoproduction and electroproduction measurements to run in parallel. In electroproduction runs, both the scattered electron and the hadronic final state are detected in the CLAS12 detector. For meson spectroscopy, scattered electrons will be detected in the FT and hadronic final states in CLAS12.

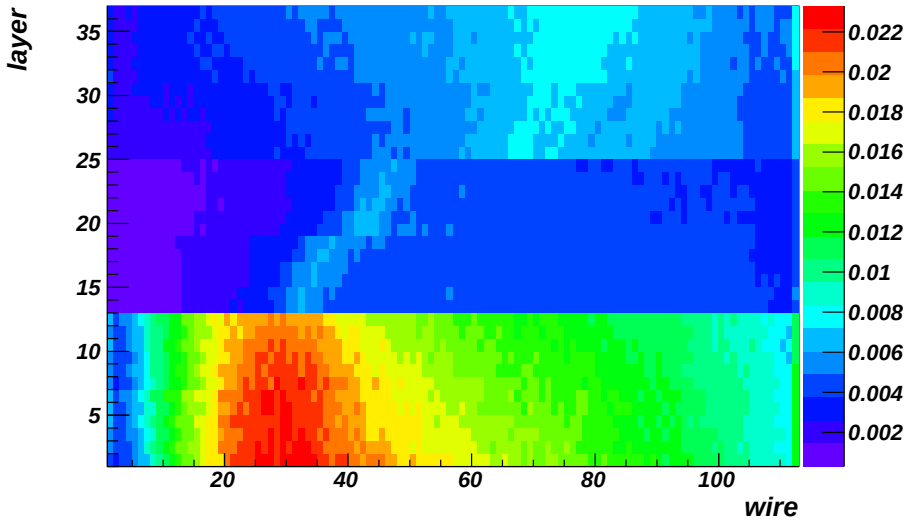

Figure 15: Drift Chamber occupancies at 10^{35} cm^{-2}s-1 luminosity as a function of wire and layer number. The maximum occupancy value of about 2% is found in Region 1 while occupancies in Region 2 and 3 are less than 1%. These values are comparable to what estimated in the standard CLAS12 configuration without the FT and are within acceptable values.

To be able to collect data for both experiments at the same time, the CLAS12 DAQ system should be able to trigger and record both types of events. For electroproduction experiments, a single electron trigger will be employed while, for meson spectroscopy, the DAQ will be triggered by the coincidence of a multi-particle final state in CLAS12 and a signal in the FT within the relevant energy range. The main requirements for the trigger is to be $\sim 100\%$ efficient for the final states of interest and not to exceed the DAQ readout limit by keeping the background rate as low as possible.

5.5.1 CLAS12 trigger system

CLAS12 will have a free running DAQ system. ADCs and TDCs will collect data in pipeline mode. Readout of data will be done after the trigger decision is made with an expected event rate of $\geq$ 10 kHz [70]. The new CLAS12-DAQ front-end electronics, in particular the use of flash ADCs (fADCs) for calorimeters, time-of-flight and Cherenkov counters, and the availability of fast field-programmable gate arrays (FPGA) will allow to employ a multi layer trigger system [70]. The trigger will have a fast cluster finding algorithm (already implemented in the CLAS-IC read-out) with energy and position reconstruction in EC, and hit position and signal strength reconstruction in Cherenkov and time-of-flight counters. These requirements will be implemented at the Level-1 trigger, using features of fADCs and crate trigger processing (CTP) boards. At Level-2, track segment finding, track linking, and track position information in drift chambers will be used. Summing all contributions, the overall time for Level-1 and Level-2 trigger decision making is < 10 μs. At the next step, before recording the event, the Level-3 software trigger will be employed: combining information from detectors and tracking will make the final decision on the event.

At luminosities and energies foreseen for CLAS12 standard electroproduction experiments, such a complex trigger is important even for single electron trigger runs. Present experience with CLAS

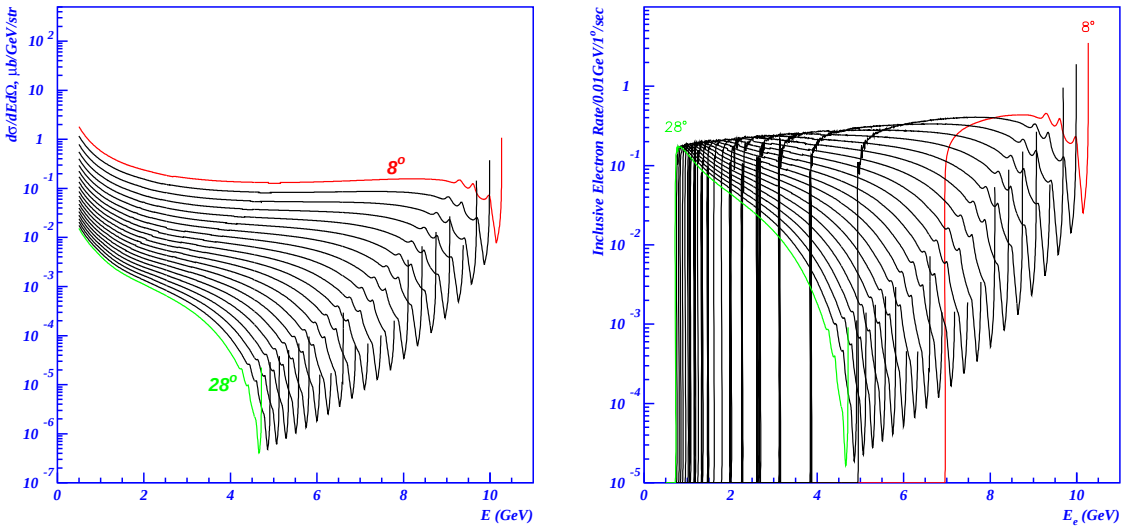

Figure 16: Cross sections (left) and rates at 10^{35} cm^{-2} sec^{-1} (right) for inclusive electron scattering, $ep \rightarrow e'X$, at 11.5 GeV as a function of scattered electron energy, for scattered angles from 8° to 28°. Calculations done using the code of Ref. [80].

showed that a trigger system that uses sector-based coincidence of signals from calorimeters (with a cut on the total energy sum) and signals from Cherenkov counters (over a certain threshold), while being very efficient, has a very poor electron-selectivity. For example, at $E_{beam} \sim 6$ GeV and L$\sim 2 \times 10^{34}$ cm^{-2} sec^{-1}, only 7% of triggered events have an electron. Moreover, a simple sector-based Level-2 trigger involving the tracking is also inefficient for rejecting the background (non-electron) events since there is almost always a track found at the sector level. From the analysis of the remaining 97% of non-electron events, it turned out that most of events were produced via forward photoproduction [21] where a fake trigger was caused by accidental coincidences between the Cherenkov counter and the electromagnetic calorimeter. With higher beam energies (11 GeV) and higher luminosities (10^{35} cm^{-2} s^{-1}), the expected purity of the trigger based on a simple, sector based trigger system will become worse.

To have a realistic estimate of requirements for trigger selectivity and to calculate the expected trigger rates, we studied the CLAS data collected in electron and real photon experiments with production of multi-particle final states. In the next two sections, we discuss the expected trigger rates for standard CLAS12 electroproduction and quasi-real photoproduction runs.

5.5.2 Electroproduction trigger rate

Inclusive electron rates were calculated using parametrization of electron scattering cross section with radiative effects from Ref. [80]. In Figure 16 left-panel, the radiative cross section for $ep \rightarrow e'X$ as a function of scattered electron energy for several values of scattered electron angle (from 8° to 28°) is shown. In the calculation the beam energy was assumed to be 11.0 GeV. The corresponding rates at L$\sim 10^{35}$ cm^{-2} s^{-1} within the CLAS12 geometrical acceptance, are shown in right plot of Fig. 16. The electron rate integrated over all angles and over the energy range from the minimum threshold energy to the end point as a function of the minimum energy is shown by the red curve in Fig. 17. Assuming a minimum momentum cut of ~ 0.5 GeV/c, the total electron rate will be of the order of 1.5 kHz. The main source of background physics triggers is high energy pion production. Pion rates were estimated using pion yields measured in the reaction $ep \rightarrow \pi^- X$ with CLAS [81], and assuming the π^+ yield to be two times higher than the π^- yield. The charged pion rate in

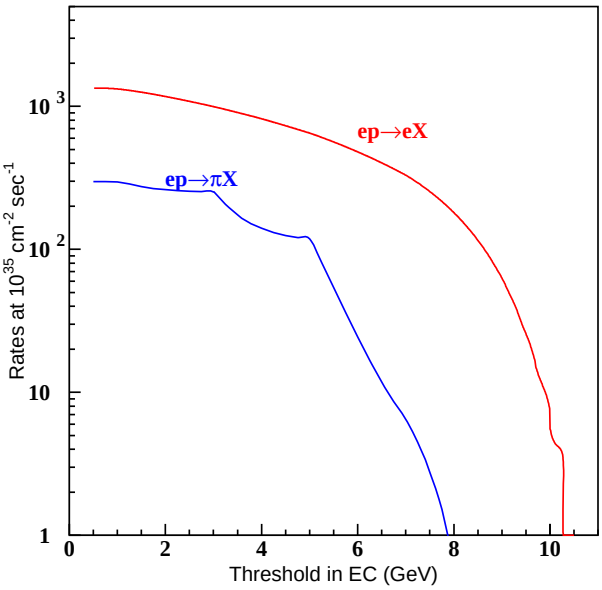

Figure 17: Trigger rates integrated over production angles as a function of the minimum energy (trigger threshold) for inclusive electron and $\pi^{+/-}$ production at luminosity of 10^{35} cm^{-2} sec^{-1}. π^- yields from Ref. [81] were used to estimate pion rates, assuming the π^+ yield is twice the π^- yield. In the trigger, cuts on the number of photoelectrons in the HTCC and on deposed energy in the EC are used.

CLAS12 was then estimated in a similar way used for electrons, using the simulated performance of the high threshold Cherenkov counter (HTCC) and electromagnetic calorimeters (EC), together with the CLAS12 geometrical acceptances. In Fig. 17 the pions trigger rate is shown with a blue curve. With a low EC threshold ($\sim$ 0.5 GeV), the pion rate is of the order of 0.3 kHz, resulting in a total trigger rate of *electron-like* particles of less than 2 kHz. We expect the CLAS12 multi-layer trigger system will be 100% efficient for *electron-like* triggers and will be able to reject the other unphysical triggers (accidentals) at the 50% level. With this assumption, we expect to have $\sim$ 4 kHz trigger rate for electroproduction events.

5.5.3 Quasi-real photoproduction trigger rate

The reactions of interest for meson spectroscopy have three or more particles in the final state. Most of the rate comes from reactions with multiple pion photoproduction. As shown in Fig. 18, the cross section of processes with three or more pions levels-out around 100μb for photon energies $>$ 3.5 GeV. With a luminosity of 10^{35}cm^{-2}s^{-1}, the inclusive electron scattering rate on the FT, in the energy range of interest (E$_{e'}$=0.5-4.5 GeV) is R$_{good}$=6.7 kHz [¶]. This is the hadronic rate useful to study meson spectroscopy. From simulations we estimated the CLAS12 geometrical acceptance

[¶]It should be noted that the equivalent real-photon flux for a typical photoproduction experiment (bremsstrahlung beam on a L$_T$=30 cm long liquid hydrogen target) that would give the same hadronic rate is:

$$\Phi_\gamma = \frac{R_{Hadronic}}{L_T \times \rho_{LH2} \times N_{Av} \times \sigma_{Total}(E_\gamma \sim 10GeV)} = \frac{6.7\ kHz}{1.3 \times 10^{10}} = 5 \times 10^7 \gamma/s \quad (2)$$

where ρ_{LH2}=0.07 g/cm^3, N_{Av}=$6 \cdot 10^{23}$ and $\sigma_{Total}(E_\gamma \sim 10GeV) \sim 100\mu$b. This value is similar to what the GLUEX experiment is expecting to run with [37].

for the dominant three particle final state is $\epsilon_{3prongs}(E_{e'} = 0.5 - 4.5GeV) \sim 20\%$ and therefore the expected trigger rate from multi-prong events (three or more particles) in CLAS12 will be: $R_{good} \times \epsilon_{3prongs} \sim 1.3$ kHz.

On top of this, we should consider accidentals between hadronic events in CLAS12 and the total rate in the FT. The latter is given by two main contributions: the elastic radiative tail and the electromagnetic background. Both of them give no multi-particle events in CLAS12. The elastic radiative rate within the acceptance of the FT was estimated to be of R_{FT-rad} ∼40 kHz. As discussed in Sec. 5.4.2, the contribution of the electromagnetic background associated to the beam (Møller electrons and secondaries) is much higher than the total hadronic rate mentioned above. The overall electromagnetic background rate is of the order of 50 MHz but, assuming a threshold on the total energy deposed in the FT calorimeter of 500 MeV and limiting the maximum energy to 4.5 GeV we calculated R_{FT-em}=200 kHz (see Sec. 5.4.2 for details). Since the optimization of the tungsten shield geometry is still in progress we are confident that R_{FT-em} can be further reduced. The suppression of the background outside the energy range of interest, requires the implementation of a trigger system, for both CLAS12 and the FT, capable of reconstructing clusters in the FT with thresholds on the minimum and maximum energy that will be developed for the experiment. To estimate the random coincidences between the FT and the CLAS12 we should consider the total hadron rate due to electroproduction. This is dominated by electron scattering below 2.5°, outside the FT coverage. From Ref. [82], the total electroproduction rate is equivalent to the photoproduction rate given by a bremsstrahlung beam at a luminosity approximately equal to 1/50 of the electron luminosity (multiplied by a factor that accounts for energy range). In our case this leads to

$$R_{CLAS12} \sim \sigma_{Total}(E_\gamma \sim 10GeV) \times 3.6 \cdot 10^{33} cm^{-2} s^{-1} \times \epsilon_{3prongs}(E_{e'} = 0.5 - 10.0GeV) \sim 36kHz \quad (3)$$

where $\epsilon_{3prongs}(E_{e'} = 0.5 - 10.0GeV)$ was estimated to be of the order of 10% when averaged over the whole energy range. Considering the total rate in the forward tagger of ∼ 270 kHz, accidentals between CLAS12 and forward tagger in a coincidence window of 50 ns are expected to be in the order of R_{RND} ∼1.0 kHz, leading to a total rate (R_{good}+R_{RND}) of coincidences between FT and CLAS12 of ∼ 2.8 kHz. Assuming, as in case of electron trigger, a CLAS12 trigger system selectivity for accidental triggers of 50%, the expected trigger rate for multi-prong events in CLAS12 from photoproduction events will be of the order of 5.6 kHz. This is a conservative estimate that can be refined by reducing rates in FT and CLAS12 and the time coincidence window between the two.

In summary, with a new, multi-level trigger system of CLAS12 and on the FT, electroproduction and quasi-real photoproduction experiments can be run together. The total trigger rate, with 50% purity of accidentals in both electron and multi-prong triggers, will be <10 kHz, within limits of the CLAS12 DAQ.

6 Data Analysis

The extraction of meson resonance signal relies on sophisticated amplitude analyses that require a good kinematic coverage, good understanding of the detector acceptance and a full analysis chain to reconstruct and fit partial waves from the measured distributions. In this Section we will discuss in more details some of the reaction channels that we aim at investigating, reporting results obtained from Monte Carlo Simulations for the detection of these channels and results of the partial wave analysis performed on benchmark channels.

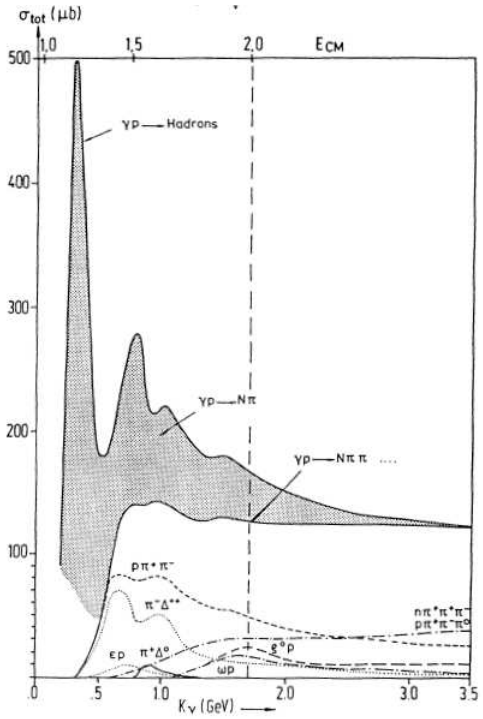

Figure 18: Total photoproduction cross section on proton as a function of photon energy, broken down into major final states which contribute.

6.1 Benchmark channels

The simulations were based on the CLAS12 Fast Monte Carlo (FASTMC) [83], which uses parametrization of the detector acceptance and resolution for different particle types. The parametrization of angular resolutions were updated to agree with the most recent Monte Carlo tracking results [70, 84] and are shown in Fig. 19.

The acceptance for the tagger was assumed to be 100% in the range $0.5 < E_{e'} < 4.5$ GeV and $2.5^\circ < \theta_{e'} < 4.5^\circ$. The angular resolution was determined from GEMC simulation studies, detailed in Sec. 5.4, assuming a spatial resolution for the tracking detector of 200 μm. The resulting angular resolutions used were, $\sigma_\theta = (0.017 \cdot \theta)$ and $\sigma_\phi = 2.8^\circ$ as quoted in Sec 5.2.3. The energy resolution of the FT was parametrized for three different assumptions on the calorimeter structure:

1. the existing CLAS-IC $PbWO_4$ calorimeter [74]
   - $\sigma_P = \sqrt{0.02^2 + 0.03^2 P + 0.024^2 P^2}$ GeV,
2. the proposed PANDA-EMC $PbWO_4$ calorimeter [73]
   - $\sigma_P = \sqrt{0.02^2 P + 0.01 P^2}$ GeV,
3. a poorer resolution sampling calorimeter or equivalent
   - $\sigma_P = 0.2\sqrt{P}$ GeV.

Different reactions were studied using reasonable assumptions on productions mechanisms. Events were generated via the Monte Carlo technique, projected onto the detector to determine acceptances and the 4-vectors smeared according to the above parameterizations.

In the following section we described the results obtained for four specific reactions:

- $\gamma p \to n\pi^+\pi^+\pi^-$,

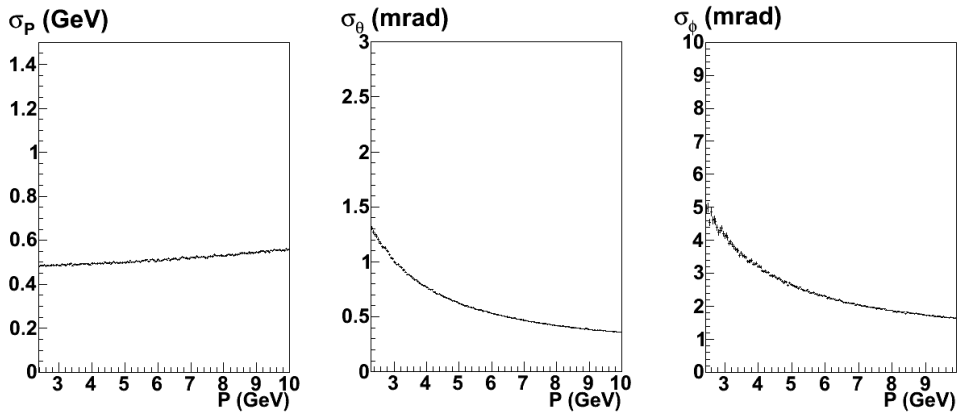

Figure 19: FASTMC resolutions for e^- at $\theta = 15°$. The curves are based on GEANT4 simulation of the CLAS12 tracking system and reconstruction by the SOCRAT package [84, 70].

- $\gamma p \to n\eta\pi^+$,
- $\gamma p \to p\eta\phi$,
- $\gamma p \ \to pK^+K^-\pi^0$.

6.1.1 The reaction $\gamma p \to n\pi^+\pi^+\pi^-$

As discussed in Section 2.1, the 3π decay mode is one of the channels where evidence for the exotic $\pi_1(1600)$ was reported. The controversy raised from the contradictory findings of different experiments makes further investigation of this final state highly desirable.

The $\gamma p \to n\pi^+\pi^+\pi^-$ reaction can be easily accessed in the CLAS12 experimental setup by detecting the three charged pions in the forward part of the CLAS12 detector. The exclusivity of the reaction can be ensured by using the FT to determine the energy of the initial state photon and then applying the missing mass technique to select events with a missing neutron. To show that amplitude analysis is possible with CLAS12, a detailed Monte Carlo simulation and PWA (Sec. 6.2.2) are performed for this channel.

Initially, events were generated with a flat 3π invariant mass and exponential t channel distribution, $\frac{d\sigma}{dt} \propto e^{-5|t|}$. The response of the CLAS12 and FT system to this channel was then analyzed after reconstruction with FASTMC. For this reaction, important kinematic dependencies of acceptance are the invariant mass of the 3π system, corresponding to the resonance mass, the momentum transfer t and the angles of the isobar (e.g. ρ) in the meson resonance decay. These are the variables that the production mechanism may depend from. The angles are commonly defined in the meson rest frame with the z-axis along the negative photon momentum and the y-axis defined as $\underline{n} \times \underline{z}$, where $\underline{n}$ is the neutron direction. These are known as the Godfried-Jackson angles θ_{GJ}, ϕ_{GJ}. The acceptances for these 4 quantities are shown in Fig. 20 for the CLAS12 half field setting and Fig. 21 for the full field setting. Clearly the overall acceptance depends strongly on $M_{3\pi}$ and the three other variables are shown for fixed $M_{3\pi} = 1.4$, 1.7 and 2.0 (GeV/c^2). Although the overall magnitude changes for the 3 masses, the shape of the other acceptances is similar for each. For the full field the acceptance is significantly poorer at low $M_{3\pi}$, approximately a factor 5 at $M_{3\pi} = 1.4$ and 2 at $M_{3\pi} = 1.7$. Nevertheless, the angular coverage is reasonable for θ_{GJ} and almost flat for ϕ_{GJ}, which is qualitatively good for a PWA, as is tested in more detail later.

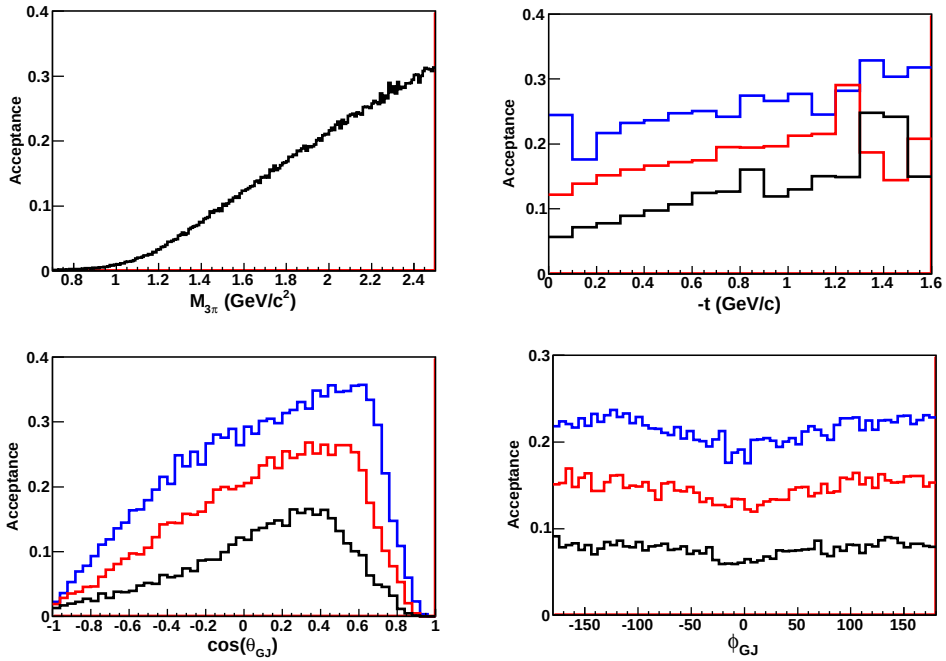

Figure 20: Acceptances for the $\pi^+\pi^+\pi^-n$ final state and half CLAS12 field setting. Top left the 3π invariant mass $M_{3\pi}$, right the momentum transfer t, bottom left, $\cos\theta_{GJ}$ and right, ϕ_{GJ}. For the latter 3 plots the black, red and blue lines correspond to $M_{3\pi}$ = 1.4, 1.7 and 2.0 (GeV/c^2) respectively.

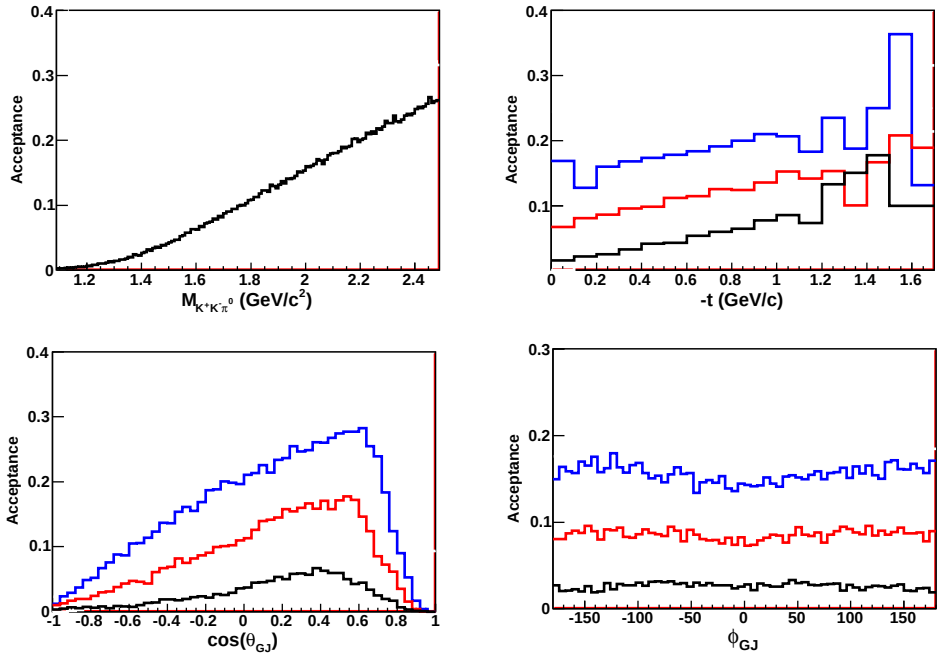

Figure 21: Acceptances for the $\pi^+\pi^+\pi^-n$ final state and full CLAS12 field setting. Top left the 3π invariant mass $M_{3\pi}$, right the momentum transfer t, bottom left, $\cos\theta_{GJ}$ and right, ϕ_{GJ}. For the latter 3 plots the black, red and blue lines correspond to $M_{3\pi}$ = 1.4, 1.7 and 2.0 (GeV/c^2) respectively.

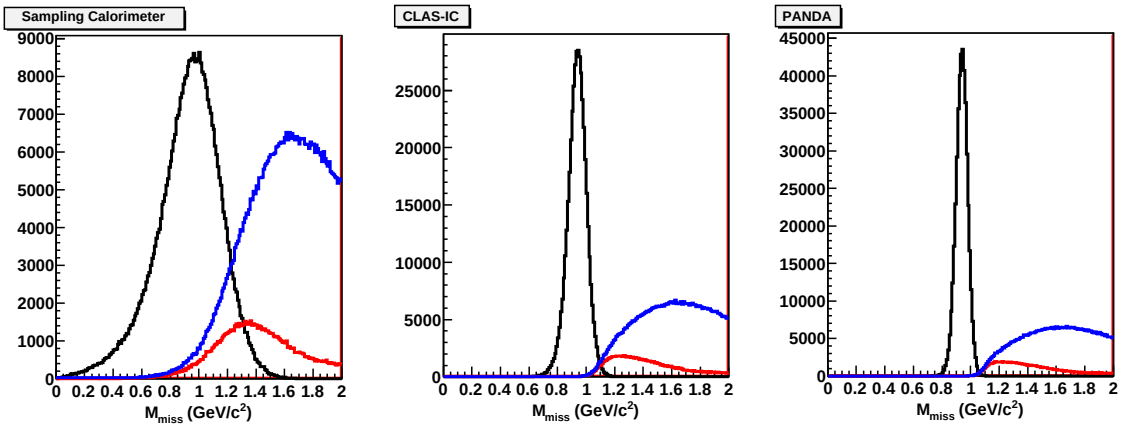

Figure 22: Missing mass of the detected 3π system for generated 3π events in black, generated 4π events with 3 charged π detected, in blue and in red the same but with an additional cut on zero π^0 decay photons detected. The left plot is for the sampling calorimeter model, middle, the CLAS-IC and right the expected PANDA calorimeter energy resolution.

Next, the exclusivity of the final state selection was tested by simulating the main possible background channel $\gamma p \to n\pi^+\pi^+\pi^-\pi^0$, which just required an additional π^0 in the generator. In this case it is possible for the CLAS12 detector to miss both of the π^0 decay photons, so only the 3 charged pions are reconstructed and this final state must be rejected by kinematics. Figure 22, shows the missing mass spectra of the 3 pions for the different models of the FT energy resolution described earlier. The plots only contain events with $M_{3\pi} < 2.5$ (GeV/c^2) since the background is lower above this mass. The 3π and 4π reactions were assumed to have the same cross sections for this test. For the 4π events two cases are shown, with and without analyzing the π^0 decay photons, to show the potential suppression from kinematics alone. It is clear from the plots that the two $PbWO_4$ calorimeters offer substantial improvement in final state selection compared to a sampling calorimeter. The PANDA calorimeter resolution gives near perfect rejection with the 4π background amounting to just 0.03% within 2σ of the neutron peak, while the CLAS-IC gives 0.7%. The sampling calorimeter by comparison contains almost 30% 4π events in the 2σ range. This analysis strongly supports the use of a homogeneous calorimeter with scintillating crystals comparable or superior to $PbWO_4$ for the FT and that such a detector would allow identification of almost background free 3π final states.

6.1.2 The reaction $\gamma p \to n\eta\pi^+$

All experimental evidences for the $\pi_1(1400)$ were found in the $\eta\pi$ final state. The good acceptance of CLAS12 for neutral particles and the extension at low angles provided by the FT calorimeter results in a sizable detection acceptance for the neutral-rich final state of the $\gamma p \to n\eta\pi^+$ reaction. Data from CLAS at 6 GeV (G12 run [20]) are currently being analyzed, exploring the possibility of $\eta\pi$ meson production off of a recoiling Δ^{++}. This channel has the advantage that the naturality of the exchanged particle, a pion, is automatically selected and the background associated to baryon resonances is reduced. An order of magnitude more data, as expected from this proposal, would provide enough statistics to explore the resonant nature of the $\eta\pi^-$ system and to search for the $\pi_1(1400)$ exotic meson.

To study the CLAS12 acceptance for this reaction, events of the form $\gamma p \to pX \to p\eta\pi^+ \to p\gamma\gamma\pi^+$ were generated according to t-channel phase space with a $d\sigma/dt \propto e^{-5|t|}$. Acceptances were

derived using FASTMC, requiring that the π^+ was measured in CLAS12 and the two photons were detected in CLAS12 or in FT. The neutron was reconstructed by using the missing mass technique. Figure 23 shows acceptances as a function of detected particle angles in the laboratory frame. The overall acceptance is of about 16% with an angular dependence as shown in the bottom-right panel of the same figure. It is worth noticing that the acceptance for this final state is only slightly dependent on the magnetic field intensity since the most part of the produced particles are neutral.

6.1.3 The reaction $\gamma p \to p\eta\phi$ and the search for strangeonium

Photoproduction is expected to be an efficient technique to produce $s\bar{s}$ mesons due to the spin-vector nature of the photon beam. This provides a natural way to favor the presence an $s\bar{s}$ component in the produced meson system. The excellent CLAS12 particle identification (k/π separation up to p=3 GeV) and acceptance in this mass range makes the upgraded Hall-B the ideal place to study strangeonium production.

The acceptance of CLAS12 for $\phi(1850)$ decay to $\phi\eta$ has been simulated using the FASTMC. The channel was identified by detecting the recoiling proton, the η, via its two photons decay, and a K^+ from the ϕ decay, while the K^- was reconstructed via the missing mass technique. Due to the good acceptance for neutrals in the forward direction, which is strongly enhanced at low angles by the FT calorimeter, we estimated an overall acceptance of about 10%. Fig. 24 shows the angular acceptances for detected particles.

The decay into $\phi\eta$ of strangeonia has never been observed before. Barnes, Black and Page predicted [49]:

$$\frac{Br(\phi\eta)}{Br(K^+K^-)} = 0.5.$$

A cross section of about 6 nb for strangeonium photoproduction decaying to K^+K^- was measured for energies between 20 and 70 GeV by the Ω Collaboration [57]. Considering the lower beam energy of our experiment we can expect the cross section to be somewhat higher, in the range of 10 nb in agreement with preliminary values from the G12 experiment [20].

6.1.4 The reactions $\gamma p \ \to pK^+K^-\pi^0$ and $\gamma p \ \to nK^+K^-\pi^+$

As for the production of strangeonium, quasi-real photoproduction is likely to be one of the more promising mechanisms for the production of exotic mesons with hidden strangeness due to the relatively large $s\bar{s}$ content of the photon. Photons are also expected to be efficient in the production of spin-1 hybrids. The first attempts to explore existing data from CLAS showed that the multiparticle reactions as

$$\gamma p \to (\phi\pi^0)p, \quad \phi \to K^+K^-, \quad \pi^0 \to \gamma\gamma \tag{4}$$

$$\gamma p \to (\phi\pi^+)n, \quad \phi \to K^+K^- \tag{5}$$

can be investigated [85].

The CLAS12 spectrometer has excellent momentum and angular resolution and particle identification. These features are extremely important for the mass determination and background reduction. The acceptance and resolution for resonances decaying to $\phi\pi^0$ was studied assuming the resonance to be produced and decay via the reaction $\gamma p \to Xp \to \phi\pi^0 p \to K^+K^-\gamma\gamma p$. Again the resonance X was produced with a t distribution, $\frac{d\sigma}{dt} \propto e^{-5|t|}$. In this case, the K^- from the decay of the ϕ meson is mainly produced at very forward angle, i.e. typically below 15 degrees in the lab with an overall detection efficiency of about 2% due to the inbending of negative particles in the toroidal field. The detection of this particle leads therefore to a very strong reduction of the

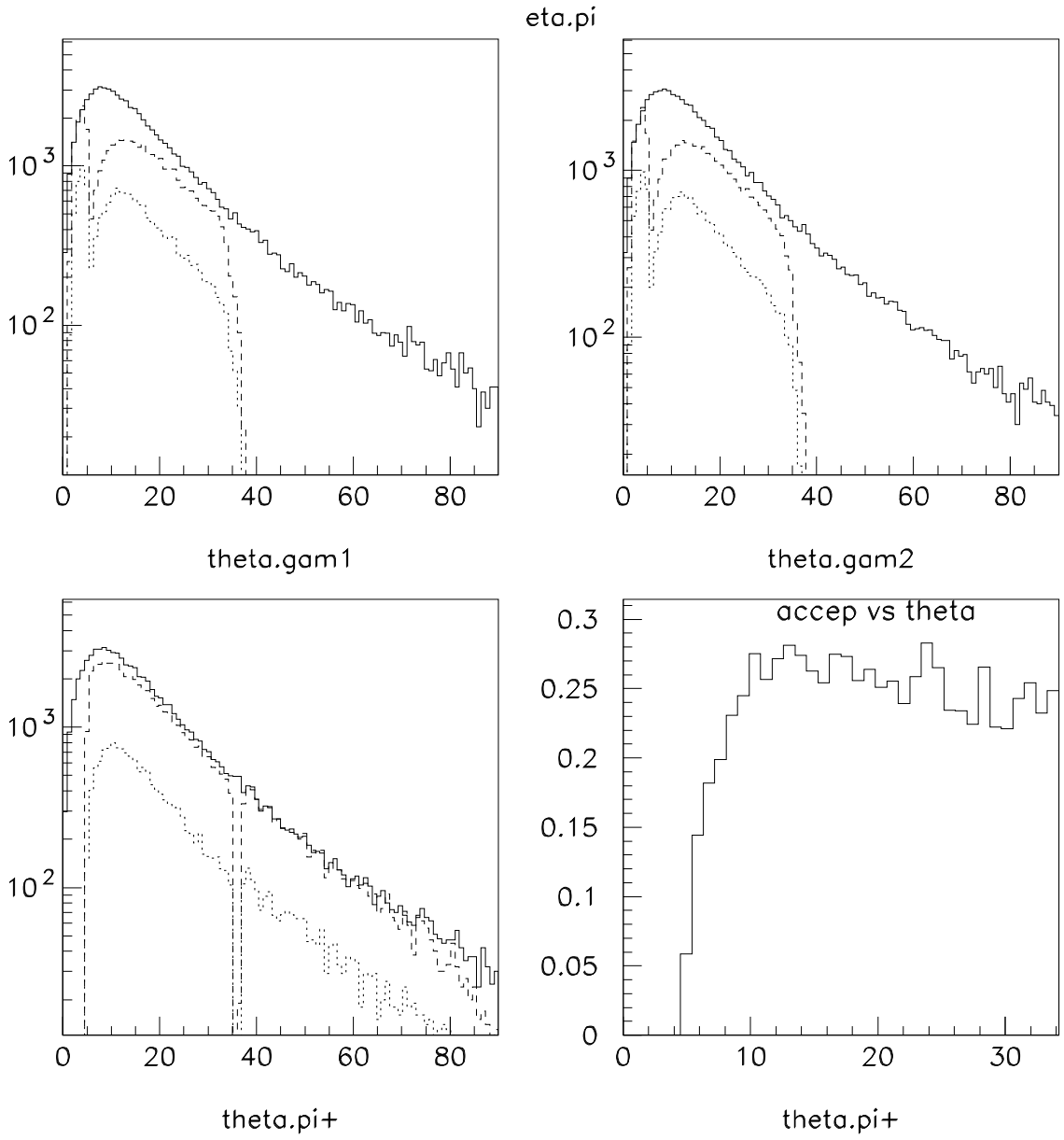

Figure 23: θ_{Lab} distributions for particles from $\eta\pi$ events. The top and bottom-left panels show the angular distributions for generated (solid) and detected (dashed) particles. In the same panels the dotted histograms show the angular distributions for particles when the whole final state is identified. The bottom-right panel shows the overall acceptance as a function of the π^+ angle.

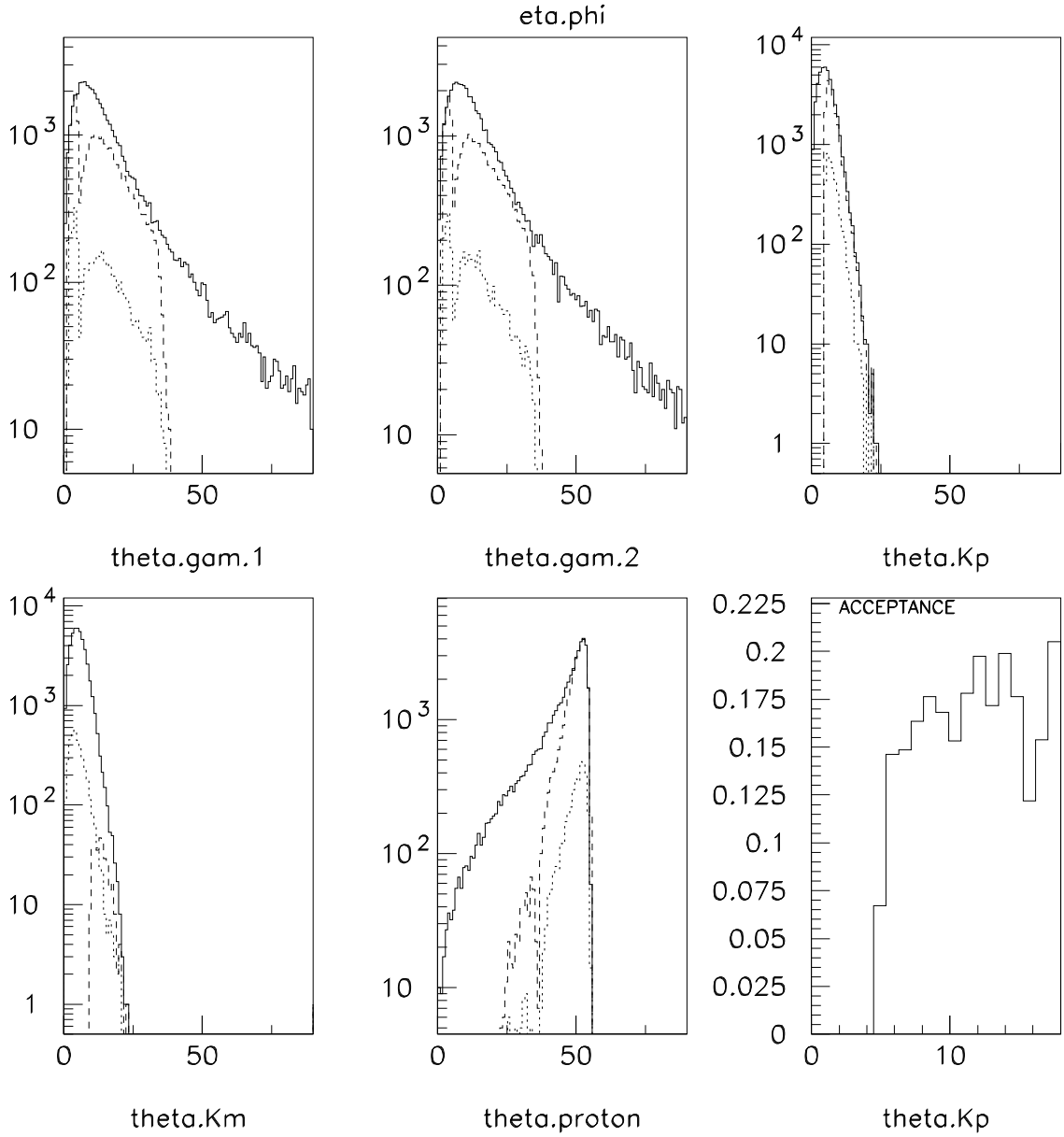

Figure 24: θ_{Lab} distributions for particles from $\phi\eta$ events and acceptance (bottom right) as a function of the polar angle of the K^+. The first five panels show the angular distributions for generated (solid) and detected (dashed) particles. In the same panels, the dotted histograms show the angular distributions for events where the final state is identified by detecting the two photons, the K^+, the proton and reconstructing the K^- with the missing mass technique.

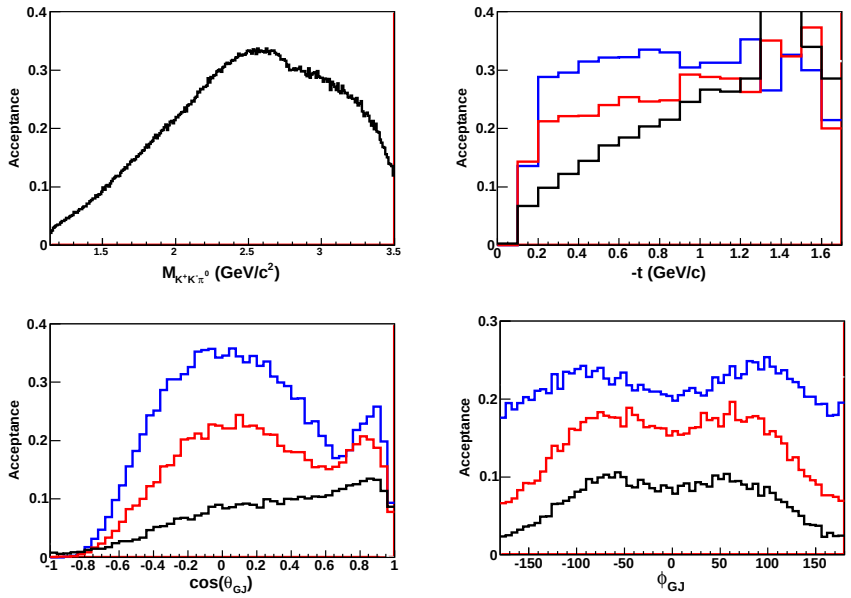

Figure 25: Acceptances for the $K^+K^-\pi^0 p$ final state, with the K^- reconstructed. Top left the $K^+K^-\pi^0$ invariant mass $M_{K^+K^-\pi^0}$, right the momentum transfer t, bottom left, $\cos\theta_{GJ}$ and right, ϕ_{GJ}. For the latter 3 plots the black, red and blue lines correspond to $M_{K^+K^-\pi^0} = 1.4$, 1.7 and 2.0 (GeV/c^2) respectively.

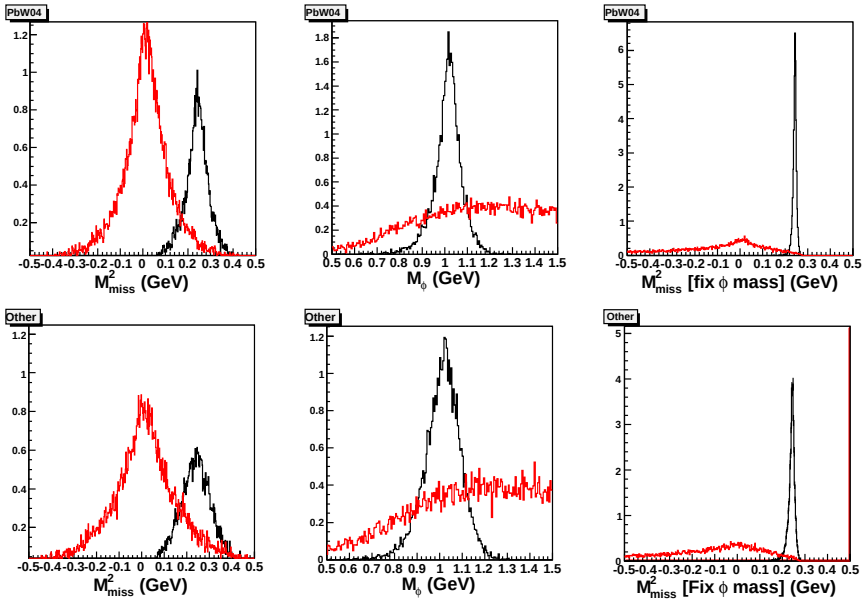

Figure 26: Reconstructed masses from the $pK^+\gamma\gamma$ final state for the CLAS-IC tagger (top) and the lowest resolution tagger (bottom). In all plots, the black line shows the final state of interest, while the red line is for a phase space $\gamma p \to K^+\pi^0\pi^- p$ reaction. The left plot shows the missing mass ($\sim K^-$), the middle the reconstructed ϕ mass and the right plot the missing, mass having fixed the reconstructed ϕ mass to 1.020 GeV.

overall acceptance. A more efficient identification of this final state is achieved by detecting the proton, the K^+, the π^0 via its decay to two photons and selecting the K^- in missing mass. The dependence of the acceptance on the mass of the $\phi\pi$ system $M_{K^+K^-\pi^0}$, t distribution and resonant decay angles θ_{GJ} and ϕ_{GJ} are shown in Fig. 25 for the half field setting for CLAS12. They are similar to those obtained for the 3π analysis and so the conclusion discussed in the next Section about the feasibility of PWA can be extended to this reaction as well. There is little effect on these acceptances for full magnetic field as the K^- is not detected in CLAS12.

Figure 26 shows the reconstructed masses from the $pK^+\gamma\gamma$ final state. Also shown is a phase space $\gamma p \to K^+\pi^0\pi^- p$ background. The missing masses have widths of 0.054 and 0.093 GeV for the CLAS-IC and low-resolution tagger respectively. The resolution is the same for the reconstructed ϕ mass. Again, the capability to determine the photon energy with a good resolution is crucial to be able to study this reaction channel with a sizable efficiency and a good signal to background ratio.

6.1.5 Conclusions

The results of the study on benchmark reactions presented in the previous sections has clearly shown that the possibility of inferring the energy of the quasi-real photon from measuring the scattered low angle electron gives significant advantages for the study of exclusive multi-particle final states. First of all, the complete determination of the initial state provided by the FT makes it possible to use the missing mass technique to ensure the exclusivity of the reaction. Without such information, a full measurement of the final state particles would be necessary, resulting in acceptances of the order of 1% or below for many of the studied reactions. To fully exploit the missing mass technique, a good energy resolution for the tagger, as planned in the current design, is desirable. In cases where full detection of the final state is possible, the determination of the initial state allows to apply further constraints to suppress backgrounds coming from other reactions and extract small cross section signals.

6.2 PWA simulations

As described in Sec. 3, the first step in partial wave analysis is to extract amplitudes from fits to the measured particle distribution. At this stage it is necessary to establish to what extent the finite detector acceptance and resolution distorts the extraction of underlying reaction mechanism. For a specific reaction this is done by generating events using a realistic differential cross-section, processing them through a detector simulation and reconstruction programs, and fitting with a set of partial waves in bins of kinematic variables. We currently have two partially independent PWA codes and two groups who are working on developing and testing these codes. Using these tools, we performed detailed partial wave analysis studies for two reactions:$\gamma p \to n\eta\pi^+$ and $\gamma p \to \pi^+\pi^+\pi^- n$.

A detailed description of the systematic studies and of the corresponding results is reported in the following sections. The results of this systematic studies can be summarized as follows. The PWA results obtained from the two channels and by the two analysis groups have demonstrated that it will be possible to perform a full and reliable partial wave analysis using CLAS12 and the Forward Tagger system. Furthermore, information from the beam polarization is maintained in asymmetries observed on the ϕ distributions. This information will be important to determine the naturality of the production mechanisms, reducing possible ambiguities in the PWA and suppressing background contribution from the wrong-naturality processes.

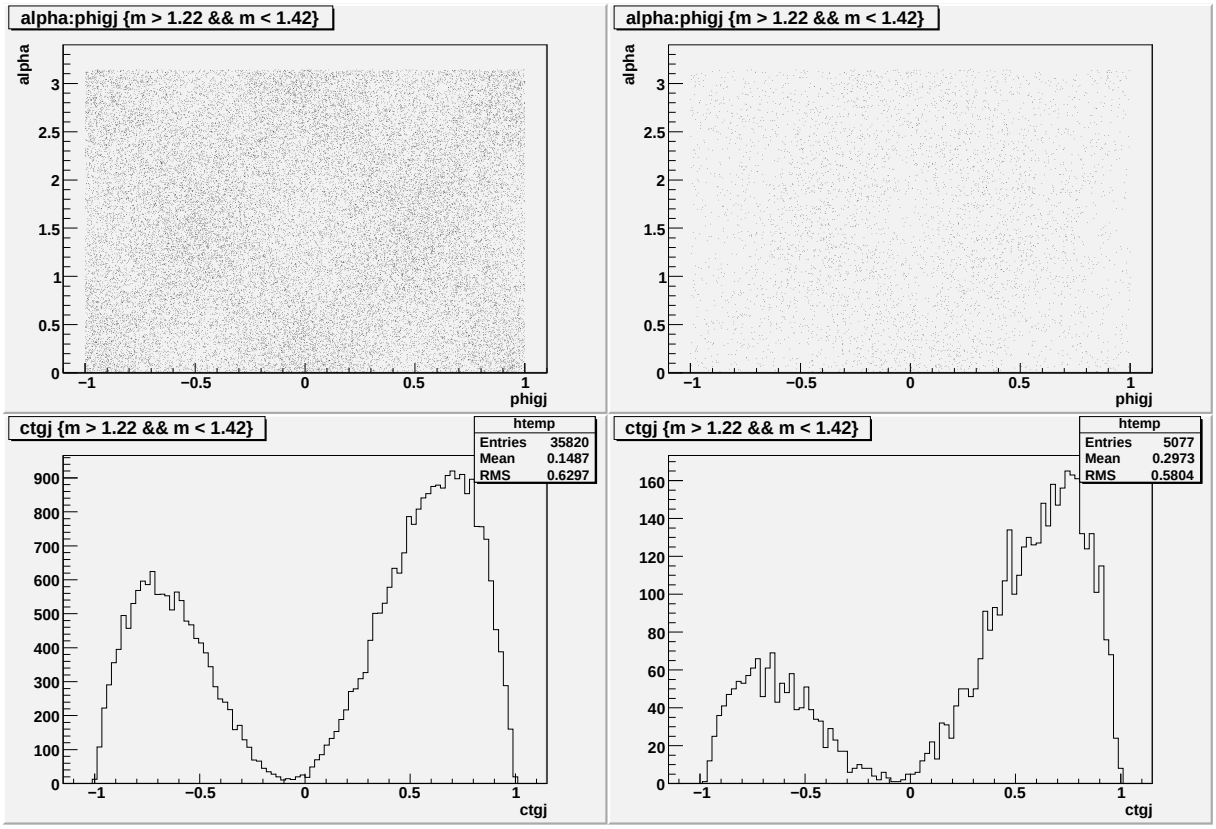

Figure 27: The raw (left) and accepted (right) ϕ_{GJ} vs α and $\cos(\theta_{GJ})$ distributions for the $\eta\pi$ final state.

6.2.1 Partial Wave Analysis of the $\eta\pi$ Channel

As discussed in Sec. 6.1.2, this final state can be measured in CLAS12 detecting the pion and the two photons from the η decay. This leads to typical acceptances of the order of 16%. For the PWA study we considered an electron beam of 11 GeV, a scattered electron of $E_{e'} = 2$ GeV (ie. a 9 GeV virtual photon) and $\theta_{e'}$=3^o. By fixing those parameters, the photon linear polarization is fixed at $\epsilon = 0.35$. The azimuthal angle $\phi_{e'}$ is taken randomly from 0 to 360 degrees, therefore, the angle α, between the polarization vector and the perpendicular to the production plane, results randomly distributed within the same interval.

The virtual photon information enters solely through its energy and spin density matrix (related to ϵ and α). Those three values were smeared with a Gaussian distribution of standard deviation calculated by propagating the energy and angles resolutions measured by the FT.

Events were then weighted according to a photoproduction cross-section for E_γ=9 GeV photons and with a one-pion-exchange production (OPE) mechanism. In addition, two resonances were included: the $\pi_1(1400)$ and the $a_2(1320)$. Decays were produced only for $m = +1$ waves leading to two combinations of quantum number: $J^{PC}M = 1^{-+}1$ and $2^{++}1$. These events were then put through FASTMC.

Our first test was to determine if the asymmetries in ϕ created by the beam polarization, remained through the angular distribution distortion produced by the CLAS12 and FT acceptance and resolution. We knew that the experimental resolution may introduce some distortions but we expected that most of the structure created by the polarization were preserved. A good test is to

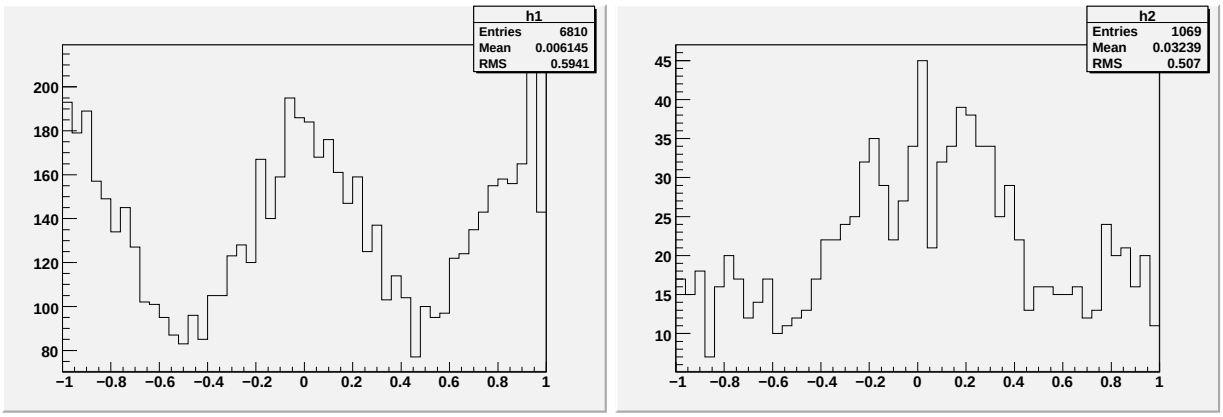

Figure 28: The raw (left) and accepted (right) ϕ_{GJ} distributions for the $\eta\pi$ final state.

look at the distributions of ϕ_{GJ} (ϕ angle in the Gottfried-Jackson frame) vs. α (polarization vector angle) before and after acceptance and resolution smearing. Figure 27 shows these distributions. Also the ϕ_{GJ} distributions for a given range in alpha, before and after acceptances, are shown in Fig. 28. We conclude that the ϕ information produced by the beam polarization is still present in the data after the acceptances and resolutions of the CLAS12 and the FT are taken into account.

Furthermore, a mass independent partial wave analysis of the simulated data was performed using 20 MeV/c^2 wide mass bins from 1.0 GeV/c^2 to 1.6 GeV/c^2. We used an updated version of the PWA2000 code used for the CLAS G6 data analysis [19, 17] that is now being used to analyze the CLAS G12 run data [20]. Three partial waves were used in the PWA fit. For each of $J^{PC}|M|L$ there was one wave corresponding to positive reflectivity (pion exchange). The waves used in the fit were: $2^{++}1D$, $1^{-+}1P$, the same used as input for the simulation, and an additional $2^{++}0D$ wave. The PWA intensities resulting from the many mass independent PWA fits are shown in Fig. 29. The fit populates the $P1$ and $D1$ waves, with no contribution to the $D0$ wave. This result demonstrates the capability of the PWA to extract different resonances in their proper partial waves.

6.2.2 Partial Wave Analysis of the 3π Channel

Even though the charged 3π state is not an eigenstate of charge conjugation, $I = 1$ vector resonance decaying to three pions would correspond to a (charged) member of the $\pi_1^{\pm,0}$ exotic multiplet. From the theoretical point of view, charge exchange photo-production is expected to be well described in terms of the leading Regge pion exchange trajectory which has been thoroughly studied in the past. The alternative, neutral 3π production is dominated by the enigmatic Pomeron exchange which leads to large backgrounds from $I = 0$ vector meson diffractive production. Furthermore, there are well established $I = 1$ 3π resonances, a_1, a_2 and π_2, that enhance the sensitivity by interfering with the small exotic wave . The model for 3 pion production, detailed in Appendix A, has been implemented in a PWA framework developed by Indiana University [86], and used to test the suitability of events reconstructed from CLAS12 and the forward tagger for Partial Wave Analysis. The model defines 8 possible final states, summarized in table 5, decaying to $\pi^+\pi^+\pi^-$, with an additional recoiling neutron in the final state. The π_1 is a proposed exotic state. In the model, its contribution to the final state is around 2%, corresponding to a 200 nb cross section, for a total $\pi^+\pi^+\pi^-$ cross section of around 10 μb. To allow a series of PWA tests to be performed

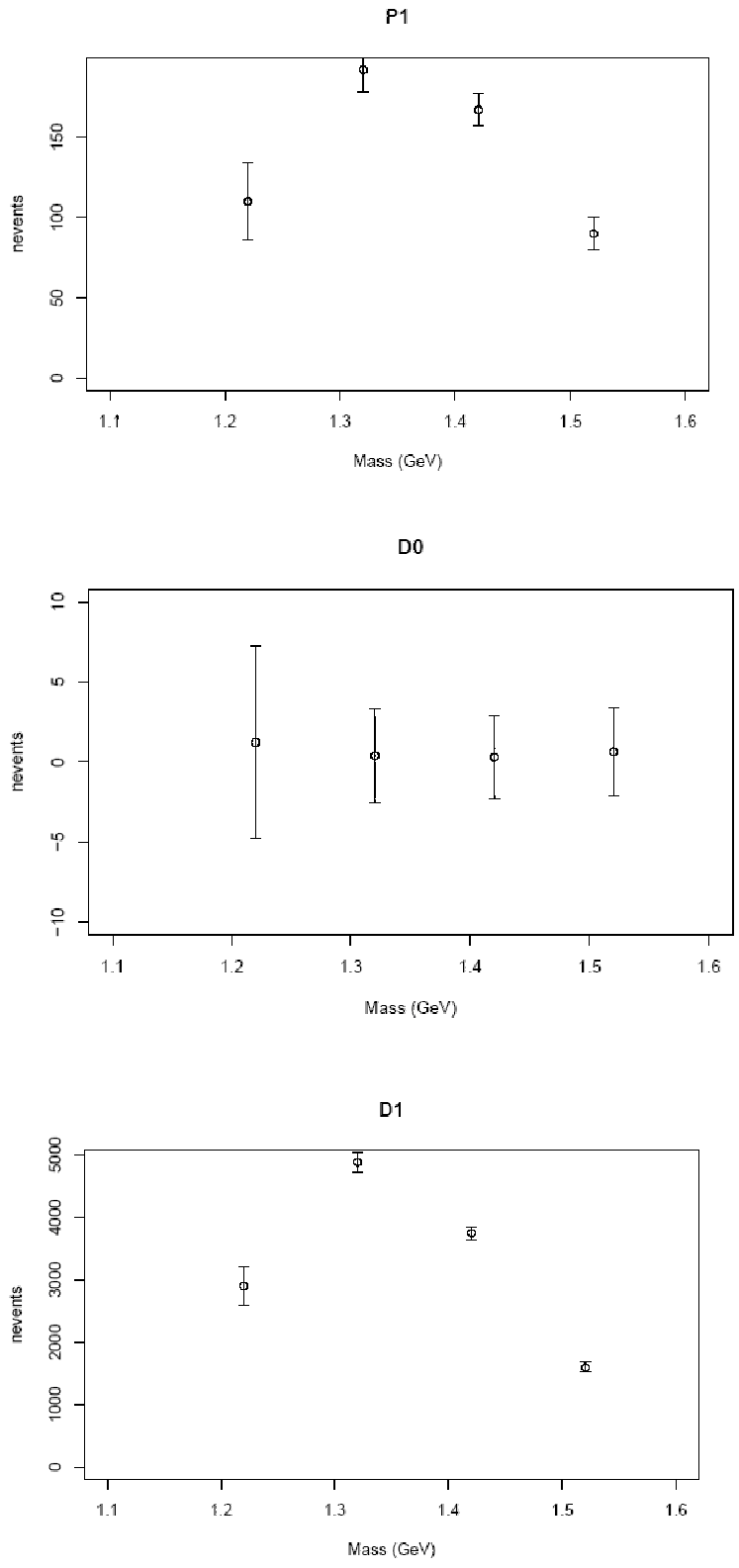

Figure 29: The PWA intensities resulting from the mass independent PWA fits of the simulated data. One expects not to observe resonance structure in these partial waves.

State	J^{PC}	L	Decay Mode
$a_1\,(1260)$	1^{++}	D	$\rho\pi$
$a_2\,(1320)$	2^{++}	D	$\rho\pi$
$\pi_2\,(1670)$	2^{-+}	P	$\rho\pi$
$\pi_2\,(1670)$	2^{-+}	F	$\rho\pi$
$\pi_2\,(1670)$	2^{-+}	S	$f_2\pi$
$\pi_2\,(1670)$	2^{-+}	D	$f_2\pi$
$\pi_1\,(1600)$	1^{-+}	P	$\rho\pi$

Table 5: The meson states produced in the model of $\pi^+\pi^+\pi^-$ production, detailed in Appendix A.

in a reasonable time, the number of generated events was limited to 1 million. This would be equivalent to around 1 thousandth of the total number of events, we estimate would be produced in this experiment. Therefore, for the experimental data we will have many more times the statistics then for our current tests, allowing fine binning in a number of kinematic variables such as E_γ, t and $M_{3\pi}$.

The testing algorithm proceeded as follows,

- The model was used to generate 1 million events, "data", from low Q^2 electron scattering reactions accepted by the forward tagger, with an electron beam energy of 11 GeV. Events were generated in two t bins at 0.2 and 0.5 $(\mathrm{GeV/c})^2$, 0.25 and 1 MeV wide respectively to give comparative numbers of events in the same beamtime.
- 5 million phase space Monte Carlo events, "mc", were generated in the same kinematics and were used to calculate the acceptance during the PWA fit.
- Both "data" and "mc", were tracked through the detectors via the FASTMC program. A number of tracking options were used including full and half CLAS12 torus field and CLAS-IC or PANDA-EMC resolutions for the forward tagger.
- Final states with 3 reconstructed pions were accepted for the PWA.
- The accepted events were split into 40 bins in the mass of the 3π system, between 0.7 and 2.2 GeV.
- Maximum likelihood fits were performed, using the model described before to calculate the event-by-event amplitudes, for each 3π mass bin. The generated and accepted "mc" events are used to calculate the normalization integrals and subsequent acceptance. The complex production amplitude of each channel was a free parameter in the fit.
- The resulting intensity of each channel was calculated from the fit results and compared to the generated one.

The first comparison presented in Figure 30 is between the generated waves and a fit for each t bin (0.2 and 0.5) at half CLAS12 field and CLAS-IC Forward Tagger resolution. The fits for both t bins reproduce the generated waves very well for all channels including the hypothetical π_1 exotic. The mass region with $M_{3\pi}(< 1.2\,GeV/c^2)$ has been excluded from this analysis because of the very low acceptance. Even with a π_1 contribution of just 2% to the total, a clear statistically significant signal is reproduced using a small statistics compared to the expected yield for the

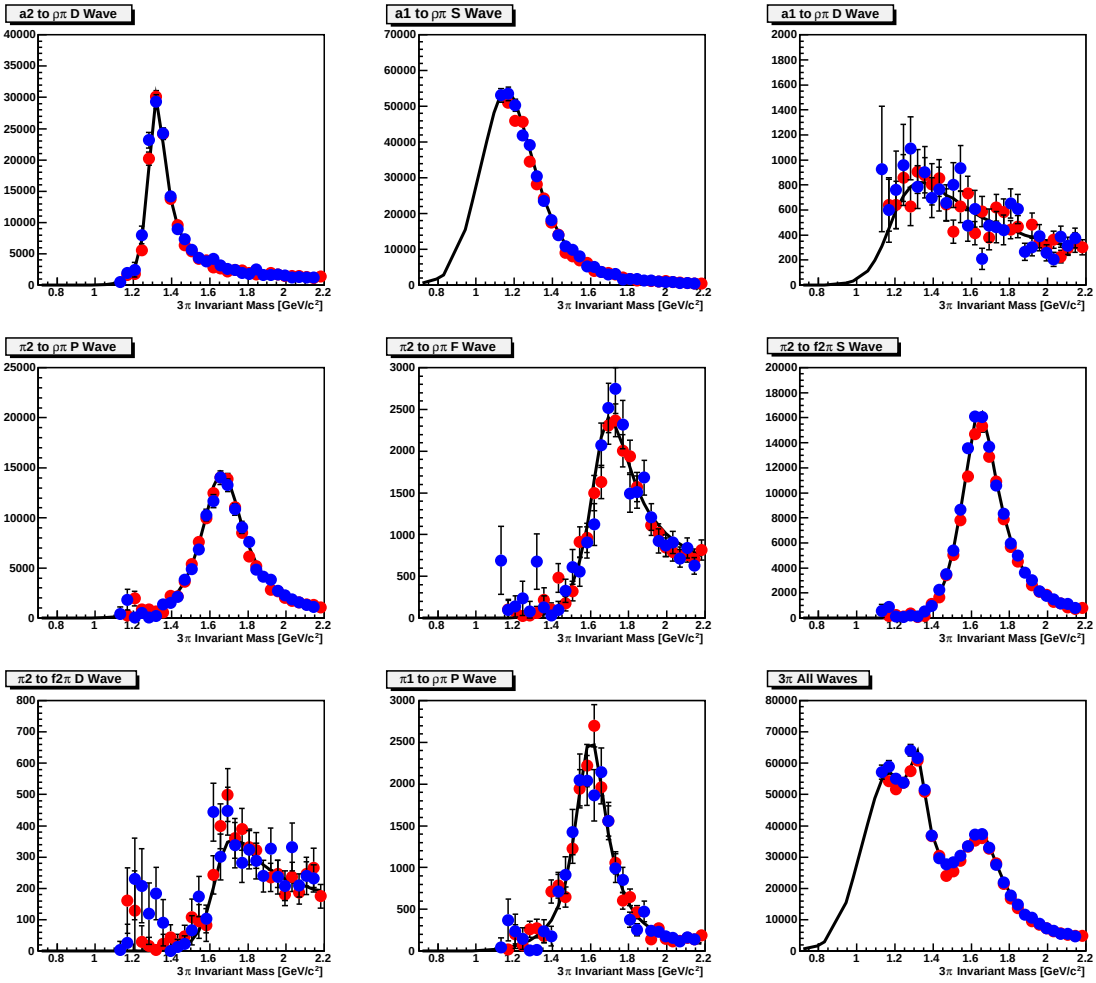

Figure 30: The intensities of the 8 different isobar channels in the 3π model, see table 5. The bottom right plot shows the total intensity. The black line shows the generated waves, while the blue and red points are the fit results for $t = 0.2$ and $0.5(GeV/c)^2$, respectively.

proposed experiment. *This leads to the conclusion that the CLAS12-Forward Tagger system is intrinsically capable of meson spectroscopy measurements via partial wave analysis.*

However, in reality we will not have such perfect knowledge of the CLAS12 response and physics of the production and decay. To test the effects of possible distortions and leakages we have performed a number of fits with imperfect knowledge of the detector or model.

1) The "data" were tracked through FASTMC with an incorrect field strength, 2% higher at the half field setting, compared to the accepted "mc" events. This effectively creates a different acceptance between the "data" and "mc" due to charged particles of a given momenta seeing different holes in the detector. The results are shown in Figure 31, and at this level of field discrepancy no sizeable distortion effect is seen on the fitted waves.

2) The angular and momentum resolutions of the FASTMC were decreased by 20% for the "data" only. This tests how accurately we will be required to know the resolutions from the tracking in CLAS12. The results are shown in Figure 32 and very little deviation in seen between the ideal case and the degraded resolution case.

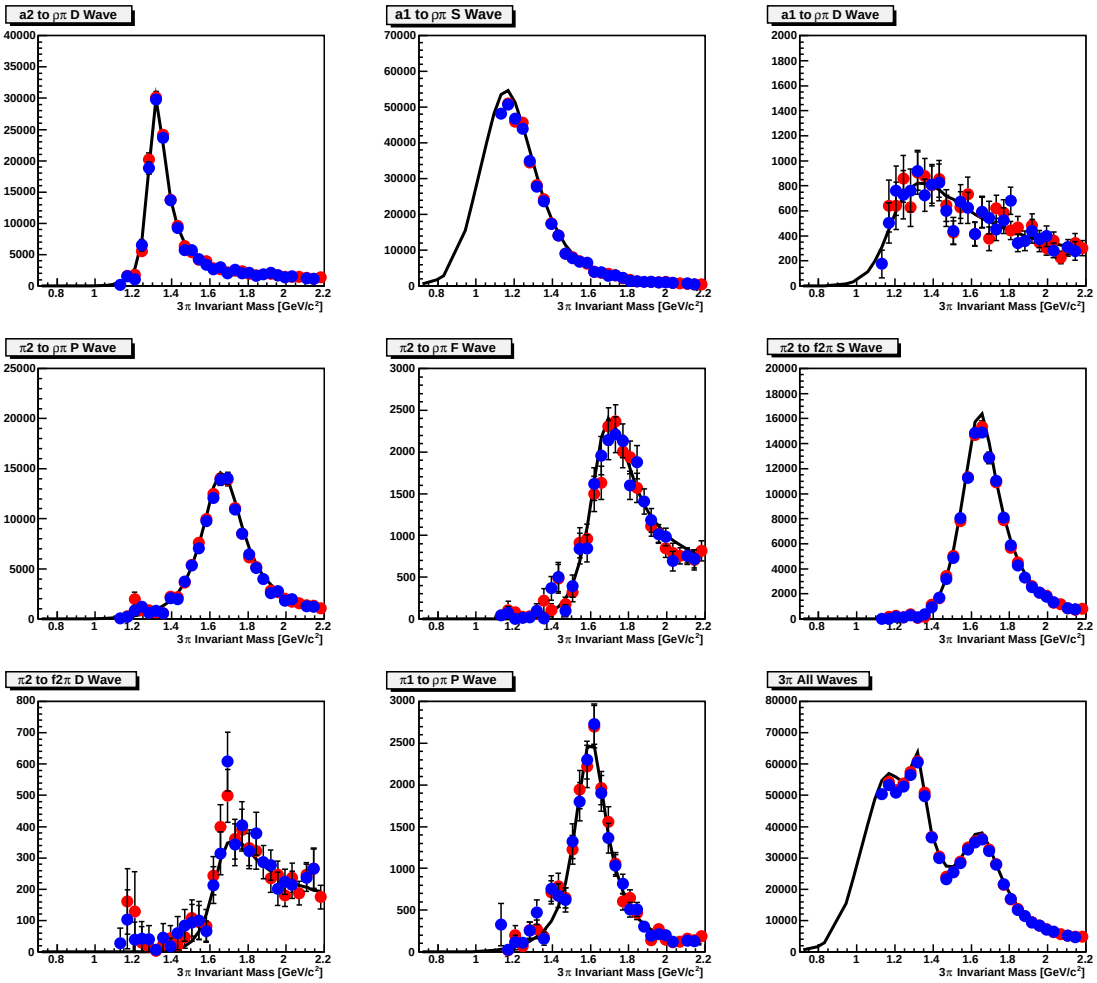

Figure 31: The intensities of the 8 different isobar channels in the 3π model, see table 5. The bottom right plot shows the total intensity. The black line shows the generated waves, while the red points are the fit results for $t = 0.5(GeV/c)^2$, half field and the blue points are for "data" tracked with the field incorrectly set 2% higher than for the "mc" events.

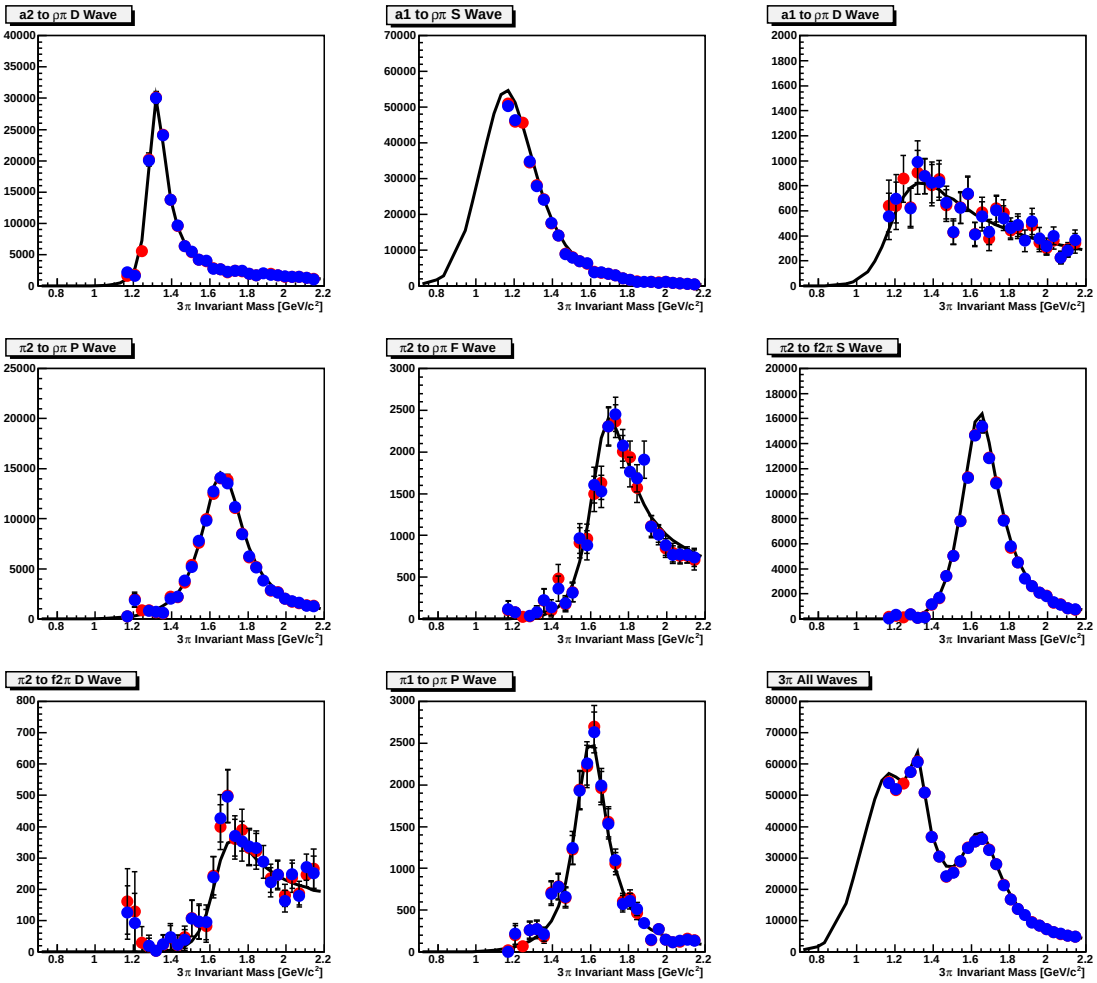

Figure 32: The intensities of the 8 different isobar channels in the 3π model, see table 5. The bottom right plot shows the total intensity. The black line shows the generated waves, while the red points are the fit results for $t = 0.5(GeV/c)^2$, half field and the blue points are for "data" tracked resolutions 20% greater than standard, while the corresponding "mc" used standard resolutions.

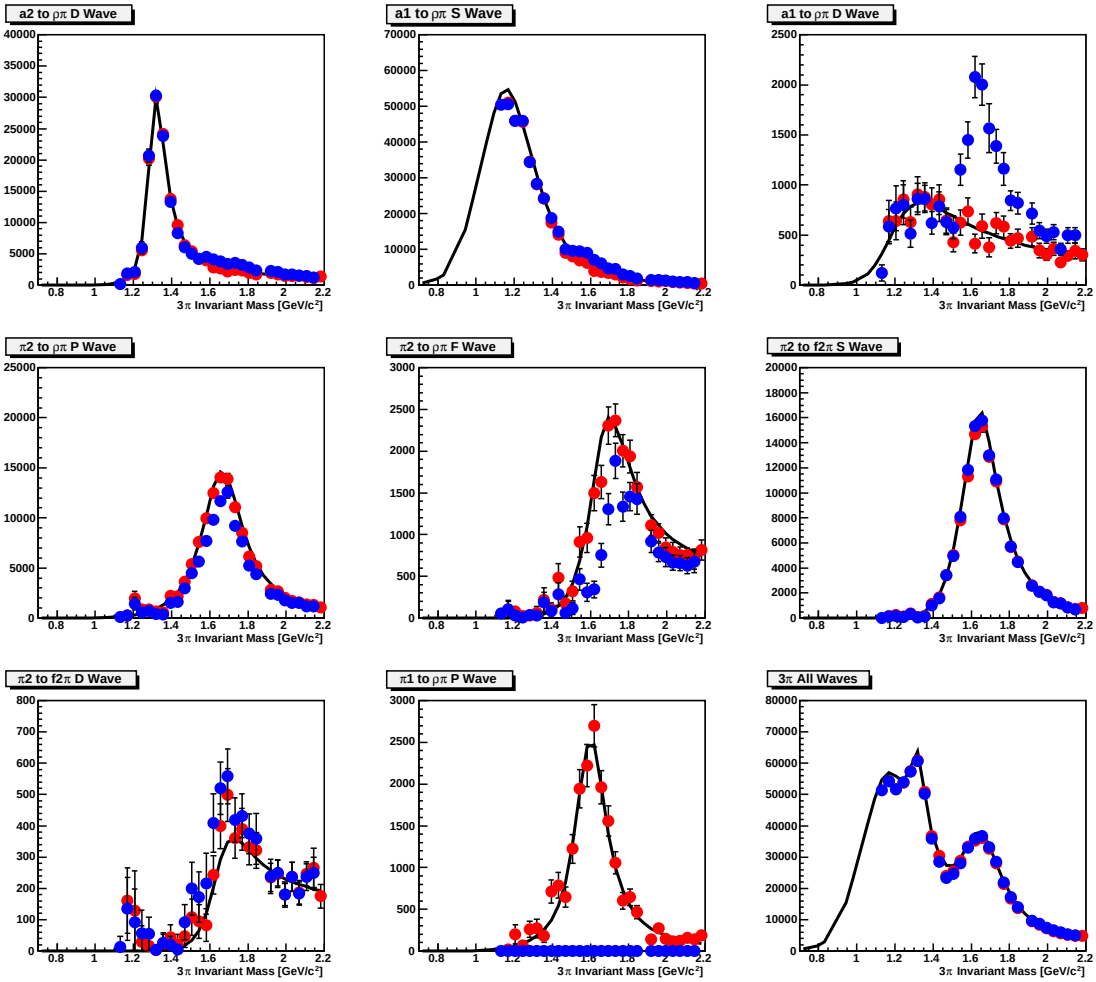

Figure 33: The intensities of the 8 different isobar channels in the 3π model, see table 5. The bottom right plot shows the total intensity. The black line shows the generated waves, while the red points are the fit results for $t = 0.5(GeV/c)^2$, half field and the blue points are for a fit without the π_1 D wave.

3) The standard model events were fit without the π_1 D-wave and the results are shown in Figure 33. The intensity of the generated π_1 clearly has to be given to another wave or waves by the fit. In this case it is the a_1 S and D wave which acquires most of the yield, while the π_2 P and F waves are underestimated. This shows the importance understanding the components of the model used to perform the fit. As discussed in Sec. 3, a collaborative worldwide effort is underway to refine the tools and models required to perform such amplitude analysis. The timescales for this work will coincide well with the prospective data from the CLAS12 experiment.

4) The full model fit was performed on events generated without a π_1. As shown in Fig. 34, the resulting π_1 intensity is consistent with zero within it uncertainty and for the statistics generated is around 10 counts at 1.6 GeV/c^2. This is a factor 200 less than for the π_1 generated in the model which contributed 2% to the 3π yield.

5) We have shown in Sec. 6.1 that the half field setting provides the optimal acceptance for this channel. However, as mentioned before, this experiment is conceived to run in parallel to other electron scattering experiments that may have higher field setting. The results of the PWA with

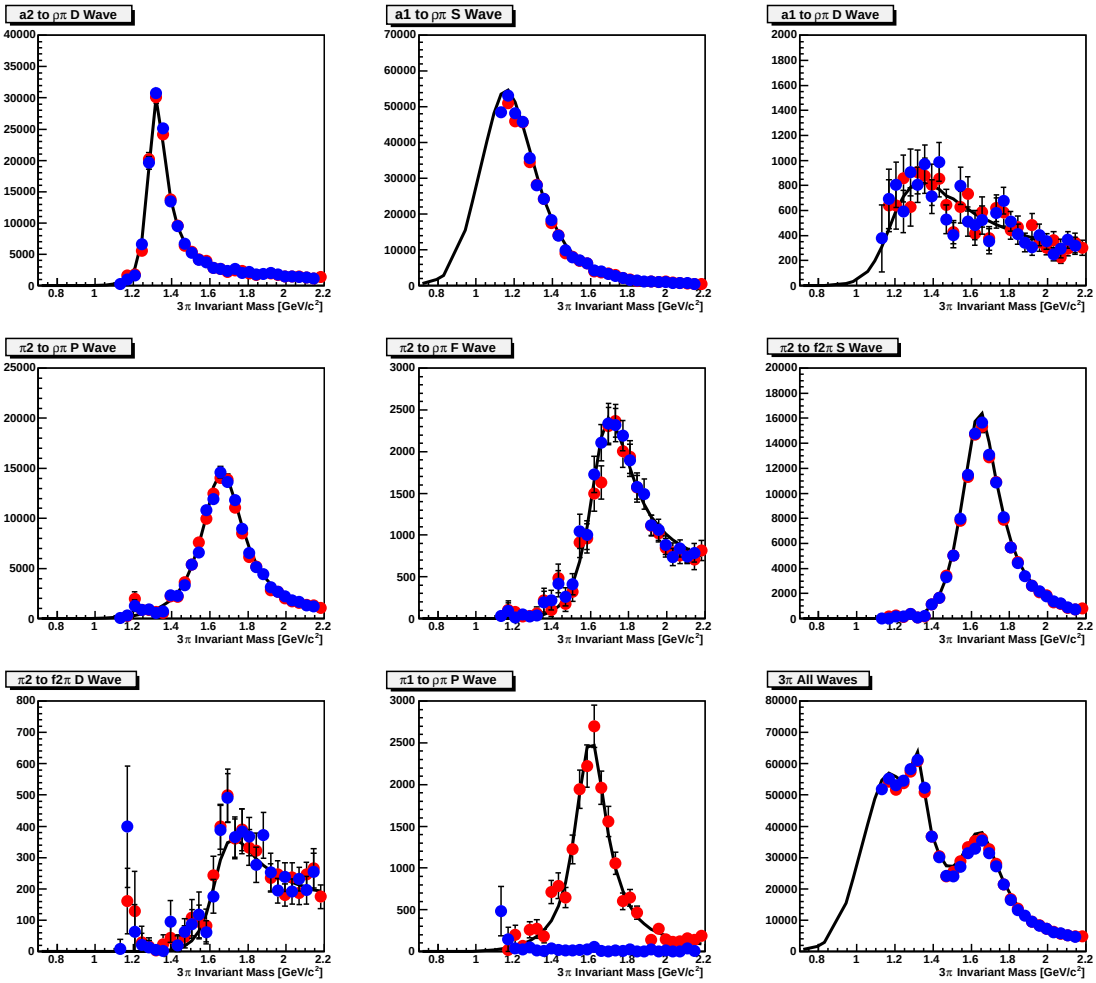

Figure 34: The intensities of the 8 different isobar channels in the 3π model, see table 5. The bottom right plot shows the total intensity. The black line shows the generated waves, while the red points are the fit results for $t = 0.5(GeV/c)^2$, half field and the blue points are for a generated without the π_1 D wave.

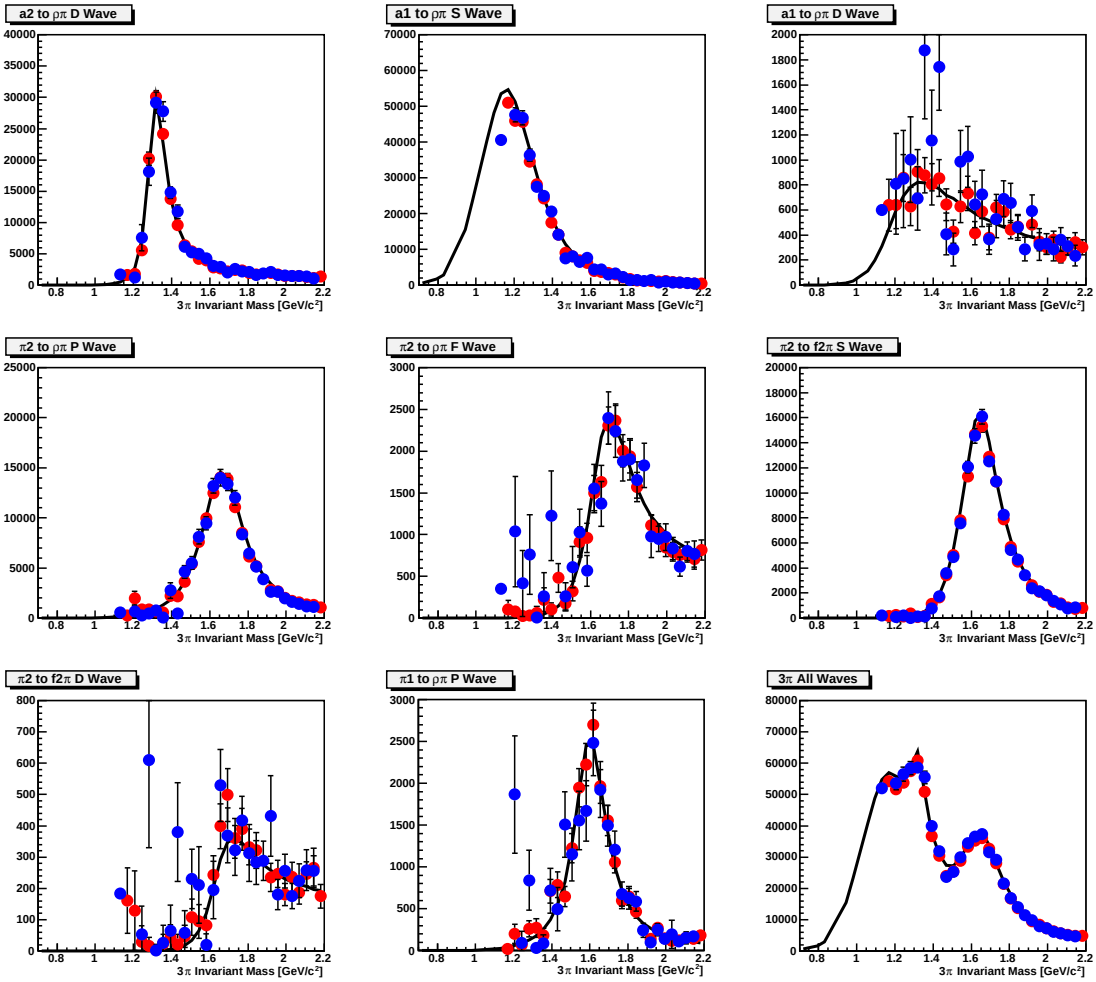

Figure 35: The intensities of the 8 different isobar channels in the 3π model, see table 5. The bottom right plot shows the total intensity. The black line shows the generated waves, while the red points are the fit results for $t = 0.5(GeV/c)^2$, half field and the blue points are for full field.

the full field setting are shown in Fig. 35. Again the fits are successful for the full field setting. In general the error bars are larger particularly at low $M_{3\pi}$, and are around 25% larger around the π_1 peak. As our test results only use a small amount of the statistics, the statistic uncertainty will be significant reduced with the full expected yield.

6.2.3 Linear polarisation

The linear polarization of the quasi-real photon beam will enhance the information extracted from PWA. On one hand, it can help separate out the signal from mesonic states with similar masses, but produced in processes involving different naturality, as outlined in Appendix A. While on the other hand it can be used to reduce contributions from background processes. For example, the model used for the bulk of these tests has assumed one-pion-exchange for the production mechanism, however, ρ exchange can also play a role. The latter exchange has opposite naturality leading to a phase shift of the ϕ distribution, of the produced meson.

An additional test was performed on π_1 events produced by a mix of these production mecha-

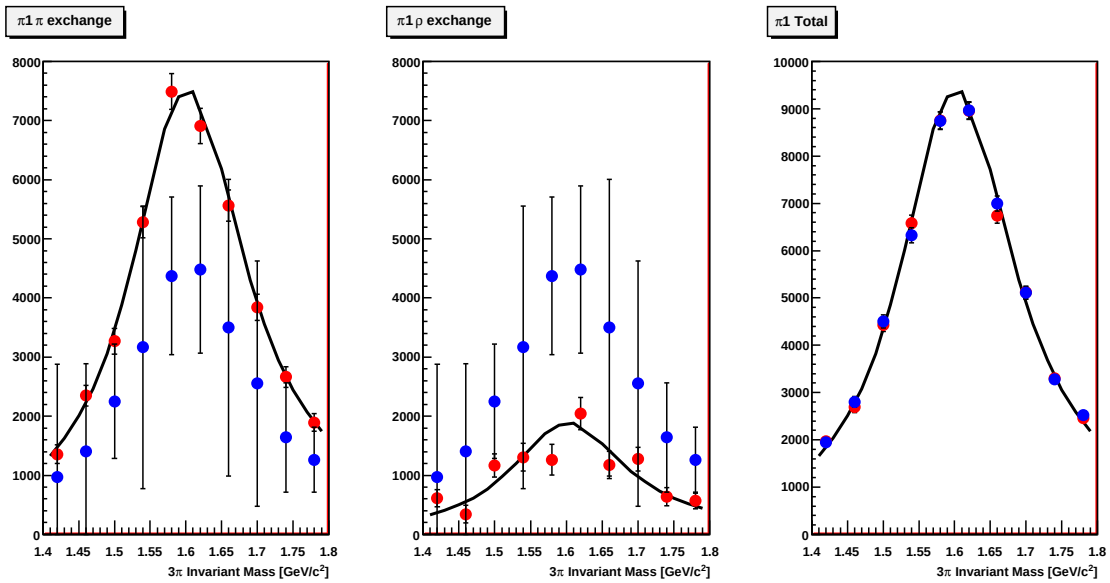

Figure 36: The fit results for the pion exchange mechanism (left), ρ exchange (middle) and total (right). The black line is the generated intensities, while the red circles show the polarized fit and blue, the unpolarized. The large error bars shown in the unpolarized fits are an artifact created by the fitting procedure.

nisms. The events were generated using both true electron scattering polarization and zero polarization. The ratio of pion exchange to ρ exchange amplitudes was 6:3. These events were passed through the detector acceptances, then fitted. The results, shown in Fig. 36, confirm that the unpolarized fits have no sensitivity to the production mechanism, while the polarized fits successfully separate out the two contributions.

7 Beam time request and expected results

This experiment requires the following beam time:

- 80 days of production beam time at full luminosity ($\sim 10^{35}\text{cm}^{-2}\text{s}^{-1}$). This time is needed to accumulate enough statistics to study the reactions with the smallest cross sections. For instance, as shown in Sec. 6.1.3, the expected cross sections for strangeonium production are in the range of 10 nb and the corresponding event rate is expected to be 3×10^{-4} ev/s in a 10 MeV mass bin. This will lead to ~ 3000 event per mass bin, which is sufficient to perform a full PWA of these final states. The right panel of Fig. 37 shows the expected yield for the reaction $\gamma p \to p\phi\pi^0$ whose cross section and acceptance are similar to the strangeounium case.

- 15 days of commissioning time to test and optimize the FT configuration. This includes full test of the new equipment (tracker, scintillation hodoscope and calorimeter), gain matching, first energy and time calibration and optimization of the trigger set-up (energy threshold, clustering algorithm, ...).

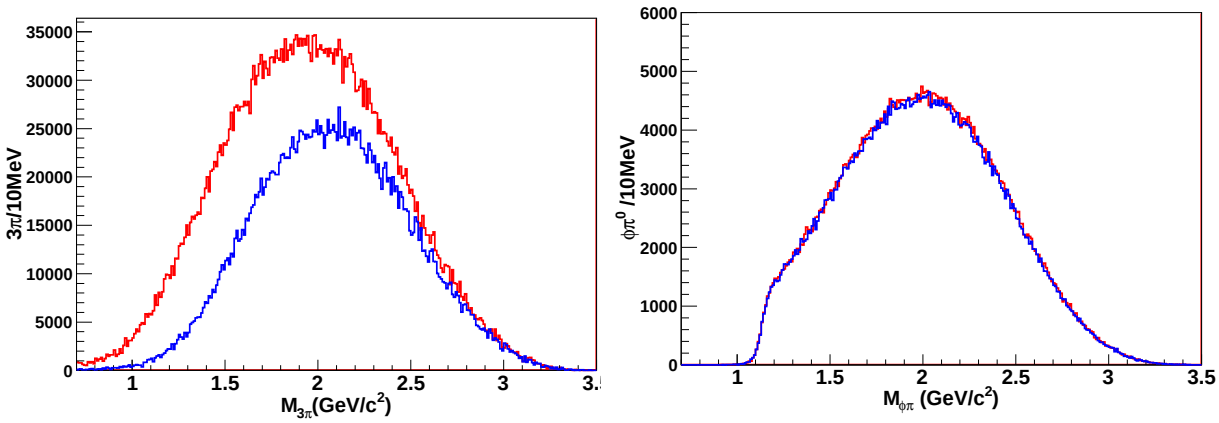

Figure 37: Left: event yield for the reaction $\gamma p \to n\pi^+\pi^+\pi^-$ as a function of the 3π mass for 20 days of beam time at $\sim 5 \times 10^{33}\text{cm}^{-2}\text{s}^{-1}$ luminosity. Right: event yield for the reaction $\gamma p \to p\phi\pi^0$ as a function of the $\phi\pi$ mass for 80 days of beam time at $10^{35}\text{cm}^{-2}\text{s}^{-1}$ luminosity. The red and blue histograms correspond to half and full field configurations of the torus magnet, respectively.

- 24 days of dedicated beam time with low luminosity ($\sim 5 \times 10^{33}\text{cm}^{-2}\text{s}^{-1}$) and minimum bias triggers to test the overall trigger configuration and event reconstruction. 20 days should be allocated before the production run to accumulate enough statistics to perform first analysis on the reactions with higher cross section in the optimal detector configuration and have a quantitative test of the reliability of the experimental setup. As shown in the left panel of Fig. 37 we estimated that the 3π yield in 10 MeV bins for a possible resonance mass of 1.6 GeV will be of the order of 10k which is adequate to perform a full and detailed PWA on this final state. Four days should be allocated in periods of 8 hours (one shift) per week to accumulate data for systematic checks and monitoring.

As mentioned above, the CLAS12 configuration we propose for the meson spectroscopy program is compatible with the experimental setup requested by the already approved electroproduction runs [87]. Therefore the requested production beamtime may be allocated in parallel to the other electroproduction experiments on hydrogen target.

8 Summary

Study of the conventional meson spectrum and search for gluonic excitations is one of the promising way to address fundamental issues in strong interactions. This investigation can provide an answer to crucial questions as what is the origin of the mass of hadrons, what is the origin of quark confinement, what are the relevant degrees of freedom to describe these complex systems and how the transition between the elementary constituents, quarks and gluons, and baryons and mesons occurs.

Spectroscopy of mesons in the 1.5 to 2.5 GeV mass range will provide insight into new or rare forms of hadronic matter such as exotics, hybrids and strangeonia. High intensity beams together with large acceptance detectors, instrumented to detect multi-particle final states, can provide the necessary precision and statistics for meson spectroscopy studies.

We propose to add to the CLAS12 detector a new quasi-real photon tagging facility (Forward

Tagger) to be able to run a meson spectroscopy program in the Hall-B at Jefferson Lab. The unique combination of a high resolution and good particle identification of CLAS12, together with a high photon flux achievable with the proposed technique, will allow us to measure rare mesonic states, extending the search to the strangeness-rich meson spectrum.

Electrons scattered at small angles, from 2.5° to 4.5°, will be detected by the FT, providing the virtual photon energy, the linear polarization and a precise determination of the interaction time. Trigger rates have been studied running complete GEANT4 simulation of the FT. Shielding and electron detection kinematics have been optimized to keep the radiation dose, mainly due to the electromagnetic background, within permissible values. The design of the FT is compatible with the CLAS12 base equipment, so that the tagger operation will be possible in parallel to electroproduction experiments on LH_2 that are part of the already approved physics program. The proposed detector will therefore extend the CLAS12 detection capabilities for electron down to 2.5°, also providing an excellent acceptance for photons emitted in the forward direction. The total trigger rate for electron and quasi real photon experiment running in parallel is expected to be <10 kHz, i.e. within limits of the CLAS12 DAQ.

Detailed studies of benchmark channels have shown that final states with four particles detected in CLAS12 have a sizable acceptance of about 15%. The blind detection area due to the complex geometry based on the toroidal magnet of the detector, does not reflect in a significant distortion of the angular distributions in the meson decay frame. Partial wave analysis of different channels performed on pseudo-data, that take into account the CLAS12 acceptance, showed that a signal up to a few % level of the whole intensity can be reliably identified and reconstructed in a specific wave.

With 80 days of run at full luminosity of ($10^{35}\mathrm{cm}^{-2}\mathrm{s}^{-1}$) it is possible to collect enough statistics to run partial wave analysis of rare mesons with cross sections down to 10 nb level. Other 35 days of commissioning and low luminosity run ($\sim 5 \times 10^{33}\mathrm{cm}^{-2}\mathrm{s}^{-1}$) are required to check and optimize the new detector, test the hardware trigger system and accumulate the necessary statistics with minimum bias trigger to perform physics analysis.

Appendix A: The model to describe $\gamma p \to \pi^+\pi^+\pi^- n$

The matrix element for unpolarized electron scattering in the one-photon exchange approximation is:

$$|\mathcal{M}|^2 = (2e^4/Q^2)T_{\mu\nu}L^{\mu\nu} \tag{6}$$

where $T_{\mu\nu}$ is the hadronic tensor and $L^{\mu\nu}$ is the virtual photon polarization density matrix.

For reaction $\gamma p \to \pi^+\pi^+\pi^- n$ the hadronic tensor $T^{\mu\nu}$ is given by the current matrix elements $T^{\mu\nu} = \langle 3\pi n|J^\mu|p\rangle^* \langle 3\pi n|J^\nu|p\rangle$ where

$$\langle 3\pi n|J^\mu|p\rangle = \sum_{\lambda_\gamma=\pm1,0} \epsilon^\mu(Q,\lambda_\gamma) T(p_i,p',p,q;\lambda',\lambda,\lambda_\gamma) \tag{7}$$

with $\lambda_\gamma, \lambda, \lambda'$ being the photon, proton and neutron, helicities in the center of mass, respectively, and p_i, $i = \pi^+(1), \pi^+(2), \pi^-(3)$, p', p, q denoting the pion, recoil, target and photon momenta, respectively. The amplitude T is symmetrized with respect to the two π^+. Assuming the pion exchange dominance and rewriting in a factorized from

$$T(p_i,p',p,q;\lambda',\lambda,\lambda_\gamma) = \sum_X \sum_{\lambda_X=-J_X}^{J_X} P^X_{\lambda',\lambda_X,\lambda,\lambda_\gamma}(s,t) D^X_{\lambda_X}(p_i) \tag{8}$$

The amplitude P^X denotes the one-pion-exchange amplitude for production of a 3π isobar, $X = a_1, a_2, \pi_1, \pi_2$ with the quantum numbers $J_X^{P_X C_X} = 1^{++}, 2^{++}, 1^{-+}, 2^{-+}$ respectively,

$$P^X_{\lambda'\lambda_X,\lambda,\lambda_\gamma} = \delta_{\lambda',-\lambda} V_{\lambda_\gamma\lambda_X} \left(-\frac{t'}{4m_N^2}\right)^{\frac{|\lambda'-\lambda|}{2}+\frac{|\lambda_\gamma-\lambda_X|}{2}} \frac{1+e^{-i\pi\alpha_\pi(t)}}{2} \Gamma[-\alpha_\pi(t)] s^{\alpha_\pi(t)} e^{-5|t|GeV^{-2}}, \tag{9}$$

with $t' = t_{min}$ where $t = (p'-p)^2$ is the momentum transfer squared, $s = (q+p)^2$ is the center of mass energy squared and $\alpha_\pi(t) = 0.9(t - m_\pi^2)\mathrm{GeV}^{-2}$ is the pion Regge trajectory. The "upper" vertex $V_{\lambda_\gamma\lambda_X}$ is given by

$$\begin{aligned} & V_{\lambda_\gamma\lambda_X} = [\delta_{\lambda_\gamma,1}\delta_{\lambda_X,0} + \eta_X\delta_{\lambda_\gamma,-1}\delta_{\lambda_X,0}]\beta_1^{\gamma\pi X} + [\delta_{\lambda_\gamma,1}\delta_{\lambda_X,|\lambda_X|} + \eta_X(-1)^{\lambda_X}\delta_{\lambda_\gamma,-1}\delta_{\lambda_X,-|\lambda_X|}]\beta^{\gamma\pi X}_{|\lambda_X|-1} \\ + & [\delta_{\lambda_\gamma,1}\delta_{\lambda_X,-|\lambda_X|} + \eta_X(-1)^{\lambda_X}\delta_{\lambda_\gamma,-1}\delta_{\lambda_X,|\lambda_X|}]\beta^{\gamma\pi X}_{|\lambda_X|+1} + \delta_{\lambda_\gamma,0}[\delta_{\lambda_X,|\lambda_X|} - \eta_X(-1)^{\lambda_X}\delta_{\lambda_X,-|\lambda_X|}]\beta^{\gamma\pi X}_{|\lambda_X|} \\ & +\delta_{\lambda_\gamma,0}\delta_{\lambda_X,0}\frac{1-\eta_X}{2}\beta_0^{\gamma\pi X} \end{aligned} \tag{10}$$

where $\eta_X = P_X(-1)^{J_X}$ and the various linear combination reflect parity conservation. The factors $\beta_n^{\gamma\pi X}$, $n = 0, 1, \cdots \lambda_X + 1$ give the strength of various helicity couplings and in simulations we have assumed dominances of s-channel helicity conservation *i.e.* only use $\beta_0^{\gamma\pi X} \neq 0$. The resonance decay amplitudes D^X are given by

$$D^X_{\lambda_X} = D^X_{\lambda_X}(12,3) + D^X_{\lambda_X}(31,2) + D^X_{\lambda_X}(23,1) \tag{11}$$

where $D^X_{\lambda_X}(ij,k)$ represents a quasi-two body decay of the X-isobar to a $(\pi^i\pi^j)$, di-pion resonance defined by its spin, j_{ij}, isospin t_{ij} and parity P_{ij}, and and the spectator, π^k, with the orbital angular

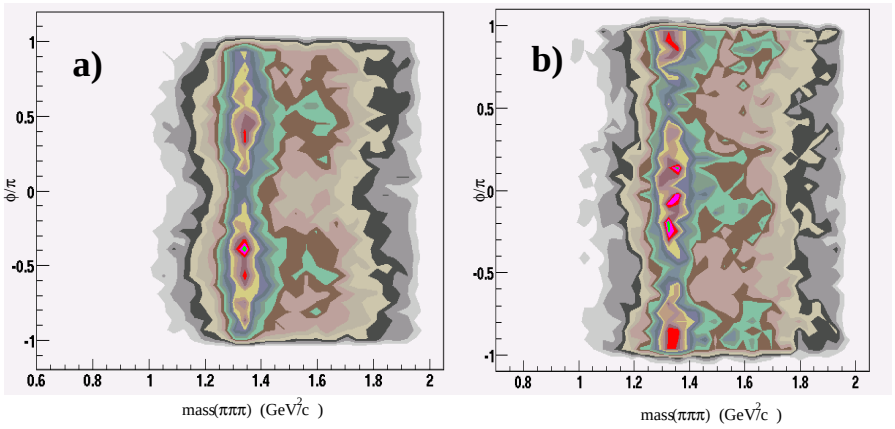

Figure 38: The ϕ/π vs. Mass[3π] for those events with the polarization perpendicular to the production plane (left) and in the production plane (right). The simulated polarization was set to 60%.

momentum L_{ij} between the di-pion resonance and the spectator,

$$D^X_{\lambda_X}(ij,k) = \sum_{t_{ij} j_{ij} L_{ij}} N_{L_{ij}} N_{j_{ij}} g^{j_X^{P_X} I_X}_{j_{ij}^{P_{ij}} L_{ij}} \frac{1+P_X P_{ij}(-1)^{L_{ij}+1}}{2} \frac{1+P_{ij}(-1)^{j_{ij}}}{2} \frac{1+(-1)^{j_{ij}+t_{ij}}}{2}$$
$$\times \sum_{m_{ij},\mu_{ij}} \langle 1 m_i; 1 m_j | t_{ij} m_{ij} \rangle \langle t_{ij} m_{ij}; 1 m_k | 1 1 \rangle \langle j_{ij} \mu_{ij}; L_{ij} 0 | j_X \mu_{ij} \rangle D^{j_{ij}}_{\mu_{ij},0}(\psi_i \theta_i 0) D^{J_X}_{\lambda_X,\mu_{ij}}(\widetilde{\phi}_k \widetilde{\vartheta}_k 0) \tag{12}$$

The angles $\widetilde{\vartheta}_k, \widetilde{\phi}_k$ are the polar and the azimuthal angle of the spectator pion (π^k) in the helicity frame of the (*i.e.* the rest frame of the 3π system with the y axis perpendicular to the hadron reaction plane and the $-z$ axis along the recoil neutron) and θ_i, ψ_i are the polar and the azimuthal angle of the π^i in the rest frame of the $\pi^i\pi^j$. In simulations we used: the $L = S, D$ decay modes of the a_1 to $\rho\pi$, the $L = D$ decay modes of the a_2 to $\rho\pi$, the $L = P, F$ decay modes of the π_2 to $f_2\pi$ and the $L = P, F$ decay modes of the π_2 to $\rho\pi$. The coupling constants g were fixed by the known decay widths for these modes. In addition we simulated the $L = P$ decay mode of the exotic, π_1 to $\rho\pi$ with varied coupling strength and mass of the π_1 resonance.

The effects related to the polarization can be directly seen in Figure 38. Because pion exchange corresponds to unnatural parity exchange the ϕ dependence of the produced 3π system will flip depending on the naturality $\eta_X = P_X(-1)^{J_X}$ of the state [88]. These two figures differ only in the direction of the photon polarization and correspond to the two eigenstates of reflectivity. In Figure 38 (a) are those events where the photon polarization is normal to the production plane, and (b) are those events where the photon polarization is in the production plane. Due to parity conservation in the production process, states of the same reflectivity but opposite naturality will have opposite ϕ distributions, which may be observed in the figure. It is most clearly seen for the band at the $a_2(1320)$ mass. This distribution is $cos^2(\phi)$ in one figure and $sin^2(\phi)$ in the other. Another band at a mass near 1.7 GeV has the opposite ϕ behavior of the $a_2(1320)$. It corresponds to the $\pi_2(1670)$ which has a naturality opposite that of the $a_2(1320)$.

Further details of the simulations are presented in Sec. 6.2

Appendix B: PAC35 Report on LOI-10-001 and response

PAC35 Report
Letter of Intent: LOI-10-001

Title: Large Hadron Spectroscopy with low Q2 electron scattering in CLAS12

Spokespersons: M. Battaglieri, R. De Vita, S. Stepanyan

Motivation: In an attempt to gain an understanding of QCD in the strong couple regime, meson and baryon spectroscopy is proposed to be investigated using high energy quasi-real linearly polarized photons by tagging scattered electrons at low energy and small angles (between 2º and 5º) in combination with the operation of the CLAS12 detector. A study of the confinement mechanism of quarks and gluons in hadrons is proposed through the search for hybrid and exotic hadrons. The physics motivation in this Letter of Intent is in many ways similar and complementary to that giving the raison d'etre *of the dedicated GlueX experiment in Hall D, its importance and impact has been established over recent years. The described capability is very attractive on one hand for its complementarity to the Hall D program and to its experimental impact on the possible discovery of hybrid mesons.*

Measurement and Feasibility: The series of measurements described in this letter require the proposed forward electron tagger and take advantage of the large acceptance, multi-particle detection capability of CLAS12. The forward tagger would provide key information on the energy and linear polarization of the quasi-real photons responsible for the hadronic reactions under studies. A post-tagging technique (that is tagging only electrons corresponding to virtual photons involved in a hadronic interactions) is proposed to allow for increased luminosity. A study of rates from electromagnetic backgrounds, in the forward tagger for energies of photons between 7 and 10.5 GeV, shows that adding such device seems feasible. A safety margin on the rates is provided with a possible increase in the total energy threshold. Several options for the calorimeter are under investigation with a PbWO calorimeter as the most promising one. On the experimental side there does not seem to be any show stopper for a given luminosity. However to access some of the physics, like charm production near threshold on hydrogen and light nuclei, mentioned in this letter, the 'high luminosity' capabilities will need to be demonstrated once the device is built or optimized.

Issues: One issue that needs to be addressed is a clear demonstration of the capability of CLAS12 in combination with the tagger to provide data that would permit the extraction of the sought over resonances in a background where no peak is seen, and not just when an obvious peak is observed. In this case, effects of acceptance and hermeticity of the detector need to be addressed for the most promising channels. As mentioned in the TAC report the hole in the acceptance at 35º shown in Fig. 26 of the LOI in the 3π channel is not reassuring and the issue needs to be addressed of its impact on the PWA analysis. Such studies have been carried out in Hall D and could be replicated for this case. There was also a concern expressed in terms of the man power needed to carry out the analysis. This issue also needs to be discussed when a full proposal is submitted. It was not clear that even with the proposed tagger facility the luminosity for a quasi-real photoproduction of charm near threshold is possible with reasonable statistics. Perhaps the proponents could show that in a full proposal.

Recommendation: The proponents are encouraged to develop a full proposal with the key reactions that form the heart of the motivation are presented and where issues of acceptance and PWA analysis are fully addressed.

Response

The response to the three issues rised by the Program Advisory Committee 35 are reported below:

- *CLAS12 acceptance and PWA, in particular for the 3π channel.*

  We addressed this issue in Sec. 6.2.2 where results from systematic studies on this channel are reported. Events were generated according to a realistic model that includes many different isobar channels, projected onto the CLAS12 detector and fit with a full partial wave analysis. This study showed that: *(i)* the reconstructed waves are fully consistent with the generated ones, *(ii)* it is possible to single out an exotic wave with a strength of few % of the whole intensity for the reaction channel, and *(iii)* that possible leakages from other stronger waves do not create fake structures in the exotic wave. We also showed that reasonable distortions in the event reconstruction procedure, e.g using an incorrect magnetic field or a worse momentum resolution for hadrons, do not prevent to successfully perform the PWA.

  Similar studies have been performed on the $\eta\pi$ channel where the partial wave analysis was carried out with a completely independent model finding consistent results. The outcomes of this study are reported in Sec. 6.2.1.

- *Man power needed to carry out data analysis.*

  We are taking very seriously this concern since a man-power problem was encountered in the baryon spectroscopy analysis at the early stage of the CLAS-JLab history. Full partial wave analysis of several reaction channels using CLAS data have been performed and first results have been published [17, 18, 61], demonstrating that tools are already available.

  During the preparation of this proposal, a dedicated effort was put in building an analysis framework and tools based on the the Isobar Model, i.e. the phenomenological approach used in most analysis worldwide. As reported in Sec. 6.2, these tools were successfully used in the analysis of some of reaction channels. To cope with the large statistics foreseen for this experiment, these tools have also been designed to use the most advanced technology (GPUs) to reduce the computation time to acceptable level. Performance tests and code optimization for the presently available graphic cards are in progress.

  In addition, well aware of the necessity of a strict collaboration with the theoretical community, as mentioned in Sec. 3, we are participating to a world-wide network of laboratories and universities to share experience and resources among the existing PWA initiatives: EBAC at JLab, SAID at GW, NABLIS at Juliech and others. A first dedicated workshop was organized at INT (Seattle 2009) to bring together experts in the field from both the theoretical and experimental communities. A second workshop is being organized at ECT* (Trento, Italy) in January 2011. In particular a strong collaboration to provide a common analysis framework between the CLAS12 and the GLUEX experiment has already started and will be strengthened from a strict collaboration.

- *Luminosity for photoproduction of charm near threshold.*

  Charm production is not included in the present proposal that is only focused on light quark meson spectroscopy.

References

[1] K. Nakamura et al. (Particle Data Group), J. Phys. G 37, 075021 (2010) .

[2] R. L. Jaffe, K. Johnson, Phys. Lett. **B60**, 201 (1976).

[3] D. Horn and J. Mandula, Phys. Rev. D **17**, 898 (1978).

[4] T. Barnes, F. E. Close, F. de Viron and J. Weyers, Nucl. Phys. B **224**, 241 (1983).

[5] N. Isgur, R. Kokoski, J. E. Paton, Phys. Rev. Lett. **54**, 869 (1985).

[6] N. Isgur, J. E. Paton, Phys. Rev. **D31**, 2910 (1985).

[7] P. Guo, A. P. Szczepaniak, G. Galatà, A. Vassallo and E. Santopinto, Phys. Rev. D **78** (2008) 056003.

[8] J. J. Dudek, R. G. Edwards, M. J. Peardon *et al.*, Phys. Rev. Lett. **103**, 262001 (2009).

[9] J. J. Dudek, R. G. Edwards, M. J. Peardon *et al.*, Phys. Rev. **D82**, 034508 (2010).

[10] M. Battaglieri *et al.* [CLAS Collaboration], LOI-10-001:*Hadron Spectroscopy with Low* Q^2 *electron-scattering in CLAS12*.

[11] C. W. Bernard *et al.* [MILC Collaboration], Phys. Rev. **D56**, 7039-7051 (1997).

[12] P. Lacock *et al.* [UKQCD Collaboration], Phys. Lett. **B401**, 308-312 (1997).

[13] C. Bernard, T. Burch, E. B. Gregory *et al.*, Phys. Rev. **D68**, 074505 (2003).

[14] J. N. Hedditch, W. Kamleh, B. G. Lasscock *et al.*, Phys. Rev. **D72**, 114507 (2005).

[15] P. Lacock *et al.* [TXL Collaboration], Nucl. Phys. Proc. Suppl. **73**, 261-263 (1999).

[16] C. McNeile *et al.* [UKQCD Collaboration], Phys. Rev. **D73**, 074506 (2006).

[17] M. Nozar *et al.* [CLAS Collaboration], Phys. Rev. Lett. **102**, 102002 (2009).

[18] M. Battaglieri *et al.* [CLAS Collaboration], Phys. Rev. Lett. **102**, 102001 (2009) and M. Battaglieri *et al.* [CLAS Collaboration], Phys. Rev. **D80**, 072005 (2009).

[19] C. Salgado *et al.*, E-99-005: *Meson Spectroscopy in Few-Body Decays*, http://www.jlab.org/exp_prog/proposals/99/PR99-005.pdf;
C. Salgado *et al.*, E-01-017: *Extensions to E-99-005, Meson Spectroscopy in Few-Body Decays*, http://www.jlab.org/exp_prog/proposals/01/PR01-017.pdf.

[20] P. Eugenio *et al.*, E-04-005: *Search for New Forms of Hadronic Matter in Photoproduction*, http://www.jlab.org/exp_prog/proposals/04/PR04-005.pdf.

[21] S. Stepanyan *et al.*, E-07-009: *Meson spectroscopy in the Coherent Production on* ^{4}*He with CLAS*, http://www.jlab.org/exp_prog/proposals/07/PR-07-009.pdf.

[22] S. Godfrey, J. Napolitano, Rev. Mod. Phys. **71**, 1411-1462 (1999).

[23] E. Klempt, [hep-ph/0404270].

[24] C. A. Meyer, Y. Van Haarlem, Phys. Rev. **C82**, 025208 (2010).

[25] D. Alde, et al. *Phys.Lett.* **B205**, 397 (1988).

[26] G. M. Beladidze *et al.* [VES Collaboration], Phys. Lett. **B313**, 276-282 (1993).

[27] H. Aoyagi, S. Fukui, T. Hasegawa *et al.*, Phys. Lett. **B314**, 246-254 (1993).

[28] D. R. Thompson *et al.* [E852 Collaboration], Phys. Rev. Lett. **79**, 1630-1633 (1997); S. U. Chung *et al.* [E852 Collaboration], Phys. Rev. **D60**, 092001 (1999).

[29] A. Abele *et al.* [Crystal Barrel Collaboration], Phys. Lett. **B423**, 175-184 (1998); A. Abele *et al.* [Crystal Barrel Collaboration], Phys. Lett. **B446**, 349-355 (1999).

[30] D. P. Weygand, *The Status of Mesonic Exotica*, **Mesons 2010**, Warsaw, Poland (2010).

[31] G. S. Adams *et al.* (E852 Collaboration), Phys. Rev. Lett. **81**, 5760 (1998).

[32] A. Dzierba *et al.*, Phys. Rev. D **73**, 072001 (2006).

[33] Y. Khokhlov *et al.* (VES Collaboration), Nucl. Phys. A **663**, 596 (2000).

[34] A. Alekseev *et al.* (COMPASS Collaboration), Phys. Rev Lett. **104**, 241803 (2010). B. Grube *et al.* (COMPASS Collaboration), arXiv:1002.1272 [hep-ex] (2010).

[35] J. Kuhn *et al.* [E852 Collaboration], Phys. Lett. **B595**, 109-117 (2004); M. Lu *et al.* [E852 Collaboration], Phys. Rev. Lett. **94**, 032002 (2005).

[36] M. Ablikim *et al.* [BESIII Collaboration], Nucl. Instrum. Meth. A **614** (2010) 345.

[37] The GlueX Collaboration, *The GlueX Experiment in Hall-D*, http://argus.phys.uregina.ca/cgi-bin/public/DocDB/ShowDocument?docid=1545; The GlueX Collaboration, *Mapping the Spectrum of Light Quark Mesons and Gluonic Excitations with Linearly Polarized Photons*, http://argus.phys.uregina.ca/cgi-bin/public/DocDB/ShowDocument?docid=1226.

[38] D. Bettoni *et al.* [PANDA Collaboration], *Physics Performance Report for PANDA: Strong Interaction Studies with Antiprotons*, arXiv:0903.3905v1 [hep-ex] (2009).

[39] F.E. Close and H.J. Lipkin, Phys. Rev. Lett. 41, 1263 (1978).

[40] S.I. Bityukov *et al.*, Sov.J.Nucl.Phys. 38, 1205 (1983).

[41] S.I. Bityukov *et al.*, Phys. Lett. **B188** 383 (1987).

[42] M. Atkinson *et al.*, Nucl. Phys. **B231**, 1 (1984).

[43] Yu.M. Antipov *et al.*, Pis'ma JETF **38**, 356 (1983).

[44] B. Aubert *et al.*, Phys. Rev. **D77**, 092002 (2008).

[45] R. L. Jaffe, Phys. Rev. D **15**, 281 (1977).

[46] L. Maiani, F. Piccinini, A. D. Polosa, V. Riquer, Phys. Rev. Lett. **93**, 212002 (2004).

[47] C. Amsler and F. Close, *Phys. Lett.* **B353**, 385 (1995).

[48] A. Donnachie and Y. Kalashnikova, arXiv:0806.3698 [hep-ph] (2008).

[49] T. Barnes, N. Black and P. R. Page, nucl-th-0208072, (2002).

[50] F. Mane *et al.* [DM1], Phys. Lett. **99B**, 261 (1981).

[51] B. Delcourt *et al.* [DM1], Phys. Lett. **99B**, 257 (1981)

[52] P.M.Ivanov *et al.*, Phys. Lett. **107B**, 297 (1981).

[53] D. Bisello *et al.*, [DM2] Z. Phys. **C39**, 13 (1988).

[54] F. Mane *et al.*, [DM1], Phys. Lett. 112B, 178 (1982).

[55] J. Buon *et al.*, [DM1] Phys. Lett. **118B**, 221 (1982).

[56] A. Antonelli *et al.*, [DM2] Z. Phys. **C56**, 15 (1992).

[57] D. Aston *et al.*, Phys. Lett. **104B**, 231 (1981).

[58] M. Atkinson *et al.*,Z. Phys. **C27**, 233 (1985).

[59] J. Busenitz *et al.*, Phys. Rev. **D40**, 1 (1989).

[60] J.M. Link *et al.* [FOCUS], arXiv:0208027 [hep-ex] (2002).

[61] M. Williams *et al.* [CLAS Collaboration], Phys. Rev. **C80**, 065209 (2009).

[62] A. Afanasev and P. R. Page, Phys. Rev. **A57**, 6771 (1998).

[63] A. Szczepaniak and M. Swat, Phys. Lett. **B516**, 72 (2001).

[64] N. Dombey, Rev. Mod. Phys. **41**, 236 (1969).

[65] E. S. Ageev *et al.* [COMPASS Collaboration], Phys. Lett. **B**, 633 (2005).

[66] S. Chekanov *et al.* [ZEUS Collaboration], Nucl. Phys. B **627**, 3 (2002).

[67] B.Andrieu et al., *Test beam results of the tungsten/quartz-fibre calorimeter for the luminosity measurement in H1, Proc. of the IX Int.Conf. on Calorimetry in Particle Physics*, CALOR2000, Annecy Oct. 2000, Frascati Physics Series (2001).

[68] I. Akushevich, H. Bottcher and D. Ryckbosch, arXiv:hep-ph/9906408.

[69] B. A. Mecking *et al.* [CLAS Collaboration], Nucl. Instrum. Meth. A **503** (2003) 513.

[70] CLAS12 Technical Design Report,
http://clasweb.jlab.org/wiki/index.php/CLAS12_Technical_Design_Report.

[71] CMS Electromagnetic Calorimeter, http://cms.web.cern.ch/cms/Detector/ECAL/index.html.

[72] D. C. Zhou *et al.* (ALICE Collaboration), J. Phys. G **34** (2007) 719.

[73] PANDA Collaboration, *Technical Design Report for PANDA Electromagnetic Calorimeter (EMC)*, arXiv:0810.1216.

[74] I. Bedlinskiy *et al.*, "An Inner Calorimeter for CLAS/DVCS experiments", unpublished.

[75] S. Janssen et. al., Nuclear Science Symposium, 1999 Conference Record, 1999 IEEE

[76] S.J. Alsvaag et. al., IEEE Transactions on Nuclear Science, Vol. 42, no.4 (1995)

[77] S. Stepanyan et. al., CLAS Note 2009-019; S. Stepanyan et. al., 2008 IEEE nuclear Science Symposium and Medical imaging Conference.

[78] M. Ungaro, CLAS12 GEANT-4 simulation package GEMC, http://clasweb.jlab.org/wiki/index.php/CLAS12_Software.

[79] A. Vlassov, *private communication*.

[80] M. Sargsyan, CLAS-NOTE 90-007 (1990).

[81] M. Mestayer, SLAC Eng.Note 72 (1977).

[82] Y.S. Tsai, Rev. Mod. Phys. **46**, 815 (1974).

[83] M. Mestayer, *private communication*.

[84] S. Procureur, *private communication*. See also http://www.jlab.org/∼procureu/CLAS12/2008-10-30_CollabMeeting.ppt

[85] V. Kubarovsky, *$\phi\pi$ Photoproduction and Search for Exotic Meson with CLAS*, CLAS-ANALYSIS Note 2000-001.

[86] H. Matevosyan, R. Mitchell and M. Shepherd, IUAmpTools, *private communication*.

[87] See for example K. Joo, F. Sabatie *et al.*, E12-06-119: *Deeply Virtual Compton Scattering with CLAS at 11 GeV*, http://www.jlab.org/exp_prog/proposals/06/PR12-06-119.pdf.

[88] S. U. Chung and T. L. Trueman, Phys. Rev. D **11** (1975) 633.